Hot electron transport in different semiconductor structures at low lattice temperatures – a theoretical analysis

THESIS SUBMITTED FOR THE DEGREE OF

DOCTOR OF PHILOSOPHY IN SCIENCE (PHYSICS)

OF

JADAVPUR UNIVERSITY

2021

By

ARNAB BASU

DEPARTMENT OF PHYSICS

JADAVPUR UNIVERSITY

KOLKATA - 700032

TO

MY BELOVED

PARENTS AND WIFE

CERTIFICATE FROM THE SUPERVISOR

This is to certify that the thesis entitled "**Hot electron transport in different semiconductor structures at low lattice temperatures - a theoretical analysis**" submitted by **Sri Arnab Basu** (Reference No. D-7/SC/349/15, Index No. 54/15/Phys./23), who got his name registered on **28th April, 2015** for the award of Ph.D. (Science) degree of Jadavpur University, is absolutely based upon his own work under the supervision of **Prof. Tapas Ranjan Middya, Department of Physics, Jadavpur University, Kolkata - 32** and that neither this thesis nor any part of it has been submitted for either any degree / diploma or any other academic award anywhere before.

Prof. Tapas Ranjan Middya 22/12/21
Retired Professor
Dept. of Physics
Jadavpur University
Email: tapas.middya@gmail.com

Declaration

I, hereby, declare that the work enclosed in the present thesis has been carried out by me under the supervision of Prof. Tapas Ranjan Middya at the Department of Physics, Jadavpur University, Kolkata - 32, India. Neither this thesis nor any part of it has been submitted for any degree whatsoever.

Dated:

……………………………………..

Arnab Basu
Research Scholar
Department of Physics
Jadavpur University
Kolkata - 32, India

ACKNODLEDGEMENTS

Firstly, I would like to express my sincere gratitude to my supervisor Prof. Tapas Ranjan Middya for the continuous support in my Ph.D study and related research, for his patience, motivation, and immense knowledge. His guidance helped me in all the time and writing of this thesis. I could not have imagined having a better advisor and mentor for my Ph.D study.

I am deeply indebted to Prof. D.P. Bhattacharya. He has guided me constantly throughout my research and always encouraged me by sharing constructive ideas and insightful comments which prompted me to widen my research from various perspectives.

I thankfully acknowledge the Department of Science and Technology, Government of India, for providing me the INSPIRE Fellowship. I would also like to thank the Physics Department of Jadavpur University and of course Institute of Enginering & Management, Kolkata for the Infrastructural Support and the computer facilities that I needed to complete this thesis.

I thank my fellow lab mates for the stimulating discussions and for all the fun we have had in the last few years.

Last but not the least, I would like to thank my family: my parents and my wife for supporting me spiritually throughout writing this thesis and my life in general.

(ARNAB BASU)

Assistant Professor
Dept. of Basic Science and Humanities
Institute of Engineering & Management, Kolkata
&
Research Scholar
Dept. of Physics
Jadavpur University
Kolkata - 700032

LIST OF PUBLICATIONS

[1] A realistic analysis of the phonon growth characteristics in a degenerate semiconductor using a simplified model of Fermi-Dirac distribution.

A. Basu, B. Das, T.R. Middya, D.P. Bhattacharya ; ***Journal of Physics and Chemistry of Solids***, Volume 100, January 2017, Pages 9–13

[2] The effects of degeneracy of the carrier ensemble on the energy loss rate and the high field mobility characteristics under the conditions of low lattice temperatures.

A. Basu, B. Das, T.R. Middya, D.P. Bhattacharya ; ***Physica B*** , Volume 506, 1 February 2017, Pages 65–68

[3] Field-effect mobility of a two dimensional electron gas in an n-channel of Si-SiO2 MOS structure with due consideration of some practical features

A. Basu, T.R. Middya, D.P. Bhattacharya ; ***Journal of Applied Physics***, Volume 122, 2017, Page 105703

[4] An analysis of phonon emission as controlled by the combined interaction with the acoustic and piezoelectric phonons in a degenerate III-V compound semiconductor using an approximated Fermi – Dirac distribution at low lattice temperatures.

A. Basu, B.Das, T.R. Middya, D.P. Bhattacharya ; ***Philosophical Magazine***, Volume 98, No. 9, 2018, Pages 803- 818

[5] A study of the average energy loss to the acoustic modes and the non-ohmic mobility characteristics of a degenerate semiconductor using an alternative model of heated Fermi –Dirac distribution

A.Basu, T.R.Middya, D.P.Bhattacharya (Communicated)

[6] Effective temperature of the non-equilibrium electrons in a degenerate semiconductor at low lattice temperature.

B.Das, **A.Basu**, J.Das, D.P.Bhattacharya; ***Physica B***, Volume 474, 1 October 2015, Pages 21-26

[7] Piezoelectric interaction in controlling the effective electron temperature and the non-ohmic mobility characteristics in GaN and other III–V compounds at low lattice temperature.

B. Das, **A. Basu**, J. Das, D.P. Bhattacharya; ***Canadian Journal of Physics*** , 2017, 95(2): 167-172

[8] Heating of carriers as controlled by the combined interactions with acoustic and piezoelectric phonons in degenerate III-V semiconductors at low lattice temperature.

D.P.Bhattacharya, J.Das, **A.Basu**, B.Das; ***Physica B***, Volume 520, 1 September 2017, Pages 106–111

Publications not included in the Thesis

[1] Piezoelectric scattering limited mobility as controlled by the transverse component of the phonon wave vector in quantum layers at low temperatures.

S.Nag, **A.Basu**, B.Das, T.R.Middya, D.P.Bhattacharya ; ***Physica E***, Volume 72, August 2015, Pages 77-83

[2] Energy loss to intravalley acoustic modes in nano-dimensional wire structures at low temperatures.

S.Nag, B.Das, **A.Basu**, J.Das, D.P.Bhattacharya, C.K.Sarkar; ***Physica E***, Volume 87, March 2017, Pages 237–241

CONTENTS

Page No.

List of Publications

List of Publications not included in the Thesis

List of Symbols

Chapter I: Introduction, Basic Assumptions and Scope of the Thesis

1.1. Introduction 1

1.2. Salient features of low temperature 2

1.3. Different semiconductor structures 6

1.4. Scattering Mechanisms 11

1.5. Classification of Scattering 12

1.6. Relative importance of different scattering mechanisms 15

1.7. Scope of the Thesis 17

References 22

Chapter II: Fermi – Dirac Distribution Function : An Effective Alternative Model 26

Chapter III: Analysis of the energy loss rate and the non-ohmic mobility characteristics in the non-degenerate sample of different III -V compound semiconductors at low lattice temperature

3.1. Introduction 34

3.2. Development

3.2.1. Field dependence of the effective electron temperature for the combined interaction with piezoelectric and deformation acoustic phonons. 36

3.2.2. Energy loss rate for the combined interaction with the piezoelectric and deformation acoustic phonons. 39

3.3. Results and Discussion 41

References 49

Chapter IV: Effective temperature of the non-equilibrium electrons in a degenerate semiconductor at low lattice temperature

4.1. Effective temperature of the non-equilibrium electrons for the interaction with the acoustic phonons.

4.1.1. Introduction 50

4.1.2. Development 52

4.1.3. Comparison of Results and Discussion 56

4.1.4. Conclusion 60

4.2. Effective temperature of the non-equilibrium electrons for the combined interaction with the acoustic and the piezoelectric phonons.

4.2.1. Introduction 62

4.2.2. Development 63

4.2.3. Results 73

4.2.4. Discussion 74

4.2.5. Conclusion 78

References 81

Chapter V: Phonon growth characteristics in a degenerate semiconductor at low lattice temperatures

5.1. Phonon growth rate for the interaction of the electrons with the acoustic phonons.

5.1.1. Introduction 83

5.1.2. Development 84

5.1.3. Results and Discussions 89

5.2. Phonon growth rate for the interaction of the electrons with the acoustic and the piezoelectric phonons

5.2.1. Introduction 93

5.2.2. Development 94

5.2.3. Results and Discussions 100
References 107

Chapter VI: Energy loss rate and the high field mobility characteristics in a degenerate semiconductor at low lattice temperatures

6.1. Calculation of the energy loss rate and the high field mobility for the interaction of the electrons with the acoustic phonons using the Fermi – Dirac distribution function

6.1.1. Introduction 108
6.1.2. Development 110
6.1.3. Results and Discussions 114

6.2. Calculation of the energy loss rate and the high field mobility for the interaction of the electrons with the acoustic phonons using the alternative model of heated Fermi – Dirac distribution function

6.2.1. Introduction 121
6.2.2. Development 123
6.2.3. Results and Discussions 131

References 140

Chapter VII: Field-effect mobility of a two dimensional electron gas in an n–channel of Si-SiO_2 MOS structure

7.1. Introduction 141
7.2. Development 143

7.2.1. Mobility characteristics at high temperatures 146
7.2.2. Mobility characteristics at low temperatures 146

7.3. Results and Discussions 148

References 159

List of symbols

$N_{\vec{q}(\vec{Q})}$: Phonon energy distribution

$\vec{q}$: Three dimensional phonon wave vector

$\vec{Q}$: Two dimensional phonon wave vector

h : Planck's constant

ω : Frequency of the lattice wave vector

u_l : Acoustic velocity

k_B : Boltzmann constant

T_L : Lattice temperature

x or X : Normalized phonon wavevector in three and two dimensions respectively

B_m : Bernoulli′s number

ε_{ph} : Phonon energy

ε_k : Electron energy

v_{th} : Velocity of the electrons at thermal equilibrium with the lattice

ε_F : Fermi energy

m^* : Effective mass of the electrons

N_D : Donor concentration

E_d : Donor ionisation energy

β_s : Screening length

e : Electronic charge

n_0 : Free electron concentration

K or ϵ_{sc} : Dielectric constant

α : Inverse of screening length

ε_0 : Energy of the lowest subband

3/2/1/0 DEG : Three/ two/ one/ zero dimensional electron gas (0 DEG : Quantum dot)

T_e : Effective electron temperature

μ : Mobility of the electrons

m_0 : Free electron mass

f_0 : Isotropic part of distributuin function

τ : Energy / Momentum relaxation time

E_1 : Deformation potential constant

$T_n = \frac{T_e}{T_L}$: Normalised electron temperature

ρ : Density of electron

K_m : Piezoelectric coupling constant

N_C : Effective density of states

$\frac{\varepsilon_F}{k_B T_L}$: Degeneracy parameter

$\frac{\varepsilon_F}{k_B T_e}$: Normalised degeneracy parameter

ω_0 : Angular frequency for optical phonons

n_{norm} : Normalised concentration

J : Current density

μ_0 : Zero field mobility

$m_{\parallel}^*$: Effective mass of the electrons parallel to the interface

m_3^* : Effective mass of the electrons perpendicular to the surface

ϵ_0 : Free space permittivity

m_μ^* : Conduction electron effective mass

μ_{eff} : Effective mobility of the electrons

μ_{FE} : Field effect mobility

V_G : Gate voltage

V_T : Threshold voltage

C_{ox} : Capacitance per unit area of the oxide layer

ϵ_{ox} : Permittivity of the oxide layer

t_{ox} : Thikness of the oxide layer

CHAPTER I

Introduction, Basic Assumptions and Scope of the Thesis

1.1. Introduction

Semiconductor devices have been considered as one of the most important inventions of 20th century because of their remarkable applications in modern technology and electronic goods. The physics of such devices is dependent upon the physics of the materials they are made of and their structures. In order to understand the purpose a device may serve and to know how to manipulate its performance, one should have a detailed knowledge of the electrical transport characteristics of the structures the device is made of. The study of electronic transport in different semiconductor structures under different prevalent conditions is a traditional subject, which has been well analysed over the past few decades. Transport properties are known to underlie numerous technical applications of semiconductors. Besides, such properties are sensitive to the dispersion laws of the current carriers and the nature of the interaction of the carriers with various defects of the crystal lattice or phonons. Therefore, many conventional methods of investigating semiconducting materials are based on the study of different kinetic effects. They become especially efficient under some extreme conditions of low temperatures. Satisfactory and reliable results are obtained when an integral investigation is carried out and the conclusions of the theory of electron transport phenomena are taken into account. Though such studies in and around room temperature are well available, but the same for low temperatures are quite scarce. Of late, particularly after the discovery of Quantum

Hall Effect (QHE) and Fractional Quantum Hall Effect (FQHE), the study of low temperature electrical transport in semiconductors has assumed high importance.

Such theoretical studies are beset with much mathematical difficulties. The low temperature features are either absent at higher temperatures or ignored to make an analysis easily tractable. The basic physics involved in high field effects at low temperatures is quite complicated and not yet well understood.

1.2. Salient features of low temperature

The low temperature features that make such studies complicated include [1.1-1.5] -

(i) Necessity of using true phonon distribution, as the simple equipartition approximation of Bose – Einstein's (B.E.) distribution function may hardly be assumed. The energy distribution for the phonons is

$$N_{\vec{q}(\vec{Q})} = \frac{1}{\exp\left(\frac{\hbar\omega_{\vec{q}(\vec{Q})}}{k_B T_L}\right) - 1}$$

where, $\vec{q}$ and $\vec{Q}$ are the three and two dimensional phonon wave vectors respectively, $\hbar = \frac{h}{2\pi}$; h being the Planck's constant, $\omega_{\vec{q}(\vec{Q})}$ is the frequency of corresponding lattice wave vectors given by $\omega_{\vec{q}(\vec{Q})} = u_l q(Q)$; u_l is the acoustic velocity of the electrons; k_B the Boltzmann constant and T_L is the lattice temperature. At high temperatures, the above expression may be simplified to the well known equipartition law i.e. [1.1,1.3]

$$N_{\vec{q}(\vec{Q})} = \frac{k_B T_L}{\hbar\omega_{\vec{q}(\vec{Q})}}$$

because of the fact that $k_B T_L \gg \hbar\omega_{\vec{q}(\vec{Q})}$ i.e. the average thermal energy of the free carriers largely exceeds the phonon energy at thermodynamic equilibrium. However, at low temperatures ($T_L \leq 20K$), $N_{\vec{q}(\vec{Q})}$ may be approximated by Laurent expansion [1.6]

$$N_{\vec{q}(\vec{Q})} = \sum_{m=0}^{\infty} \frac{B_m}{m!} [x(X)]^{m-1}; x(X) \leq \bar{x}(\bar{X})$$

$$N_{\vec{q}(\vec{Q})} = \exp[-x(X)]\,;\ x(X) > \bar{x}(\bar{X})$$

where $x(X)$is the normalised phonon wave vector given by $\frac{\hbar u_l q\,(Q)}{k_B T_L}$ and B_m is the Bernoulli's number. The value of $\bar{x}(\bar{X})$ may be taken to be 3.5 (3.31) [1.6-1.8].

In addition, at the low temperature regime, the full form of the phonon distribution function may be expressed as [1.9-1.10]

$$N_{\vec{q}(\vec{Q})} = \sum_{n=0}^{\infty} \exp\left[-\frac{(n+1)\hbar\omega_{\vec{q}(\vec{Q})}}{k_B T_L}\right] \ll 1$$

Though the phonon population at low temperatures is indeed limited, putting $N_{q(Q)} \approx 0$ seems to be an oversimplification.

(ii) Inelasticity of the electron-phonon interaction as the phonon energy becomes comparable with the average thermal energy of the electrons. Under the condition when T_L is high, the analyses neglect the phonon energy (ε_{ph}) compared to the electron energy (ε_k). Hence, the electron-phonon collisions are treated to be elastic. The ratio $\frac{\varepsilon_{ph}}{\varepsilon_k}$ is of the order of $\frac{2u_l}{v_{th}}$; v_{th} being the velocity of the electron which is in thermodynamic equilibrium with the lattice. At higher temperatures, the ratio being very small, the phonon energy is indeed only a negligible fraction of the carrier energy. But with the lowering of T_L, the ratio increases, eventually making the phonon energy comparable with the electron energy. Hence, at low temperatures, the assumption that the electron-phonon collisions are elastic, can no longer be made. However the interaction of the electron – phonon system is assumed to be elastic even at low temperatures to overcome the mathematical difficulties in solving a problem. But such study will indeed incur some errors in the results [1.1-1.3,1.9,1.11].

(iii) The carrier ensemble may be non-degenerate or degenerate. But, one of the important low temperature features is the degeneracy of the carrier ensemble. At low temperatures, if the Fermi energy ε_F is not much lower than $k_B T_L$ of the conduction band edge and the electron densities are beyond the insulator to metal transitions, the free electron ensemble in the semiconductor is to be treated as degenerate. With the increase of doping level, as the electron concentration of an n-type material exceeds the effective density of states, the Fermi level moves into the conduction band and the material seems to exhibit

degeneracy. The critical concentration of the donor N_D required for the onset of degeneracy, may roughly be calculate from [1.1,1.3,1.12]

$$\varepsilon_F = \frac{\hbar^2}{2m^*}\left(3\pi^2 N_D\right)^{\frac{2}{3}} > E_d$$

where, m^* is the effective mass of an electron and E_d is the donor ionization energy. The degree of degeneracy is generally expressed in terms of $\frac{\varepsilon_F}{k_B T_L}$.

(iv) At low temperatures, the carrier ensemble being degenerate, the distribution function for the electrons should be expressed in terms of Fermi-Dirac (F.D.) distribution rather than simple Maxwellian function, which is used when the carrier ensemble is assumed to be non-degenerate.

(v) Electrical non-linearity may set in due to significant perturbation of the electron ensemble from the state of thermodynamic equilibrium for a fraction of few volts or less at low temperatures. This will lead the electrons to be hot. Hot electron transport has become an important phenomenon for the understanding of all the modern semiconductor devices. Such devices are categorized into two groups – the ballistic devices and the quasi thermal devices, depending on the type of a hot electron ensemble essentially employed in their operation.

(vi) The scattering potential due to lattice imperfections may be significantly screened, particularly in microstructures. In the absence of any potential, one may assume that the free electrons are uniformly distributed in a sample. But the electrons either collect or are removed from the region where any potential discontinuity occurs depending upon the sign of the discontinuity. This resulting space charge causes an extra potential and modifies the prevalent one thereby effectively screens its effects at large distances. This behavior of an electron ensemble describes the electrostatic screening of the electron-electron, electron-lattice and electron-impurity interactions in the material. As a result, the transition probability of an electron from any state is finite for interactions with ionized impurities and piezoelectric phonons. A non-degenerate ensemble of electrons yields an inverse of screening length $\beta_s = \left[\frac{4\pi e^2 n_0}{K k_B T_L}\right]^{1/2}$, where n_0 is the free electron concentration and K is the dielectric constant of the material

[1.13,1.14]. Evidently the effect of screening is felt more and more with the lowering of the lattice temperature and for higher concentrations. As the sizes of the electronic devices have become smaller and the carrier densities become larger, the role of screening has become of much importance within the devices. In addition, screening is important in many cases like in heavily doped materials when the carrier concentration becomes high or when impurity breakdown takes place at low temperatures due to impact ionization giving rise to a sharp increase in the concentration at a field of only a few volt/cm. Thus one can hardly neglect the effect of screening when studying the electron transport in semiconducting materials at low temperatures.

The physics of lower dimensional systems is more complex compared to that of bulk materials. For example, the inverse of the screening length calculated for the systems of 2DEG (two dimensional electron gas) in the semiconductor surface assumes a complex form [1.13,1.14]

$$\alpha = \left(\frac{e^2 N_i}{2K}\right)\left[k_B T_L (1 + e^{-y}) \ln(1 + e^{y})\right]^{-1}$$

where $y = (\varepsilon_F - \varepsilon_0)/k_B T_L$, N_i is the surface carrier density, ε_F is the Fermi energy, ε_0 is the energy of the lowest subband. Obviously, the screening factor may be neglected for moderate carrier concentration and if the lattice temperature is not too low. Since the analyses here have been carried out at low temperatures, the screening of the perturbing potential must significantly come into play.

(vii) Magnetic quantization of the energy bands.

(viii) Transition from 1s → 2p of the neutral impurity atoms.

(ix) Mobility becomes field dependent and non linearity comes into play.

(x) Concentration becomes field dependent. But for such study, knowledge of recombination and generation kinetics are required.

It is apparently a formidable task to solve each part of the problem analytically at a time. As such, there remains ample scope of work with physically realistic approximations without compromising the validity of the model. In theoretical research,

whenever one wants to develop a mathematical formulation for the physically realistic systems, some assumptions may have to be made very often so that the mathematical problem becomes amenable to solution. These assumptions need to be physically realistic so that the results that follow from the subsequent investigation can describe the characteristics of the real system under the prevalent condition. In the present thesis, to carry out the theoretical investigations on different semiconductor structures, we too have made some basic assumptions which identify the structure and the prevalent physical conditions.

1.3. Different semiconductor structure

Since a long time, the bulk semiconductors have been used for device applications. However, there have been remarkable developments and inventions in the field of low dimensional semiconductor structures during the last few decades. Due to the advancement of new techniques like Molecular Beam Epitaxy (MBE), Czochralski method, Bridgman-Stockbarger technique etc, it has become possible to control the growth of the materials as per our desired dimension. One can precisely control the compositions of modern semiconductor heterostructures in the atomic scale to develop low dimensional systems that have revolutionized the physics of semiconductor device and their impact on modern information technology [1.1,1.4,1.5]. The importance of the microstructures lies on the fact that, it is possible to segregate impurities from the carrier ensemble, unlike the bulk semiconductors. Thus, a large carrier concentration may be realized without any associated reduction in the mobility. Whereas, in the bulk materials, the carrier concentration may be increased by increasing the concentration of the impurity, which in turn cause a decrease in the carrier mobility. Advancement of semiconductor technology makes it possible to realized quantum confined structures that offer higher mobility, higher concentration, higher transconductance etc. and hence improved performance of the devices in comparison to the bulk ones. Such properties have been realized in a number of devices like narrow channel FET of Si or heterojunctions made of GaAs and GaAlAs that are used in High Electron Mobility Transistor (HEMT), Modulation Doped FET (MODFET), Selectively Doped FET (SDFET) etc. Emergence of these devices has been possible for deeper understanding of carrier transport in the semiconductor microstructures.

In the low dimensional structures, the free electrons lose one or more degrees of freedom when subjected to some potential barriers thereby making them confined along certain directions. Degree of such confinement may be described on comparing the sizes L_x, L_y and L_z along X, Y and Z axes respectively with the electron wavelength (λ). Different structures may be categorized as [1.15,1.16]

(i) If $\lambda << L_x, L_y, L_z$: One gets a bulk structure. The electrons are free to move along all the three dimensions and the system is termed as three dimensional electron gas (3DEG).

(ii) If $\lambda \cong L_Z << L_x, L_y$: One gets a quantum well structure. The quantization of the electron motion is now along Z- axis. However, they freely move along X and Y axes. Hence, the motion of the electrons are now confined on the X-Y plane and the electrons have lost one degree of freedom. The electron ensemble is now two dimensional and termed as two dimensional electron gas (2DEG).

(iii) If $\lambda \cong L_Z \cong L_y \ll L_x$: One gets a quantum wire structure. The quantization of electron motion takes place along Y and Z axes. Along X axis, the electrons move as free particles. Thus electrons have lost two degrees of freedom and one gets a one dimensional electron gas (1DEG).

(iv) If $\lambda \cong L_Z \cong L_y \cong L_x$: One gets a quantum dot structure. The quantization of the electrons takes place along all the three axes. The electrons having lost three degrees of freedom, the ensemble is now zero dimensional electrons gas (0DEG).

In the first few chapters, different transport properties in bulk semiconductor structure have been extensively analysed under different prevalent conditions.

Minimisation of the electronic devices is acceptable which leads to better performance. When the anticipated quantum confinement of the free electrons in semiconductor microstructures was first observed, there has been phenomenal growth of interest in the study of such structures for the last three decades or so. Subsequently, this has opened up the world of useful Low –Dimensional Structures and mesoscopic devices.

The almost insatiable demands for the growth of memory and computational capabilities and the race for increasing the processing and transmission speeds of signals, have stimulated the research studies in these areas since the advent of metal-oxide-semiconductor-field effect transistors (MOSFET) with easily controllable surface characteristics. In general, the practical realization of the mesoscopic devices and making them economically viable, have become possible because of mastering a knowledge of the physics of the constituent structures, the device is made of.

Extensive experimental and theoretical studies in the field of electronic transport in semiconductor quantum well structures have been carried out over the last few decades, since the significantly higher mobility of the free carriers could be observed in such structures. Much of these studies have been carried out at quite low temperatures. This is because the enhancement of the mobility values due to reduction of the effect of the impurities is prominent at low temperatures. The quality of the samples can be assessed from such studies. But the studies at higher temperatures are usually relevant to the performance of the devices [1.17,1.18]. As a result of these studies, there have been lots of advancement in the Solid State devices and experimental methods producing more and more accurate results. Without going for an elaborate review of the studies, a brief account of it may be made here. Since it is now possible to get a Si-SiO_2 interface with a high degree of perfection, the bipolar devices are now being replaced by the field effect devices, for many applications. The Metal-Oxide-Semiconductor (MOS) structures having similar interfaces are now widely used in digital integrated circuits. The free carriers in the conducting channel of those structures are not provided by the usual method of doping, but by the process of inversion and depletion of the surface layer. A typical concentration of about $10^{16}/m^2$ in the surface layer of SiO_2 gives rise to a rather strong surface electric field Es 10^7 V/m. Such a strong field effectively quantifies the motion of the carriers in a direction perpendicular to the interface. But the electrons move freely on the interfacial surface. This is thus one of the structures that exhibit a quasi two dimensional ensemble of electron gas (Q2D). The study of an ensemble of Q2D has become important since the advent of the metal-oxide-semiconductor field effect transistor (MOSFET) with easily controllable surface characteristics. Still much work of potential interest remains to be done. Yu et al. [1.19] have studied electron–acoustic phonon scattering in a GaAs quantum wire. Their results demonstrate that a proper treatment of confined acoustic phonons may be essential to correctly model electron scattering rates at low energies in low–dimensional structures. From the Hall-effect

measurements of electron mobility in anti modulation–doped GaAs/AlGaAs quantum wells, made by Masselink [1.20] it is observed that the ionised-impurity scattering of the Q2D immersed in the identical concentration of impurities is greater than that of a bulk electron gas of the same density. Balkan et al. [1.21] reported their results of the hot electron energy and momentum relaxation experiments obtained from high–- field parallel transport measurements in GaAs quantum wells. Their observations suggest that the hot phonon drift in modulation doped quantum wells is negligible. Redwing et al. [1.22] made some measurements on high quality AlGaN/ GaNheterostructures grown on SiC. They obtained low temperature mobility of Q2D as high as 7500 cm2 /V s. Moreover, the sample is reported to have exhibited strong Subnikov–de Hass oscillations (SdH) and well-defined plateaus in the quantum Hall resistance as a function of magnetic field. A theoretical investigation of the electrical characteristics of GaN/AlGaN modulation doped field effect transistor has been carried out by Stengel et al [1.23]. A relationship between the gate bias and the Q2D concentration has been obtained for a flat quasi Fermi level in AlGaN. A model for the drain current and the transconductance of the device has been developed. Their theoretical results have shown striking agreement with the experimental observations. The Q2D concentration has been found to be as high as $10^{13}/cm^2$, and transconductance as high as 1000 mS/mm. Nakajima et al. [1.24] obtained conductance–gate voltage characteristics for a Si quantum wire, which they fabricated using the separation by implanted oxygen (SIMOX) technique. The step-like characteristics thus obtained indicate the occurrence of a strong one-dimensional transport effect in the physically confined Si system with a SiO_2 barrier. The correlation between inversion layer mobility of MOSFETs and surface micro-roughness of the channel has been studied by Yamanaka et al [1.25]. The mobility at high normal field has been found to decrease with increasing the surface roughness over a wide range of roughness. The trend has been found to be the same even for very thin gate oxides. It has been shown that the gate oxide thickness does not affect the surface roughness, and this supports the independence of mobility on the gate oxide thickness. Subsequently, a quantitative analysis of the Si-SiO_2 interface roughness based on atomic force microscopy (AFM) and mobility measurement has been presented by Pirovano et al [1.26]. The results which they obtained make questionable the validity of the correlations between AFM measurements and carrier mobility as reported by Yamanaka et al [1.25]. Based on the numerical model of the roughness scattering, they have proposed a new, physically based correlation, highlighting the impact of the roughness correlation length

on the carrier mobility. Of late, nitride structures are being used for many optoelectronic and high power devices. In spite of the large value of the effective mass of the electrons in GaN, a quite high value of the electron mobility is shown for quantum wells of AlGaN/GaN. Obviously, studies on quantum wells of nitrides have gained much momentum. A theory of dislocation scattering in semiconductor heterostructure Q2D has been developed Jena [1.27]. Their theory could explain the observed low temperature mobility enhancement in the AlGaN/GaN High Electron Mobility Transistor (HEMT) upon reduction of dislocation density. The strong screening effect by carriers in a Q2D which helps to achieve much higher mobilities is highlighted. The Q2D electron scattering mechanisms in AlGaN/GaNheterostructures have been analysed by Gurusinghe et al [1.28]. A new analytical model to calculate the time constant for dislocation like scattering as a function of temperature has been developed. Their Hall effect measurement data for different heterostructures have been in good agreement with the data obtained from their theory. One of the present authors, along with others, made the same theoretical analysis in the field of electronic transport in quantum wells of Si and some compound semiconductors, taking due account of some of the low temperature features, which are usually neglected in the studies under the condition of high temperature. Their studies include the problems of (i) the interaction of the electrons with deformation potential and piezoelectric phonons, (ii) energy loss to intravalley acoustic modes, (iii) ohmic and non-ohmic mobility characteristics, etc. The results which they obtained have been found to be interesting and significantly different from what can be obtained under the condition of high temperature, and inspire further studies in the field [1.29-1.37]. Notwithstanding such advancement, even now there remains ample scope for work of potential interest in the field.

It is well known that the transport characteristics of the Q2D in the channel of MOS are controlled by one or more such interactions of the electrons, like the interaction with the acoustic mode lattice vibrations, and with the charged impurities near the oxide-semiconductor interface. However, the interaction with the intravalley acoustic phonons is intrinsic in nature and turns up as the most important mechanism in interpreting the available experimental results on the surface mobility characteristics at relatively higher lattice temperatures [1.38]. Although the surface-impurity scattering may seem to dominate under the condition of low surface electric fields, it is well known that this interaction mechanism can hardly explain the details of the field-effect mobility characteristics when the surface electric field is high [1.38,1.39]. Moreover, the carriers

in high purity materials interact dominantly with the intravalley acoustic phonons, over a range of low lattice temperatures [1.39]. Hence, the problem of electrical transport at the low lattice temperatures turns out to be important [1.40–1.42]. Useful experimental results of the electrical transport in Q2D at the lower lattice temperatures are also available. SdH has been observed in the quantum well of GaAs–GaxAl1-xAs heterostructures around 4.2 K [1.41]. Interesting results on the mobility characteristics of the electrons in the n-type inversion layer of Si for different crystallographic orientations at temperatures around 77 K are also reported in the literature [1.43]. Wu and Thomas made theoretical analysis of the surface mobility characteristics of the thermally oxidised Silicon surface layer for the two-dimensional electron-lattice scattering at high surface electric fields, under the conditions of both high and low lattice temperatures [1.39]. The analysis is based on a number of simplified approximations. Some of them include (i) even though the lattice wave is three dimensional, it is assumed that the two dimensional electrons interact only with the two dimensional phonons, and so, takes into account only the components of the electron and phonon wave vectors $\vec{k}$ and $\vec{q}$ which are parallel to the interface. Thus, the effects of the transverse component of the phonon wave vector has been neglected, (ii) at sufficiently low temperatures, it has also been assumed that the phonons that can be excited are quite limited; hence, the phonon population nq has been taken to be effectively zero. Hence, the agreement of their theoretical results with the experimental values has been hardly satisfactory. Some efforts have already been made by many, including some of the present authors [1.33–1.36] to take into account the effects of the transverse component of the phonon wave vector in the light of Ridley's momentum conservation approximations (MCA) [1.44]. But the framework of MCA of Ridley has been developed only for an infinite rectangular quantum well. Whereas, on the surface channel of the MOS structure, which has been considered by Wu and Thomas [1.39] the well is actually represented by an infinite triangular potential well. Lee and Vassel [1.45] have made a refinement of Ridley's analysis of MCA, for such a well, and obtained phonon limited mobility in semiconductor heterostructures under the condition, when the lattice temperature is high.

1.4. Scattering Mechanisms

The wave function of an electron in a perfectly crystalline material is given by the stationary Bloch function. When subjected to an electric field, the drift velocity of the

electron should increase indefinitely with time. But in a real crystal, the average drift velocity gets limited by the collisions, the electron may suffer with various lattice imperfections. These imperfections, whenever they occur, produce a perturbation in the periodic potential of the perfect crystal. The electron is said to be scattered whenever it interacts with any such perturbing potential and changes its wave vector and, or the energy states [1.46].

The dynamic imperfection is intrinsic and is produced by the thermal vibration of the lattice atoms about their equilibrium positions. On the other hand, the static imperfections arise due to the crystal defects or impurity atoms, introduced at the time of crystal growth.

If the imperfections are not much frequent and the perturbing potential due to it be small, the effects of such potential may be worked out in the framework of the time dependent perturbation theory [1.1].

All the scattering mechanisms of bulk materials are also effective in quantised surface layers. In addition to these, a few more mechanisms may come into play due to the multilayer structure of the later [1.4,1.5,1.47].

In a quantised surface layer, the momentum of the electron is quantised in the direction perpendicular to the well interface. When an electron interacts with the lattice or the impurity atom, the component of the lattice wave vector or of the Fourier wave number for the impurity potentials is not altered in the direction of quantisation. The density of states is also different for the 2DEG. All these would cause distinct changes in the characteristics of the bulk scattering mechanisms too [1.18,1.47].

1.5. Classification of Scattering

On interacting with any imperfection an electron can make a transition to a state that belongs to either the same or a different valley. As such, the transitions may be classified either as intravalley or as intervalley respectively. In case of holes, the respective transitions are called either intraband or interband. The most important sources of scattering that may cause electronic transitions include [1.1,1.3,1.15,1.16,1.18]

(a) Lattice vibrations

(b) Defects

(c) Other carriers

(d) Interface roughness

The interaction of the free charge carriers with the lattice vibrations takes place through phonons which are produced as a result of deformation of an otherwise perfect crystal. Such an interaction, typical of covalent semiconductors, is called deformation potential interaction, involving both acoustic and non-polar optical phonons. In polar materials having no inversion symmetry, however, the electrostatic potentials produced by the polarization waves due to lattice vibrations may also result in an interaction, which is either the piezoelectric interaction involving the acoustic phonons or the polar interaction that involves the optical phonons.

The lattice scattering for which the final and initial states of the electron are in the same valley in the $\varepsilon - \vec{k}$ space is called intravalley scattering. In some materials with the lowest minima in the <100> or <111> directions the lattice scattering may transfer an electron from one valley to another valley having its energy minima at the same level. Such scattering is termed as intervalley scattering.

In semiconductors, defects can arise owing to various types of dislocation in crystals and to impurity atoms. The impurity atoms may be either ionized or neutral or they may give rise to dipoles, depending upon the lattice temperature, the concentration of the impurity atoms and the compensation ratio [1.1,1.15,1.47]. In semiconducting alloys, the defects may also arise due to random distribution of the constituent atoms among the available lattice sites.

When the concentration of the free electrons in semiconductor is high enough, the effects of an electron changing states by collision with another free electron through their Coulomb field, may become important. Such collisions called inter-electronic or carrier-carrier collisions, become important on increasing the electron concentration. The effects of this collision may be neglected compared to the effects produced by other scattering mechanisms for concentrations of the order of 10^{13}-10^{14} cm^{-3}. Carrier-carrier scattering acting alone cannot restore a perturbed distribution of the carrier ensemble to its normal

equilibrium condition. Actually there would be a mixture of energy and momentum of electrons and that would lead to a modification of the distribution function.

In many cases, the interfaces in a semiconductor structure, like that which occurs between Si and SiO_2 in a FET or between GaAs and AlGaAs in a HEMT are not perfectly smooth. This is another type of imperfection which may constitute a major cause for scattering and is called surface roughness scattering. It is known to be effective especially at high concentration of the carriers and for low temperatures [1.39].

A schematic diagram of different scattering mechanisms is shown below.

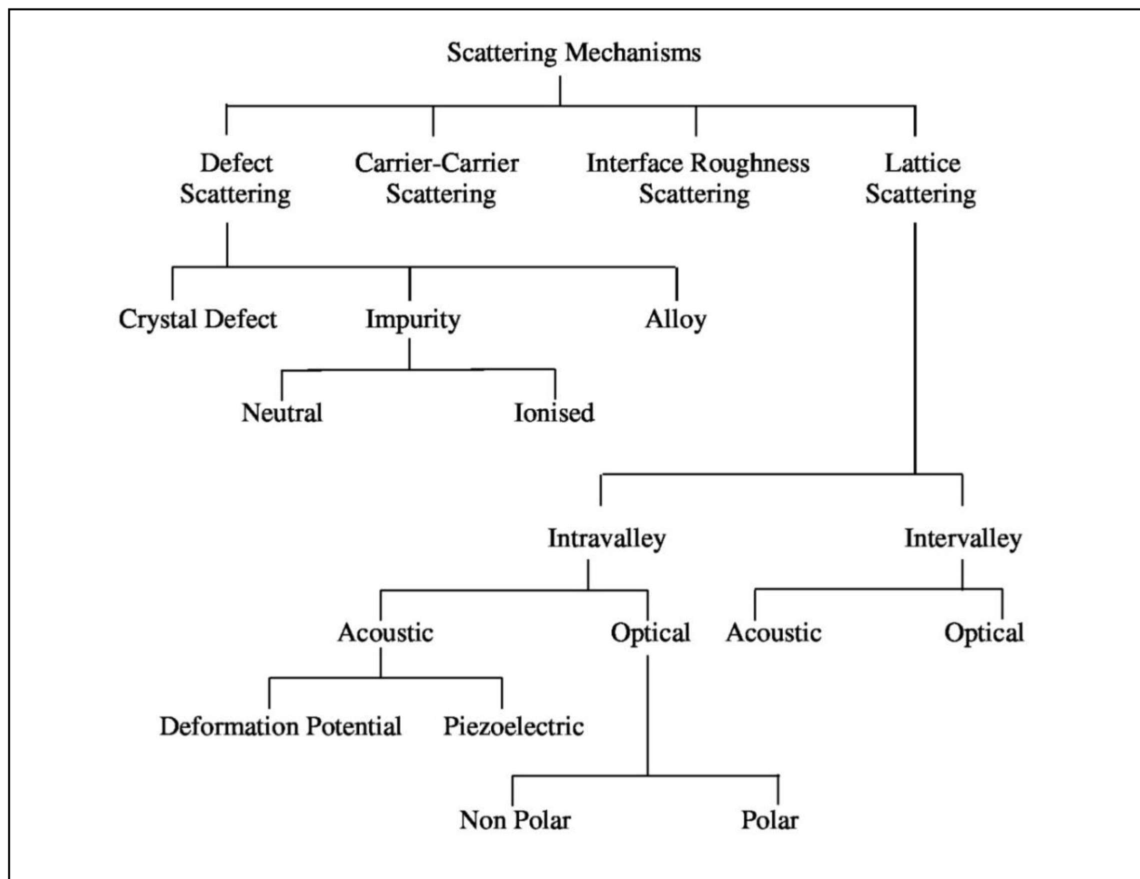

1.6. Relative importance of different scattering mechanisms

All the scattering mechanisms as described in the previous section are not always equally important. The electronic transport characteristics of any semiconductor structure are determined by the scattering mechanisms which seem to be dominant under the prevalent experimental conditions in respect of the lattice temperature, impurity or carrier concentration etc.

The impurity atoms occupy the lattice sites as substitutional atoms and cause a perturbation in the periodic crystal potential. At very low temperatures, near 4K, these atoms remain neutral. Therefore, the neutral impurity scattering of the electrons may dominate when the lattice temperature is very low. For the high purity semiconductors, the impurity scattering can hardly play any significant role even at low temperatures. With the increase of the lattice temperature, the impurity atoms are more and more ionized and the interaction with ionized impurity atoms tends to be important. The ionized impurity scattering is significant when the carrier concentration is high enough and the lattice temperature is not very low [1.2]. Moreover, due to non-uniform distribution of the impurities in the 2DEG systems, the remote impurity scattering plays an important role in addition to local impurity scattering [1.18,1.48]. The field produced by an impurity atom may be assumed to be time independent and the collisions between the electrons and the impurity atoms are essentially interaction with fixed force fields. This type of collision, being elastic in nature, cannot alone limit the drift velocity of the carriers in the presence of an external electric field. As such it must be supplemented by some other scattering mechanisms which would be responsible for the dissipation of the electron energy and thus would limit the drift velocity.

Apart from these, some structural defects may be introduced during the crystal growth. They include edge dislocations and screw dislocations etc. The carriers may be scattered at these sites when charges collect there. The dislocation scattering prevails at low lattice temperature and the mobility value is affected strongly by high density of the dislocation [1.49-1.57]. However, if the crystal is properly grown, the effects of such dislocations can be neglected.

In alloys of two semiconducting compounds the dissimilarities of the constituent compounds lead to distortions in the band structure at the points where they meet. These boundaries are randomly positioned and act as individual scattering centres similar to an

impurity atom. But the scattering being due to discontinuities in the band edges, the mechanism is similar to that for deformation potential acoustic scattering. For $In_{0.53}Ga_{0.47}As$, the alloy scattering is more dominant than impurity and surface roughness scattering at low lattice temperature [1.58].

The scattering due to lattice imperfections that are produced by crystal defects or impurity atoms may be controlled through improved techniques of crystal preparation. However, the phonon scattering of the free carriers in any material, due to interaction with lattice vibrations, is intrinsic in nature and cannot be controlled like the former mechanisms.

The deformation potential scattering becomes important for relatively higher temperatures. But in high purity samples, if the carrier concentration is not high enough the deformation potential scattering may also dominate at $T_L < 20$ K [1.3,1.18,1.59-1.62].

The piezoelectric scattering of the carriers is important in all compound semiconductors, particularly at low temperatures. It is, however, stronger in materials with wurtzite structure than in the materials with sphalerite structure due to the lower symmetry of the former. It may be mentioned here that due to strong piezoelectric interaction in compounds like CdS, ZnO etc. they are usually the chosen materials for acoustoelectric devices [1.18,1.63-1.65].

The optic strain due to lattice vibrations produces a perturbing potential with which the carriers may interact depending upon the symmetry of the band structure. This interaction is rather weak for electrons at the Γ- point minima or for the <100> minima. Since in most of the compound semiconductors the lowest minimum is at the Γ - point, this kind of scattering is of little importance there. The aluminium and gallium and lead compounds are exceptions where the non-polar optic scattering may be important. The dipole moment resulting from the displacement of the neighbouring atoms with the opposite ionic charges gives rise to perturbing potential with which the carriers may also interact. Such scattering, termed as polar optic phonon scattering, is often the most important scattering mechanism, particularly at liquid-nitrogen or higher temperatures [1.2,1.18].

The electrical transport in semiconductor structures is determined by the dominant interactions which the free carriers may have with various static and dynamic lattice

defects in the materials. The free carriers interact with optical and intervalley phonons at the lattice temperatures above some 100K and with impurities at lower temperatures. Between these two extreme situations a range of lattice temperature exists where the free carriers in a high purity covalent semiconductor interact dominantly only with intravalley acoustic phonons through the deformation potential and in compound semiconductors having no inversion symmetry they interact dominantly with both the deformation and the piezoelectric acoustic phonons [1.2,1.3,1.17,1.18,1.63,1.66-1.71].

Here in the present Thesis, the various transport properties are studied considering mainly the interaction of the electrons with the deformation acoustic and the piezoelectric phonons under different prevalent conditions.

1.7. Scope of the Thesis

In the present thesis the theories have been developed on some aspects of the electronic transport in the bulk as well as in the quantum confined, two-dimensional structures, under the condition when the lattice temperature is low. The chapter-wise orientation is as follows:

Chapter II:

The high-field distribution function of the carriers given by Fermi-Dirac (F.D.) function at the field dependent carrier temperature, has been approximated here by a well tested model that apparently overcomes the intrinsic problem of correct evaluation of the integrals involving the product and powers of the Fermi function. The results thus obtained are more reliable compared to the rough estimation that one may obtain from the exact F.D. function, but taking recourse to some over simplified approximations. The comparison of the model F.D. function and the exact form of the same has been made.

Chapter III:

The purpose here is to solve the energy balance equation for the electron–phonon system for the combined interaction of the electrons with the deformation potential and piezoelectric phonons and thus to obtain the electric field dependence of the effective electron temperature in non degenerate semiconductors. Next, the high field mobility characteristics are obtained for the same combination of interactions. Because the energy loss rate due to acoustic interaction is already known, the same is calculated for the piezoelectric interaction to get the total energy loss rate for the combined interaction. Numerical results are obtained for Insb, InAs and GaN. The results are analyzed in detail and compared with other available data. The results clearly exhibit the importance of the piezoelectric scattering in controlling the non-ohmic transport characteristics in the presence of relatively high fields under the condition of low lattice temperature.

Chapter IV:

The energy balance equation for the electron–phonon system is recast taking the degeneracy of the carrier ensemble into account. The effect of degeneracy on the field dependence of the temperature of the non-equilibrium carriers has been studied by solving the same equation. The high field distribution function of the carriers is assumed to be given by the Fermi Dirac function at the field dependent carrier temperature. The proposed F.D. distribution function has been used here that facilitates analytical solution of the problem without any serious loss of accuracy. The field dependence of the electron temperature thus obtained seems to be significantly different from what follows had the degeneracy not been taken into account. The agreement of the results obtained from the present analysis with the available experimental data for Ge and InSb are quite satisfactory. Low temperature features like the inelasticity of the electron-phonon collision and the true phonon distribution instead of the equipartition law have duly been considered here.

In the next section, the analysis of the field dependence of electron temperature in some degenerate III-V compounds, as controlled by the combined interaction with the acoustic and piezoelectric phonons has been made in the same framework as above. The numerical results obtained for InSb, InAs and GaN are compared with other theoretical

and available experimental data. The results reveal the importance of the piezoelectric interaction in controlling the characteristics of the effective electron temperature in degenerate materials, under the conditions of low lattice temperature.

Chapter V:

The phonon growth characteristic in a degenerate semiconductor due to the interaction of the electrons with the acoustic phonons has been calculated here under the condition of low temperature. If the lattice temperature is high, the energy of the intravalley acoustic phonon is negligibly small compared to the average thermal energy of the electrons. Hence one can traditionally assume the electron-phonon collisions to be elastic and approximate the Bose-Einstein (B.E.) distribution for the phonons by the simple equipartition law. However, in the analysis here at the low lattice temperatures, the interaction of the non equilibrium electrons with the acoustic phonons becomes inelastic and the simple equipartition law for the phonon distribution is not valid. Hence the analysis is made taking into account the inelastic collisions and the complete form of the B.E. distribution. The study has been carried out in the light of the model F.D. function, as described in Chapter II. The results thus obtained are more reliable compared to the rough estimation that one may obtain from using the exact F.D. function, but taking recourse to some over simplified approximations.

In the next section, the similar characteristics have been studied for the combined interactions of the electrons with the acoustic and the piezoelectric phonons. Compound semiconductors being piezoelectric in nature, the intrinsic thermal vibration of the lattice atoms at any temperature gives rise to an additional potential field that perturbs the periodic potential field of the atoms. This is over and above the intrinsic deformation acoustic potential field which is always produced in every material. The scattering of the electrons through the piezoelectric perturbing potential is important in all compound semiconductors, particularly at the low lattice temperatures. Thus, the electrical transport in such materials is principally controlled by the combined interaction of the electrons with the deformation potential acoustic and piezoelectric phonons at low lattice temperatures. The study here, deals with the problem of phonon growth characteristics, considering the combined scattering of the non-equilibrium electrons in compound semiconductors, at low lattice temperatures. Beside degeneracy, other low temperature

features, like the inelasticity of the electron–phonon collisions, and the full form of the phonon distribution have been duly considered. The analysis once again is carried out by making use of the model F.D. function as proposed earlier.

Chapter VI:

The rate of loss of energy of the non-equilibrium electrons to the acoustic mode lattice vibration in a degenerate semiconductor is obtained under the condition, when the lattice temperature is low enough, so that the traditional approximations like the elastic nature of the electron-phonon collisions and the truncation of the phonon distribution to the equipartition law are not valid any more. Using the results of the energy loss rate, the non-ohmic mobility is then calculated. Evaluating the loss rate and the non-ohmic mobility in degenerate samples of Si and Ge, significant changes in both the characteristics have been effected compared to that in the non-degenerate samples, in the regime of lower energy and for relatively lower fields. The effected changes are found to be more significant, the lower the lattice temperature is.

The same analysis has been made in the next section to study the effect of degeneracy on the average energy loss rate of the non-equilibrium electrons and the non-ohmic mobility characteristics in a semiconductor under similar prevalent conditions, giving due regard to the proposed model of the F.D. function. Because of the intrinsic complexity of the Fermi function, it is hardly possible to analytically integrate when product and powers of the same are involved. Hence the analysis has been made here in the framework of a simplified, well tested model distribution, in place of the heated Fermi – Dirac distribution. The model paves the way for correct evaluation of the integrals without making any oversimplified approximations. The numerical results for Si and InSb have been obtained from the present analysis and seem to be significantly different when compared with the results which have been reported earlier, for the non-degenerate samples of the same materials. The validity of the proposed model for the F.D. function is once again established here.

Chapter VII:

The field-effect mobility characteristics of a non-degenerate ensemble of a two dimensional electron gas for interaction with acoustic mode lattice vibrations in the Si-SiO_2 MOS structure at the high surface electric fields are calculated here for the low and high temperature cases. The calculation takes due account of some features which are usually neglected. These include the effects of (i) the transverse component of the phonon wave vector, (ii) the realistic model of the infinite triangular potential well along the transverse direction, while applying the momentum conservation approximation, and (iii) the full form of the phonon distribution function at low temperatures. The results seem to be interesting in that they are significantly different from what follows from other theories that neglect the effects of the above features. Moreover, the agreement between the results which are obtained here with the experimental data seems to be significantly better. The scope for further refinement of the present theory has been discussed.

References

[1.1] B.R.Nag, Theory of Electrical Transport in Semiconductors, Pergemon Press, Oxford,1972

[1.2] B.R.Nag, Electron Transport In Compound Semiconductors, Springer, Berlin, Heidelberg, New York, 1980

[1.3] E.M.Conwell, High Field Transport in Semiconductors, Academic Press, New York,1967

[1.4] C.Hamaguchi, Basic Semiconductor Physics, Springer, Berlin, Heidelberg, New York, 2010

[1.5] C.Jacoboni, Theory of Electron Transport in Semiconductors, Springer-Verlag Berlin Heidelberg, 2010

[1.6] Canali C., Jacoboni C, Nava F., Ottaviani G. and AlberigiQuaranta A., Phys. Rev. B 12, (1975) 2265

[1.7] S. Nag and D. P. Bhattacharya, Physica E 42, 1319 (2010)

[1.8] S.Nag, A.Basu, B.Das, T.R.Middya, D.P.Bhattacharya, Physica E ,Volume 72, August 2015, Pages 77-83

[1.9] A. Basu, B. Das, T.R. Middya, D.P. Bhattacharya ; Journal of Physics and Chemistry of Solids, Volume 100, January 2017, Pages 9–13

[1.10] A. Basu, T. R. Middya, and D. P. Bhattacharya, Journal of Applied Physics 122, 2017, 105703

[1.11] A. Basu, B. Das, T.R. Middya, D.P. Bhattacharya ; Physica B , Volume506, 1 February 2017, Pages 65–68

[1.12] S.Midday, S.Nag, D.P.Bhattacharya, Physica B 458 (2015) 18-21

[1.13] F. Stern and W. E. Howard, Phys. Rev. 163, 816 (1967)

[1.14] B. K. Ridley: Quantum Processes in Semiconductors, Clarendon Press, Oxford, 1993.

[1.15] C.Kittel, Elementary Statistical Physics ,John Wiley & Sons, Inc., New York, 1958

[1.16] S.M.Sze, Physics of Semiconductor Devices, Wiley Eastern Limited, New Delhi, 1983

[1.17] T. Ando, A. B. Fowler and F. Stern, Rev. Mod. Phys. 54, 437 (1982).

[1.18] B. R. Nag, Physics of Quantum Well devices, Kluwer Academic Publisher, Dordrecht, 2000

[1.19] S. G. Yu, K. W. Kim, M. A. Stroscio, G. J. Iafrate, and A. Ballato, Phys.Rev. B 50, 1733 (1994).

[1.20] W. T. Masselink, Phys. Rev. Lett. 66, 1513 (1991).

[1.21] N. Balkan, R. Gupta, M. E. Daniels, B. K. Ridley, and M. Emery, Semicond. Sci.Technol.5, 986 (1990).

[1.22] J. M. Redwing, M. A. Tischler, J. S. Flynn, S. Elhamri, R. S. Newrock, and W. C. Mitchel, Appl. Phys. Lett. 69, 963 (1996).

[1.23] F. Stengel, S. Noor Mohammad, and H. Morkoc, J. Appl. Phys. 80, 3031 (1996).

[1.24] Y. Nakajima, Y. Takahashi, S. Horiguchi, K. Iwadate, H. Namatsu, and M. Tabe, Appl. Phys. Lett. 65, 2833 (1994).

[1.25] T. Yamanaka, S. J. Fang, H. C. Lin, J. P. Snyder, and R. Helms, IEEE Electron Device Lett. 17, 178 (1996).

[1.26] A. Pirovano, A. L. Lacaita, G. Ghidini, and G. Tallarida, IEEE Electron Device Lett. 21, 34 (2000).

[1.27] D. Jena, A. C. Gossard, and K. K. Mishra, Appl. Phys. Lett. 76, 1707 (2000).

[1.28] M. N. Gurusinghe, S. K. Davidsson, and T. G. Anderson, Phys. Rev. B 72, 045316 (2005).

[1.29] S. S. Paul, A. K. Ghorai, and D. P. Bhattacharya, Phys. Rev. B 48, 18268 (1993).

[1.30] A. K. Ghorai and D. P. Bhattacharya, J. Appl. Phys. 80, 3130 (1996).

[1.31] A. K. Ghorai and D. P. Bhattacharya, Surf. Sci. 380, 293 (1997).

[1.32] S. Nag and D. P. Bhattacharya, Superlattices Microstruct. 50, 359 (2011).

[1.33] D. P. Bhattacharya, S. Midday, S. Nag, and A. Biswas, Physica E 47, 264 (2013).

[1.34] D. P. Bhattacharya, S. Midday, and S. Nag, Superlattices Microstruct. 72, 126 (2014).

[1.35] S. Nag, A. Basu, B. Das, T. R. Middya, and D. P. Bhattacharya, Physica E 72, 77 (2015).

[1.36] S. Nag and D. P. Bhattacharya, J. Phys. Chem. Solids 76, 59 (2015).

[1.37] S. Nag, B. Das, A. Basu, J. Das, D. P. Bhattacharya, and C. K. Sarker, Physica E 87, 237 (2017).

[1.38] F. F. Fang and A. B. Fowler, Phys. Rev. 169, 619 (1968).

[1.39] C.-Y. Wu and G. Thomas, Phys. Rev. B 9, 1724 (1974).

[1.40] C. Canali, C. Jacoboni, F. Nava, G. Octaviani, and A. Alberigi-Quaranta, Phys. Rev. B 12, 2265 (1975).

[1.41] H. L. St€ormer, R. Dingle, A. C. Gossard, W. Wiegmann, and M. D. Struge, Solid State Commun. 29, 705 (1979).

[1.42] H. L. St€ormer, L. N. Pfeiffer, K. W. Baldwin, and K. W. West, Phys. Rev. B 41, 1278 (1990).

[1.43] T. Sat^o,Y. Takeishi, H. Hara, andY. Okamoto, Phys. Rev. B 4, 1950 (1971).

[1.44] B. K. Ridley, J. Phys. C: Solid State Phys. 15, 5899 (1982).

[1.45] J. Lee and M. O. Vassel, Jpn. J. Appl. Phys., Part 1 23, 1086 (1984). [1.46] D.J.Griffiths, Instroduction to Quantum Mechanics, Prentice Hall, New Jersey, 07458

[1.47] John H. Davies, The Physics of Low-Dimensional Semiconductors: An Introduction, Cambridge University Press, 1998

[1.48] J. Lee, H. N. Spector and V. K. Arora, J. Appl. Phys. 54,6995 (1983).

[1.49] S. Gökden, A. Ilgaz, N. Balkan and S. Mazzucato, Physica E 25, 86 (2004).

[1.50] D. Zanato, S. Gökden, N. Balkan, B. K. Ridley, W. J. Schaff, Semicond. Sci. Technol. 19, 427 (2004)

[1.51] B. Tanatar and S-T. Chui, J. Phys.: Condens. Matter 6, L485 (1994).

[1.52] H. M. Ng, D. Doppalapudi, T. D. Moustakas, N. G. Weimann and L. F. Eastman, Appl. Phys. Lett. 73, 821 (1998).

[1.53] D. C. Look and J. R. Sizelove, Phys. Rev. Lett. 82, 1237 (1999).

[1.54] Debdeep Jena, A. C. Gossard and U. K. Mishra, Appl. Phys. Lett. 76, 1707 (2000).

[1.55] S. Gökden, Physica E 23, 19 (2004).

[1.56] J. Kundu, C. K. Sarkar and P. S. Mallick, Semicond. Phys. Quantum Electronics and Optoelectronics 10, 1 (2007).

[1.57] L. Reggiani, Hot Electron Transport in Semiconductors, Springer-Verlag, Berlin, 1985.

[1.58] P. K. Basu and B. R. Nag, Surf. Sci. 142, 256 (1984).

[1.59] S. S. Paul, A. K. Ghorai and D. P. Bhattacharya, Phys. Rev. B 51, 5445 (1995).

[1.60] A. K. Ghorai and D. P. Bhattacharya, J. Appl. Phys. 80, 3130 (1996).

[1.61] S. S. Paul, A. K. Ghorai and D. P. Bhattacharya, Phys. Rev. B 48, 18268 (1993).

[1.62] S. N. Patra and D. P. Bhattacharya, J. Phys. Chem. Solids 58, 829 (1997).

[1.63] P. K. Basu and B. R. Nag, J. Phys. C: Solid State Phys. 14, 1519 (1981).

[1.64] F. Comas, C. Trallero, H. Leon and J. Tutor, Physica B 152, 352 (1988).

[1.65] D. N. Quang, V. N. Tuoc and T. D. Huan, Phys. Rev. B 68, 195316 (2003).

[1.66] P. K. Basu and B. R. Nag, Phys. Rev. B 22, 4849 (1980).

[1.67] C. Jacoboni and L. Reggiani, Rev. Mod. Phys. 55, 645 (1983).

[1.68] H. L. Störmer, L. N. Pfeiffer, K. W. Baldwin and K. W. West, Phys. Rev. B 41, 1278 (1990).

[1.69] P. K. Basu and K. Bhattacharya, J. Phys. C: Solid State Phys. 15, 5711 (1982).

[1.70] W. Knap, E. Borovitskaya, M. S. Shur, L. Hsu, W. Walukiewicz, E.Frayssinet, P. Lorenzini, N. Grandjean, C. Skierbiszewski, P. Prystawko, M. Leszczynski and I. Grzegory, Appl. Phys. Lett. 80, 1228 (2002).

[1.71] D. Chattopadhyay, Phys. Stat. Sol. (b) 135, 409 (1986).

CHAPTER II

Fermi – Dirac Distribution Function : An Effective Alternative Model

The high-field distribution function of the carriers in a degenerate semiconductor is given by the Fermi-Dirac (F.D.) function at the field dependent carrier temperature T_e. The exact expression for the well known Fermi – Dirac distribution is given by

$$f_0(\varepsilon) = \frac{1}{1 + \exp\left(\frac{\varepsilon - \varepsilon_F}{k_B T_e}\right)}$$

Because of the complex nature of the Fermi function, the integrations involving the product and the powers of the function could hardly be carried out analytically without taking recourse to some over-simplified approximations. Sometimes, only the tail of the Fermi function, which is essentially the Maxwellian function is used for the analysis. Obviously, such an approximate analysis is not expected to yield much reliable results.

Such problem of analytical integration involving the Fermi function is frequently encountered in many theoretical analyses. To overcome this difficulty, an approximate model for the F.D. distribution function has been proposed [2.1]. The model is apparently quite simple and is more convenient. This is because of the fact that, using this model one can now analytically evaluate the integrals much easily, and that too without incurring significant errors in the subsequent results. To have a direct test of the validity of the proposed model, a comparison of the model with the exact F.D. distribution function is

made in Figure 2.1, considering a degenerate ensemble of electrons in equilibrium with the lattice i.e. putting $T_e = T_L$. The validity seems to be satisfactory. Moreover, the theoretical results which have been obtained earlier in the light of the model, on some high-field transport characteristics in degenerate samples of Ge and InSb at the low lattice temperature, have been found to be in good agreement with the experiments [2.1] and other theoretical results [2.1-2.3].

The energy domain is divided into three regions, demarcated on both the sides of the Fermi energy ε_F, and the Fermi function is approximated for each regime in the following manner:

Region 1: For the energy values $0 < \varepsilon \leq \beta_1 \varepsilon_F$, $\beta_1 \lesssim 1$

$$f_0(\varepsilon) = 1 + \sum_{m=1}^{\infty} (-1)^m e^{mx} \quad \text{where } x = \frac{\varepsilon - \varepsilon_F}{k_B T_e} < 0 \tag{2.1}$$

Region 3: For the energy values $\beta_2 \varepsilon_F \leq \varepsilon < \infty$, $\beta_2 \gtrsim 1$

$$f_0(\varepsilon) = \sum_{m=1}^{\infty} (-1)^{m+1} e^{-mx} \quad \text{where } x > 0 \tag{2.2}$$

Region 2: Transition Region (T): for energy values $\beta_1 \varepsilon_F \leq \varepsilon \leq \beta_2 \varepsilon_F$

Over this narrow transition region, in the light of Karlovsky's model of linear approximation [2.4], which has been used in order to obtain the V-I characteristics of a tunnel diode in a closed form, and the results thus obtained have been in good agreement with the experimental data, we assume

$$f_0(\varepsilon) = c\varepsilon + \gamma$$

where c and γ are the constants and are determined from the boundary conditions that $f_0(\varepsilon)$ at $\varepsilon = \beta_1 \varepsilon_F$ and $\beta_2 \varepsilon_F$ should be identical to the values that the exact F.D function assumes at those points, and at $\varepsilon = \varepsilon_F$, $f_0(\varepsilon) = \frac{1}{2}$. Thus one can obtain:

$$c = \frac{e^{(\beta_1 - 1)\varepsilon_F / k_B T_e} - e^{(\beta_2 - 1)\varepsilon_F / k_B T_e}}{[1 + e^{(\beta_2 - 1)\varepsilon_F / k_B T_e}][1 + e^{(\beta_1 - 1)\varepsilon_F / k_B T_e}]} \quad \text{and} \quad \gamma = \frac{1}{2} - c\varepsilon_F$$

Thus, $$f_0(\varepsilon) = \frac{1}{2} + c(\varepsilon - \varepsilon_F) \qquad (2.3)$$

While choosing the proper values of β_1 and β_2 ,it is to be kept in mind that at a finite temperature the F.D distribution around $\varepsilon = \varepsilon_F$ fuzzes out over a width of the order of a few $k_B T_e$ [2.5-2.6]. Hence one can assume that β_1 is less than unity by $nk_B T_L/\varepsilon_F$, where as β_2 exceeds unity by the same factor, where $n \cong 1$.

The proposed distribution has been obtained for m = 3, i.e. just taking only the first three terms in the expressions (2.1) and (2.2). The figure shows that the agreement of the proposed distribution with the actual F.D. function is quite satisfactory.

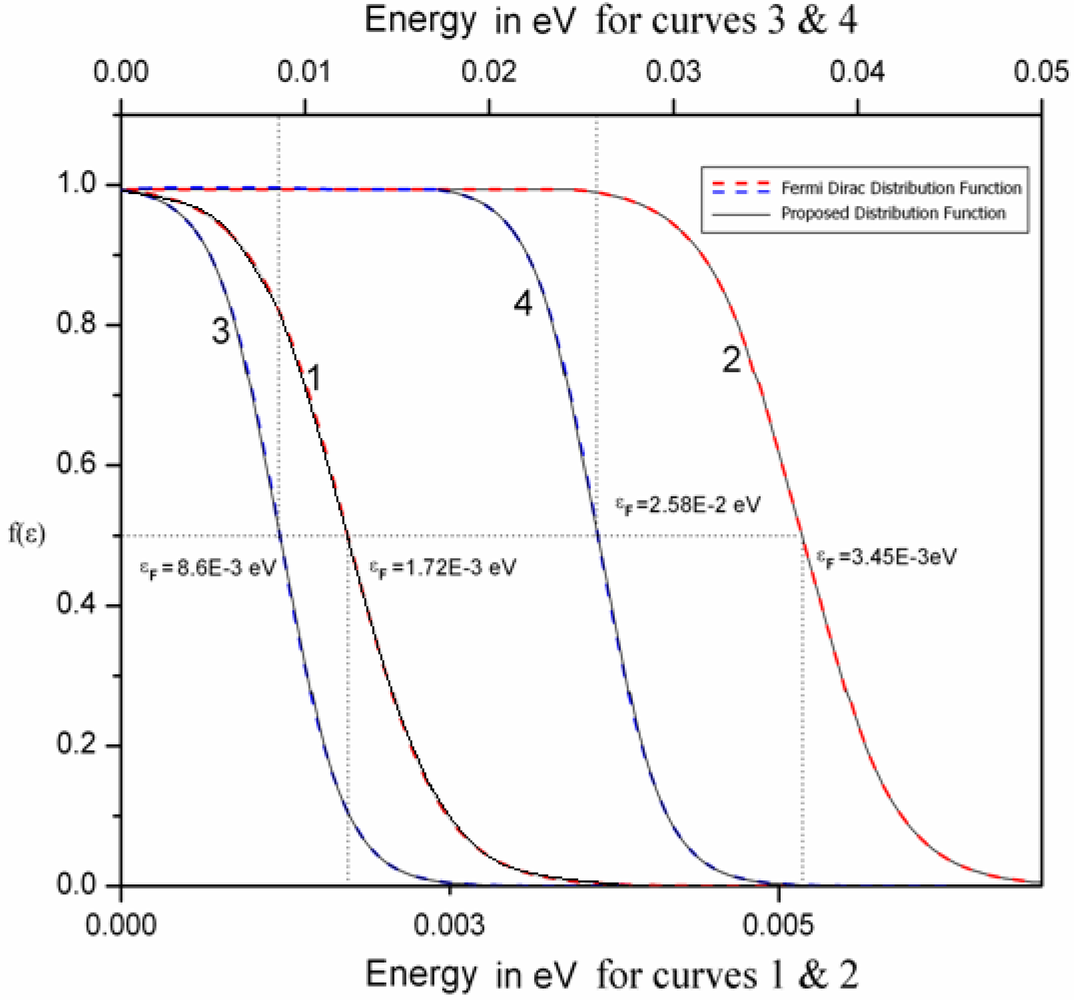

Fig. 2.1 : Comparison of Fermi-Dirac distribution function with the proposed distribution function that is calculated for just m = 3, for different values of the degeneracy parameter $\frac{\varepsilon_F}{k_B T_L}$ and lattice temperature T_L, considering an electron ensemble in the equilibrium with the lattice i.e. putting T_e=T_L . Curves 1 and 2 may be obtained respectively for $\frac{\varepsilon_F}{k_B T_L}$ = 5 and 15 and at T_L = 4K. Curves 3 and 4 are for $\frac{\varepsilon_F}{k_B T_L}$ = 5 and 15 at T_L= 20K.

To assess the extent of validity of the model distribution functions (2.1), (2.2) and (2.3) once again over their respective domain, the average energy $\langle\varepsilon\rangle$ is calculated using them by solving the following standard method

$$\langle\varepsilon\rangle = \frac{\int_0^\infty \varepsilon^{\frac{3}{2}} f_0(\varepsilon)d\varepsilon}{\int_0^\infty \varepsilon^{\frac{1}{2}} f_0(\varepsilon)d\varepsilon} \tag{2.4}$$

To carry out the integrations, the energy domain in both the numerator and the denominator of (2.4) is divided into three regimes, as has already been discussed, and the proposed model functions are accordingly used in the respective domain. Thus one obtains,

$$\langle\varepsilon\rangle = \frac{[\mathbf{I_{11}}]_{\mathbf{0}}^{\beta_1\varepsilon_F} + [\mathbf{I_{12}}]_{\beta_1\varepsilon_F}^{\beta_2\varepsilon_F} + [\mathbf{I_{13}}]_{\beta_2\varepsilon_F}^{\beta_2\varepsilon_F + nk_BT_e}}{[\mathbf{I_{21}}]_{\mathbf{0}}^{\beta_1\varepsilon_F} + [\mathbf{I_{22}}]_{\beta_1\varepsilon_F}^{\beta_2\varepsilon_F} + [\mathbf{I_{23}}]_{\beta_2\varepsilon_F}^{\beta_2\varepsilon_F + nk_BT_e}} \tag{2.5}$$

where,

$$[I_{11}]_0^{\beta_1\varepsilon_F} = \frac{2}{5}(\beta_1\eta k_BT_L)^{5/2} + \sum_{m=1}^{\infty}(-1)^m\left(\frac{3}{5}\beta_1\eta k_BT_L\right)^{3/2}\left(\frac{k_BT_e}{m}\right)\exp\left[m\eta(\beta_1 - 1)\frac{T_L}{T_e}\right]$$

$$[I_{12}]_{\beta_1\varepsilon_F}^{\beta_2\varepsilon_F} = \frac{2}{5}\left(\frac{1}{2} - c\eta k_BT_L\right)(\eta k_BT_L)^{\frac{5}{2}}\left(\beta_2^{\frac{5}{2}} - \beta_1^{\frac{5}{2}}\right) + \frac{2}{7}c(\eta k_BT_L)^{7/2}\left(\beta_2^{7/2} - \beta_1^{7/2}\right)$$

$$[I_{13}]_{\beta_2\varepsilon_F}^{\beta_2\varepsilon_F + nk_BT_e} = \sum_{m=1}^{\infty}(-1)^m H^{3/2}\left(\frac{k_BT_e}{m}\right)\exp\left(m\eta\frac{T_L}{T_e}\right)\left[\exp\left(-m\beta_2\eta\frac{T_L}{T_e}\right)\{\exp(-mn) - 1\}\right]$$

$$[I_{21}]_0^{\beta_1\varepsilon_F} = \frac{2}{3}(\beta_1\eta k_BT_L)^{3/2} + \sum_{m=1}^{\infty}(-1)^m\left(\frac{3}{5}\beta_1\eta k_BT_L\right)^{1/2}\left(\frac{k_BT_e}{m}\right)\exp\left[m\eta(\beta_1 - 1)\frac{T_L}{T_e}\right]$$

$$[I_{22}]_{\beta_1\varepsilon_F}^{\beta_2\varepsilon_F} = \frac{2}{3}\left(\frac{1}{2} - c\eta k_B T_L\right)(\eta k_B T_L)^{3/2}\left({\beta_2}^{3/2} - {\beta_1}^{3/2}\right) + \frac{2}{5}c(\eta k_B T_L)^{5/2}\left({\beta_2}^{5/2} - {\beta_1}^{5/2}\right)$$

$$[I_{23}]_{\beta_2\varepsilon_F}^{\beta_2\varepsilon_F+nk_BT_e} = \sum_{m=1}^{\infty}(-1)^m H^{1/2}\left(\frac{k_BT_e}{m}\right)\exp\left(m\eta\frac{T_L}{T_e}\right)\left[\exp\left(-m\beta_2\eta\frac{T_L}{T_e}\right)\{\exp(-mn) - 1\}\right]$$

and $H = \frac{3}{5}\frac{[(\beta_2\eta k_BT_L+nk_BT_e)^{5/2}-(\beta_2\eta k_BT_L)^{5/2}]}{[(\beta_2\eta k_BT_L+nk_BT_e)^{3/2}-(\beta_2\eta k_BT_L)^{3/2}]}$

On the other hand, $\langle\varepsilon\rangle_{F.D}$which is the well known in terms of the Fermi integrals $F_k(\eta)$ that follows from the exact F.D. distribution is given by [2.7]

$$\langle\varepsilon\rangle_{F.D} = k_BT_e\frac{F_{\frac{3}{2}}(\eta)}{F_{\frac{1}{2}}(\eta)} \tag{2.6}$$

where $\eta = \frac{\varepsilon_F}{k_BT_e}$ is the reduced Fermi energy in both the cases.

The average energy $\langle\varepsilon\rangle$ as given by (2.5) is now normalized with $\langle\varepsilon\rangle_{F.D}$ and plotted in figure 2.2 for two values of the parameter η.

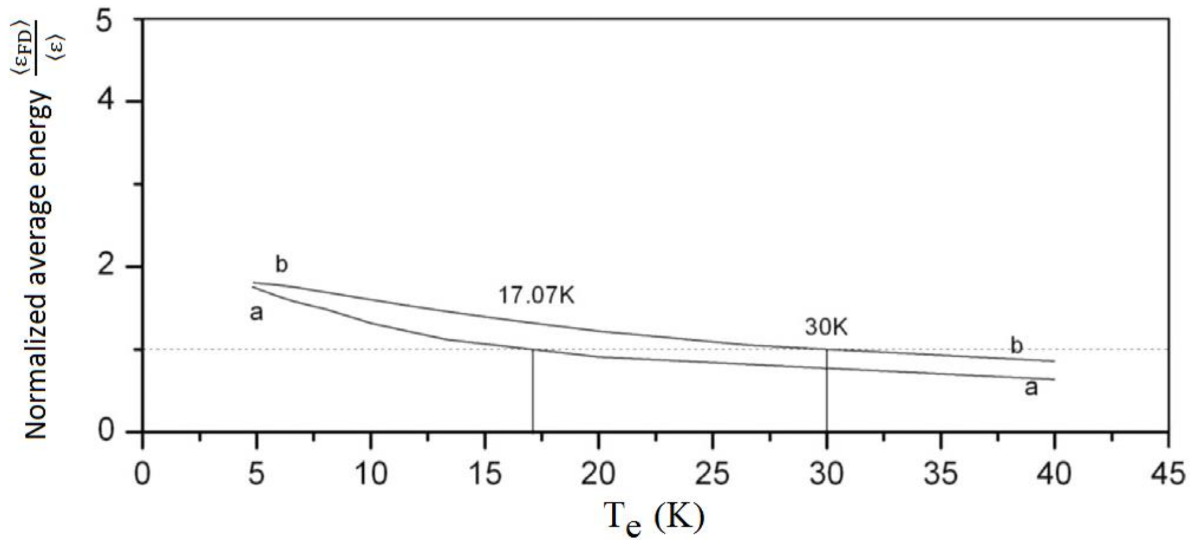

Fig. 2.2 : Dependence of the normalized average energy upon the effective electron temperature. The curves are drawn for the lattice temperature T_L=4 K. The curve 'a' is for η = 5 and the curve 'b' for η=10.

It may be seen that the values of the normalized average energy hovers around unity over the range of the electron temperature of interest here. This indicates that the approximate distributions are valid to a good extent.

On using this model distribution, evaluations of the different transport parameters have been made here and the results thus obtained are compared with the similar results carried out on using the exact F.D. function.

References:

[2.1] B.Das, A.Basu, J.Das, D.P.Bhattacharya, Physica B 474 21 (2015).

[2.2] A.Basu, B.Das, T.R.Middya, D.P.Bhattacharya, J.Phys.Chem. Solids 100 9 (2017).

[2.3] D.P.Bhattacharya, J.Das, A.Basu, B.Das; Physica B, 520 106–111 (2017).

[2.4] Jaroslav Karlovsky, Phys. Rev. 127 419 (1962).

[2.5] J. S. Blackemore, Semiconductor Statistics ,Pergamon Press Oxford, (1962).

[2.6] C.Kittel, Elementary Statistical Physics ,John Wiley & Sons, Inc., New York, (1958).

[2.7] G.Bauer, Springer Tracts in Modern Physics, Springer, Berlin, Heidelberg, New York, (1974).

CHAPTER III

Analysis of the energy loss rate and the non-ohmic mobility characteristics in the non-degenerate sample of different III -V compound semiconductors at low lattice temperature

3.1 Introduction

In compound semiconductors, the intrinsic acoustic vibrations of the lattice atoms produce an additional electric field that gives rise to piezoelectric scattering potential along with the deformation potential. The piezoelectric scattering is known to be quiet important in many semiconductors under the condition of relatively lower lattice temperature. Eventually, the electrical transport at low lattice temperatures is principally controlled by the combined interactions of the electrons with the piezoelectric and acoustic phonons. Some of these semiconductors possessing finite values of piezoelectric coupling constant K_m^2 over a wide range, are now widely used for the device purposes. For example: GaN (K_m^2 =0.0324) is commonly used for light emitting diodes, InSb (K_m^2 =7.29×10^{-4}) for infrared detectors, InAs (K_m^2 =2.8×10^{-4}) as well as InSb for galvanomagnetic devices. In the low temperature regime, where the piezoelectric scattering is important, the onset of the non-linearity may start even for a field of only few volt cm^{-1}or even less [3.1-3.4].

Traditionally, the theory of high field transport is developed through solving the Boltzmann Transport equation. An analytical solution of the transport equation is beset with much mathematical difficulties, as has already been said, unless one makes simplifying approximation, which more often than not compromises with the physical validity of the results.

If the carrier concentration is large, so that the energy exchange between the carriers is much faster than that between the carriers and the lattice, the carriers share their energy ε mainly amongst themselves and the energy distribution for a non-degenerate ensemble of carriers may be approximated by the Maxwellian distribution at a field dependent carrier temperature T_e [3.1,3.4,3.5]. The field dependence of T_e may be obtained from the solution of the energy balance equation of the electron phonon system. Such dependence has already been obtained solely for the individual interactions, like acoustic, piezoelectric etc. [3.6]. To calculate the field dependence of the effective electron temperature for some combined interactions of the electrons, the energy balance equation needs to be solved afresh taking into account all the individual scatterings simultaneously.

The non-ohmic mobility characteristics μ(E) in the presence of relatively high fields may now be obtained from [3.5]

$$e\mu E^2 = \left\langle \frac{d\mathcal{E}}{dt} \right\rangle_{\text{combined interaction}} \tag{3.1}$$

where e is the electronic charge, E is the applied electric field, and $\left\langle \frac{d\mathcal{E}}{dt} \right\rangle$, the average energy loss rate for the same combination of interactions, that needs to be calculated taking all the individual scattering into account simultaneously.

For some compounds, particularly with lower values of the effective mass m*, like InSb or InAs having $m^* \sim 10^{-2}\ m_0$ (m_0 being the free electron mass), an electric field of a fraction of a volt cm^{-1} or so, may appear to be high enough to perturb the electron ensemble significantly, and thus electrical non-linearity may set in at that field. On the other hand, for GaN, which possesses quite a high value of the piezoelectric coupling constant, the onset of the electrical non-linearity takes place at somewhat high fields because of its nearly ten times heavier effective mass compared to that of the Indium compounds.

Here, the analysis is to solve the energy balance equation for the electron phonon system considering the combined interaction of the electrons with the deformation acoustic and piezoelectric phonons and thus to obtain the electric field dependence of the effective electron temperature. From this, the high field mobility characteristics are obtained using eq. (3.1) for the same prevalent conditions. The energy loss rate due to

acoustic interaction is already known [3.5]. Here the same is calculated for the piezoelectric interaction in order to get $\langle\frac{d\mathcal{E}}{dt}\rangle$ for the combined interaction.

3.2 Development

3.2.1. Field dependence of the effective electron temperature for the combined interaction with piezoelectric and deformation acoustic phonons.

The energy balance condition for the electron phonon system can be symbolically written as [3.4-3.6]

$$\int_{\vec{k}} \left.\frac{\partial f(\vec{k})}{\partial t}\right|_{field} \varepsilon\, d\vec{k} = \sum_{\vec{k}} \int \left.\frac{\partial f(\vec{k})}{\partial t}\right|_{j} \varepsilon\, d\vec{k} \tag{3.2}$$

where $\left.\frac{\partial f(\vec{k})}{\partial t}\right|_{j}$ is the time rate of change of the high field distribution function $f(\vec{k})$ of the electron ensemble due to the jth collision mechanism,$\varepsilon$is the energy of an electron with wave vector $\vec{k}$. The distribution function $f(\vec{k})$ for the non-equilibrium carriers may be written in the diffusion approximation as [3.6]

$$f(\vec{k}) = f_0(\varepsilon) + k\, f_1(\varepsilon)\cos\theta \tag{3.3}$$

$f_0(\varepsilon)$ being the isotropic part of the distribution and θ is the angle between $\vec{k}$ and the drift field $\vec{E}$. $f_1(\varepsilon)$ is given later on.

We consider a volume of an isotropic, non-degenerate semiconductor material with a single, parabolic, spherically symmetric conduction band. Taking into account the four processes of absorption and emission of a phonon of wave vector $\vec{q}$ in course of the electronic transition between the states $|\vec{k}+\vec{q}\rangle$ and $|\vec{k}-\vec{q}\rangle$ due to the combined interaction with the piezoelectric and the deformation potential acoustic phonons, one can obtain from the perturbation theory [3.5, 3.6]:

$$\sum_{j} \left.\frac{\partial f_0(\vec{k})}{\partial t}\right|_{j} = \left(\frac{W}{\tau_{ace}} + \frac{1}{\tau_{pze}}\right) W^{\frac{1}{2}} \frac{d^2 f_0}{dW^2} + \left[\frac{W^{\frac{1}{2}}(W+2)}{\tau_{ace}} + \frac{W^{-\frac{1}{2}}(W+1)}{\tau_{pze}}\right] \frac{\partial f_0}{\partial W}$$

$$+ \left(\frac{2W^{\frac{1}{2}}}{\tau_{ace}} + \frac{W^{-\frac{1}{2}}}{\tau_{pze}}\right) f_0 \tag{3.4}$$

where, $W = \frac{\varepsilon}{K_B T_L}$; τ_{ace} and τ_{pze} are the energy independent factors of the expressions for the energy relaxation time for the interaction with the acoustic and the piezoelectric phonons respectively. They are given by,

$$\tau_{ace} = \frac{\pi\rho\hbar^4}{2\sqrt{2}m^{*5/2}{E_1}^2(k_B T_L)^{1/2}}$$

$$\tau_{pze} = \frac{\sqrt{2}\pi\hbar^2\epsilon_{sc}(k_B T_L)^{1/2}}{m^{*3/2}e^2{K_m}^2{u_l}^2}$$

ρ is the density, $\hbar = \frac{h}{2\pi}$; h being the Planck's constant, k_B is the Boltzmann constant, E_1 is the deformation potential constant, ϵ_{sc} is the static dielectric constant and u_l is the average aoustic velocity.

Now using (3.4) one can carry out the collision integral in (3.2) in the energy domain and obtain

$$\sum_j \int \frac{\partial f_0(\vec{k})}{\partial t}\bigg|_j \varepsilon d\vec{k} = \left[\frac{2\pi(2m^*)^{\frac{3}{2}}}{\hbar^3}\right]\left[\frac{n_0\hbar^3(k_B T_L)^{\frac{5}{2}}T_n}{(2\pi k_B T_e)^{\frac{3}{2}}\tau_{ace}}\right]\left[2(3T_n + P) - T_n\left\{2(T_n + 2) + P\left(1 + \frac{1}{T_n}\right)\right\}\right] \quad (3.5)$$

where, $T_n = T_e/T_L$, $P \equiv \frac{\tau_{ace}}{\tau_{pze}} = \frac{\rho\hbar^2 e^2{K_m}^2{u_l}^2}{4m^* k_B T_L {E_1}^2\epsilon_{sc}}$

The rate of change of the distribution function due to the field for the combined interaction is given by [3.4-3.6]

$$\frac{\partial f_0(\vec{k})}{\partial t}\bigg|_{field} = \frac{2}{3}\frac{eE}{\hbar}\int \mathcal{E}^{-1/2}\frac{d(\mathcal{E}^{3/2}f_1)}{d\mathcal{E}}\varepsilon d\vec{k} \quad (3.6)$$

where, $f_1 = \frac{-e\hbar\tau_{eff}}{m^*}\left(\frac{\mathcal{E}}{k_B T_L}\right)^{-1/2} E \frac{\partial f_0}{\partial \mathcal{E}}$; $\tau_{eff} = \frac{\tau_{acm} * \tau_{pzm} W^{1/2}}{\tau_{acm} + \tau_{pzm}}$; .$\tau_{acm}$ and τ_{pzm} are the momentum relaxation time for the interaction with the acoustic and the piezoelectric phonons respectively. They are given by,

$$\tau_{acm} = \frac{\pi\rho\hbar^4 {u_l}^2}{\sqrt{2} m^{*3/2} {E_1}^2 (k_B T_L)^{3/2}}$$

$$\tau_{pzm} = \frac{e^2 m^* (k_B T_L)^{1/2} {K_m}^2}{\pi 2^{3/2} \hbar^2 \epsilon_{sc}}.$$

Now using (3.6) one can in principle carry out the integral in (3.2) that involves the field term, in the energy domain. But the presence of the piezoelectric scattering in the combined interactions, characteristically makes the integral diverge as $\varepsilon \to \infty$ [3.5,3.6]. As such, the upper limit of energy is set at several times the average thermal energy, say $nk_B T_e$ ($n \gg 1$), beyond which there would be hardly any electron. The finite, maximum value of n is to be suitably chosen so as to make the result convergent. Thus one can obtain

$$\int \frac{\partial f(\vec{k})}{\partial t}\bigg|_{\vec{k}, field} \varepsilon d\vec{k} = \frac{4 n_0 (T_L)^{\frac{1}{2}} e^2 E^2 \tau_{acm}}{3\sqrt{\pi} m^* {k_B}^2 {T_e}^{\frac{5}{2}}} I_P \qquad (3.7)$$

where

$$I_P = \frac{(nk_BT_e)^3 e^{-n}}{(nk_BT_e + Pk_BT_L)}$$

$$- (k_BT_e)^2 \left[n^2 e^{Y_1} \left\{ \ln(Y_2) + \sum_{i=1}^{\propto} \frac{(-Y_2)^i}{i.\,i!} \right\} \right.$$

$$- 2e^{Y_1} \left[\left(\frac{{Y_2}^2}{2} \right) \left(\ln(Y_2) - \frac{1}{2} \right) - Y_1 Y_2 (\ln(Y_2) - 1) \right.$$

$$\left. \left. + \sum_{i=1}^{\propto} \frac{(-1)^i}{i.\,i!} \left\{ \frac{{Y_2}^{i+2}}{i+2} - Y_1 \frac{{Y_2}^{i+1}}{i+1} \right\} \right] \right]$$

$$- (k_BT_e)^2\, 2e^{Y_1} \left[\left(\frac{{Y_1}^2}{2} \right) \left(\ln(Y_1) - \frac{1}{2} \right) - {Y_1}^2 (\ln(Y_1) - 1) \right.$$

$$\left. + \sum_{i=1}^{\propto} \frac{(-1)^i}{i.\,i!} \left\{ \frac{{Y_1}^{i+2}}{i+2} - \frac{{Y_1}^{i+2}}{i+1} \right\} \right]$$

And $Y_1 = \frac{P}{T_n}$ and $Y_2 = n + \frac{P}{T_n}$

Now equating (3.5) with (3.7) one can obtain the field dependence of the effective electron temperature for the combined interaction with the piezoelectric and deformation acoustic phonons.

3.2.2. Energy loss rate for the combined interaction with the piezoelectric and deformation acoustic phonons.

The field dependence of the effective electron temperature being known, one can now calculate the non-ohmic mobility characteristics using (3.1), when the average energy loss rate of the non-equilibrium ensemble of electrons for the same combination of interactions is known.

Again starting from the perturbation theory, one may first calculate the energy loss rate of a carrier of energy ε by summing over all the possible emission and absorption processes that such a carrier may undergo in making transition to and from the states $|\vec{k}+\vec{q}\rangle$ and $|\vec{k}-\vec{q}\rangle$. Then the loss rate needs to be averaged over the distribution of carrier energies. Proceeding in this way the expression for the average loss rate for the

interaction with deformation acoustic phonons has already been available [3.5]. It takes the form

$$\langle\frac{d\mathcal{E}}{dt}\rangle_{ac} = \frac{8\sqrt{2}}{\pi^{3/2}}\frac{{E_1}^2 m^{*5/2}}{\hbar^4\rho}(k_B T_e)^{3/2}\left(\frac{T_L}{T_e} - 1\right) \tag{3.8}$$

Proceeding in the same manner one can get the following expression for the average loss rate for interaction with the piezoelectric phonons

$$\langle\frac{d\mathcal{E}}{dt}\rangle_{pz} = \frac{e^2 {K_m}^2}{2\pi^3(2\pi)^{3/2}}\frac{{u_l}^2 m^{*3/2}}{\epsilon_{SC}\hbar^2}(k_B T_e)^{1/2}\left(\frac{T_L}{T_e} - 1\right) \tag{3.9}$$

Finally, the average energy loss rate may be obtained by adding (3.8) and (3.9). Thus,

$$\langle\frac{d\mathcal{E}}{dt}\rangle_{Combintion} = \langle\frac{d\mathcal{E}}{dt}\rangle_{ac} + \langle\frac{d\mathcal{E}}{dt}\rangle_{pz} \tag{3.10}$$

Using (3.10) a relationship between $\langle\frac{d\mathcal{E}}{dt}\rangle_{Combintion}$ and T_e can be plotted. Figure 3.1 describes the dependence of energy loss rate of the electrons upon their effective temperature in samples of InSb, InAs and GaN, and the data is further used to determine the non-ohmic mobility for the three samples respectively.

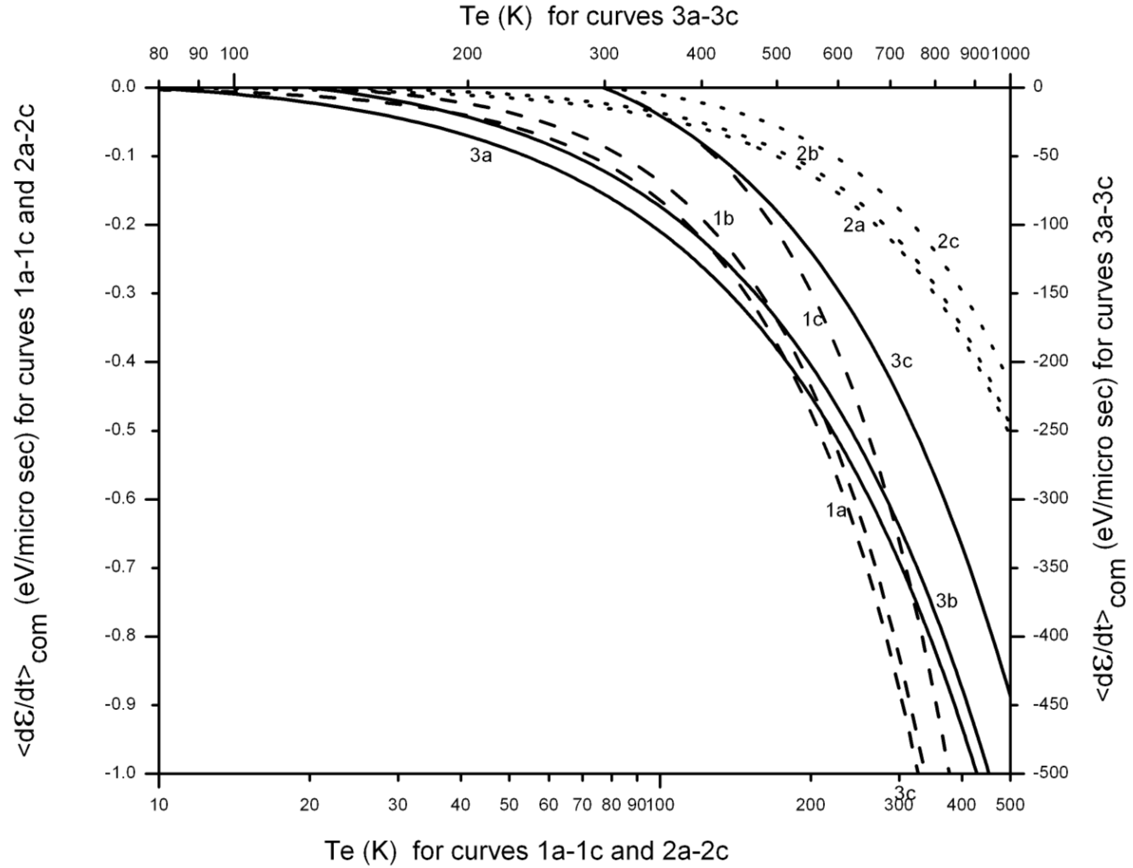

Fig. 3.1 : Dependence of energy loss rate of electrons upon the effective electron temperature in the samples of InSb, InAs and GaN. The combined interaction of the electrons with the acoustic and the piezoelectric phonons are taken into account. The curves 1a-1c for the samples of InSb and similarly the curves 2a-2c for the samples of InAs, are obtained from (3.10) at the lattice temperatures of 4.2K, 20K and 77K respectively. The curves 3a-3c for the samples of GaN are also obtained from (3.10) at the lattice temperatures of 77K, 125K and 300K respectively.

Now the non-ohmic mobility characteristics for the combined interaction of the non-equilibrium carriers may be obtained from (3.1).

3.3 Results and Discussion

Here the theoretical analysis is made to study the importance of the piezoelectric scattering relative to that of acoustic scattering in controlling the non-ohmic transport characteristics of some III-V compound semiconductors. Since the piezoelectric

interaction is important at relatively low temperatures, and at such low temperature regime the electron ensemble in compounds like InSb or InAs which possess a low value of the effective mass, gets heated up even for a field of a fraction of a volt/cm. So, such a low field appears to be effectively high enough to perturb the electron ensemble significantly from the state of thermodynamic equilibrium with the lattice atoms. As such, we choose to limit our discussion mainly over the portion of the transport characteristics that may be obtained for low lattice temperatures and for apparently low fields. Such a choice would ensure that (i) piezoelectric scattering remains an important interaction. (ii) The electron ensemble is heated up and (iii) sufficient number of polar optical phonons are not generated, so that the interaction with such phonons hardly comes into play. The results of similar studies for the importance of piezoelectric scattering in controlling the ohmic characteristics of compound semiconductors are already available [3.3].

In the present analysis, the effective electron temperature characteristics are first obtained for the combined interactions with the piezoelectric and the acoustic phonons. The non-ohmic mobility characteristics are then obtained from the electron temperature characteristics using the energy balance equation.

The field dependence of the effective electron temperature for the individual scattering is known to be quite simple, obeying the laws $T_n (T_n-1) \sim E^2$ and $(1-1/T_n) \sim E^2$ respectively for the interaction with the deformation acoustic phonons and the piezoelectric phonons [3.6]. But it appears from (3.5) and (3.7) that the same field dependence for the combination of the two interactions is quite complex. As such, this results in a much complex field dependence of the mobility of the non-equilibrium electrons.

To depict a quantitative picture of the two characteristics, we consider non-degenerate samples of InSb, InAs and GaN. The material parameters that are used for the numerical evaluation of the characteristics of these materials are given in Table 3.1.

Table 3.1: Material Parameters

Material	m^*/m_0	u_l (m/s)	ρ(kg/m^3)	K_m^2	ϵ_{SC} (F/m)	E_1 (eV)
InSb	0.014	3.7E+3	5.78E+3	7.29E-4	1.55E-10	20
InAs	0.022	3.09E+3	5.61E+3	2.822E-4	1.286E-10	5.8
GaN	0.2	5E+3	6.1E+3	3.24E-2	8.41E-11	8

Each of the samples are lightly doped with shallow donors, whose ionization energy is of the order of or lower than $k_B T_L$. The concentration of the materials is less than the effective density of states N_C, so that the Fermi level remains within the band gap. Under these conditions, the degeneracy sets in for $N_D \sim 5N_C$ and the carrier concentration $n_0 \sim 0.15\ N_D$, where N_D is the donor concentration [3.7,3.8]. As such the carrier concentrations may be taken to be $10^{12}/cm^3$, $10^{13}/cm^3$ and $10^{14}/cm^3$ for InSb, InAs and GaN respectively. However, it may be noted that, when (3.5) is equated to (3.7) to obtain the field dependence of the effective electron temperature, under the prevalent conditions of interest here, the concentration n_0 cancels out. As has already been said, n is suitably chosen for the convergent results. The effective electron temperature characteristics have been calculated from the present analysis taking n = 5 for both InSb and InAs and n = 10 for GaN.

It may be noted that, for the lower values of P, the consideration of only a few terms are sufficient for the convergence of the summation over P that are involved in the expression for the function I_P. Obviously for Indium compounds, the lower values of K_m^2 and the higher values of E_1^2 keep P quite low even for lower temperatures, around 4.2K. The values are 3.55 and 8.35 for InSb and InAs respectively. As T_L increases, P reduces more and more, that in turn makes it possible to truncate the summation earlier, without compromising with the convergence of the results. On the other hand, the value of P turns out to be nearly two orders of magnitude higher at T_L= 4.2K for GaN. Hence this requires quite a large number of terms to get the convergent results for GaN unless the lattice temperature is increased accordingly, say around 77K, so as to reduce the value of P sufficiently, which in turn makes the truncation of the summation possible after a much lesser number of terms.

The characteristics of the effective electron temperature and that of the non-ohmic mobility of the electrons relative to μ_0, the zero field value, as obtained from the present analysis under the condition when the combined interaction with the piezoelectric and acoustic phonons takes place in the samples considered here, are represented in the figures 3.2, 3.3 and 3.4. To make a ready comparison of the importance of the piezoelectric scattering relative to that of the intrinsic acoustic scattering in controlling the non-ohmic transport of the electrons, the figures for the non-ohmic characteristics for the sole interaction with the intrinsic acoustic phonons have also been included.

It may be seen from the figures that, when the piezoelectric interaction is considered in combination with that due the deformation acoustic phonons, significant qualitative as well as quantitative changes in the non-ohmic transport characteristics are effected over the low ranges of the electric field and the lattice temperature. The changes are much more perceptible for the mobility characteristics compared to the effective electron temperature characteristics. In any case, however, the combination with the piezoelectric interaction effects greater changes, the lower the temperature is. At higher fields, the characteristics for the combined interaction tend to that due to the acoustic interaction only, as the importance of the piezoelectric interaction reduces more and more. This picture continues till the lattice temperature and the field is high enough so that the interaction with the polar optical phonons begins to be more and more important.

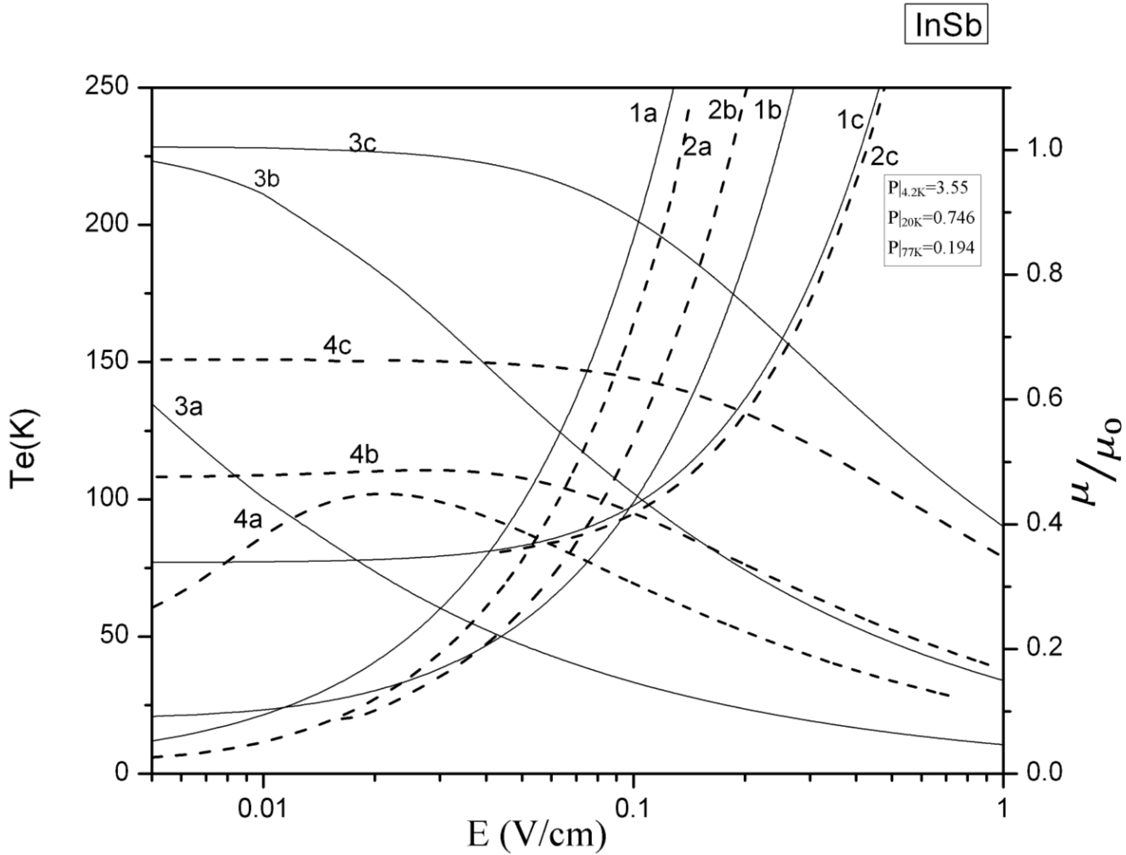

Fig. 3.2 : Dependence of effective electron temperature and normalized non-ohmic mobility upon the electric field in InSb. Curves 1a-1c and 3a-3c show the effect of acoustic scattering in determining the field dependence of the effective electron temperature and the normalized non-ohmic mobility respectively for the different lattice temperatures. Curves 2a-2c and 4a-4c give respectively the field dependence of the effective electron temperature and of the non-ohmic mobility for the combined scattering of the electrons with the acoustic and the piezoelectric phonons. The curves marked a, b and c are respectively for the lattice temperatures of 4.2K, 20K and 77K. A comparison of the curves 1a-1c with the curves 2a-2c reveals the effects of the piezoelectric scattering on the field dependence of the effective electron temperature. Similarly the comparison of the curves 3a-3c with the curves 4a-4c displays the effects of the same piezoelectric interaction on the field dependence of the non-ohmic mobility.

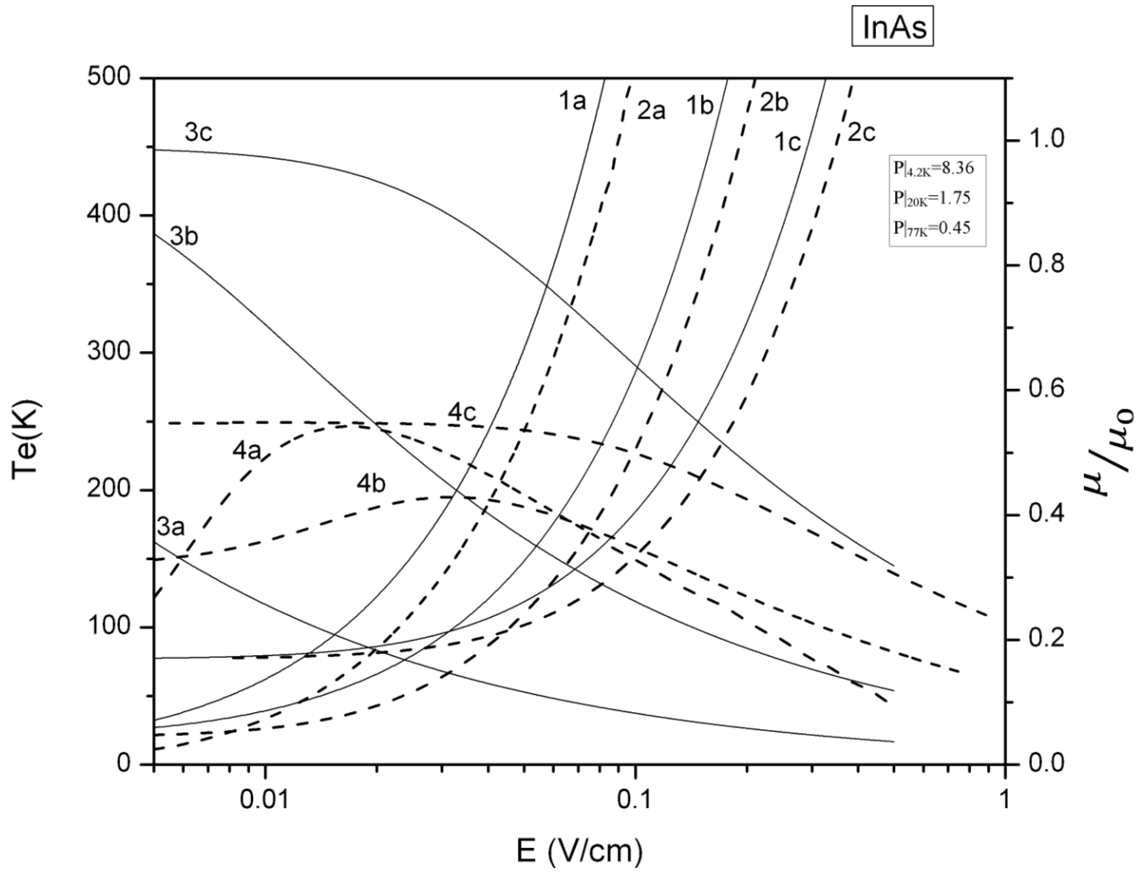

Fig. 3.3 : Dependence of effective electron temperature and normalized non-ohmic mobility upon the electric field in InAs. Curves 1a-1c and 3a-3c show the effect of acoustic scattering in determining the field dependence of the effective electron temperature and the normalized non-ohmic mobility respectively for the different lattice temperatures. Curves 2a-2c and 4a-4c give respectively the field dependence of the effective electron temperature and of the non-ohmic mobility for the combined scattering of the electrons with the acoustic and the piezoelectric phonons. The curves marked a, b and c are respectively for the lattice temperatures of 4.2K, 20K and 77K. A comparison of the curves 1a-1c with the curves 2a-2c reveals the effects of the piezoelectric scattering on the field dependence of the effective electron temperature. Similarly the comparison of the curves 3a-3c with the curves 4a-4c displays the effects of the same piezoelectric interaction on the field dependence of the non-ohmic mobility.

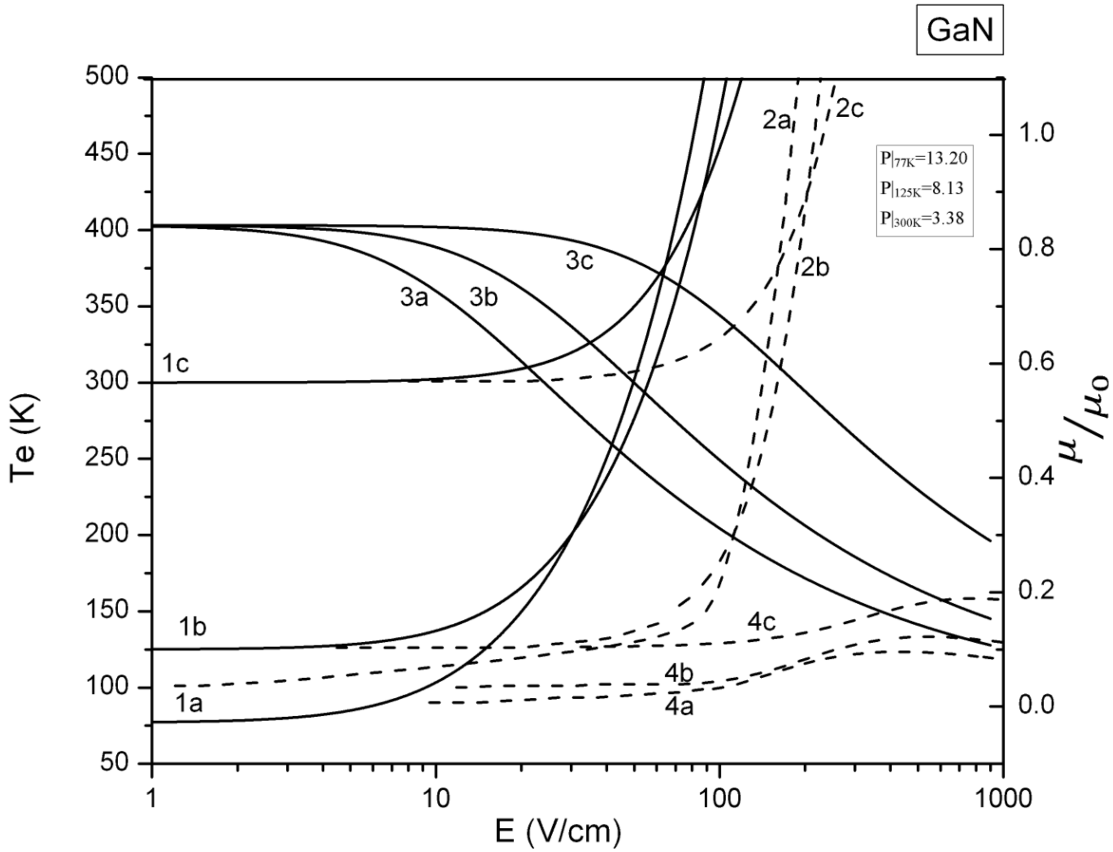

Fig. 3.4 : Dependence of effective electron temperature and normalized non-ohmic mobility upon the electric field in GaN. Curves 1a-1c and 3a-3c show the effect of acoustic scattering in determining the field dependence of the effective electron temperature and the normalized non-ohmic mobility respectively for the different lattice temperatures. Curves 2a-2c and 4a-4c give respectively the field dependence of the effective electron temperature and of the non-ohmic mobility for the combined scattering of the electrons with the acoustic and the piezoelectric phonons. The curves marked a, b and c are respectively for the lattice temperatures of 77K, 125K and 300K. A comparison of the curves 1a-1c with the curves 2a-2c reveals the effects of the piezoelectric scattering on the field dependence of the effective electron temperature. Similarly the comparison of the curves 3a-3c with the curves 4a-4c displays the effects of the same piezoelectric interaction on the field dependence of the non-ohmic mobility.

There is no such experimental data available, which shows the importance of only the piezoelectric scattering relative to that of acoustic scattering in controlling the non-ohmic transport in semiconductors. Experiments which have been performed, provide data of the non-ohmic transport characteristics over a wider regime of the lattice temperature and the electric field [3.4,3.9-3.12]. Such experimental data reflects the results of the combination of all relevant types of interaction of the electrons, not just for the combination of the piezoelectric scattering only with the acoustic scattering. However, the results obtained here for InSb and InAs over the limited range of the lattice temperature and the field provide qualitatively the same picture in respect of the variation of the mobility with the electric field as that which follow from the experiments [3.11,3.12].

Apart from piezoelectric scattering, some other low temperature features need to be considered for the refinement of the present analysis. Under the condition, when the lattice temperature is low, the equipartition approximation for the phonon distribution is hardly valid [3.5, 3.13]. Hence the true phonon distribution should be taken into account. However, at low temperatures, the average thermal energy of electrons being comparable with the energy of the acoustic phonons, the electron –phonon collision becomes inelastic. Thus phonon energy needs to be considered carefully in the energy balance equation of the electron phonon system. Apart from that, at low temperatures the electrostatic screening of the scattering potential should also be taken into account [3.1]. Still again, the piezoelectric coupling constant being highly anisotropic, the tensorial nature of the constant should also be considered [3.5, 3.14]. All these factors need to be given due consideration for further refinement of the present analysis. All the factors cannot be taken up at a time for a detailed analysis. Each may have to be considered separately. However, the results obtained from the present analysis being already interesting, it stimulates further work in the same field.

References:

[3.1] B. R. Nag *Electron Transport in Compound Semiconductors* (*Springer Series in Solid State Sciences vol 11*) ed M Cardona, P Fulde and H J Queisser (New York: Springer) (1980).

[3.2] P. K. Basu and B. R. Nag, *Phys. Rev. B*22 4849 (1980).

[3.3] P. K. Basu and B. R. Nag , *J. Phys. C: Solid State Phys*14 1519 (1981).

[3.4] G. Bauer, Springer *Tracts in Modern Physics* (New York: Springer) (1974).

[3.5] E. M. Conwell, *High Field Transport in Semiconductors* (New York: Academic) (1967).

[3.6] B. R. Nag, *Theory of Electrical Transport in Semiconductors* (Oxford Pergamon) (1972).

[3.7] S. M. Sze, *Physics of Semiconductor Devices* (New Delhi: Wiley Eastern Limited) (1983).

[3.8] B. G. Streetman and S. Banerjee *Solid State Electronic Devices* (New Delhi: Prentice Hall of India) (2003).

[3.9] H. Miyazawa, *J. of Phy. Soc. J*. 26 700 (1969).

[3.10] G. Bauer and H. Kahlert, *Phys. Rev B*.5 566 (1972).

[3.11] A. Neukemans and G. S. Kino, *Appl. Phys. Lett.*17 102 (1970).

[3.12] R. C. Curby and D. K. Ferry, *Phys. Rev. B*3 3379 (1971).

[3.13] C. Canali*et al*, *Phys. Rev. B*12 226 5 (1975).

[3.14] H. Saitoh, *J. of Phy. Soc. J*. 21 2540 (1966).

CHAPTER IV

Effective temperature of the non-equilibrium electrons in a degenerate semiconductor at low lattice temperature.

4.1. Effective temperature of the non-equilibrium electrons for the interaction with the acoustic phonons.

4.1.1. Introduction

To make a theoretical analysis of the transport characteristics of a material in the presence of a relatively high field at any lattice temperature, low or high, one needs to solve the Boltzmann Transport equation taking into account the various interactions of the electrons with the lattice defects. In the presence of a relatively high field, the free carriers in a semiconductor may be significantly perturbed from the state of thermodynamic equilibrium with the host lattice atoms. The critical field at which the electrons may be drifted to such a significantly perturbed state in any material increases with the increase of the lattice temperature and with the decrease of the values of the initial mobility. For example, in n-Ge, when the lattice temperature is low, say around 5K, the electrons may be so perturbed for a field of only a few Vcm^{-1}, and in InSb, when the lattice temperature is around 2K, similar perturbation may be observed for a fraction of a Vcm^{-1}. On the other hand, if the lattice temperature is raised to around room

temperature, significant perturbation of the carriers requires fields of several $kVcm^{-1}$ in Ge and some hundred Vcm^{-1} in InSb. Such a perturbed ensemble is known to exhibit a number of novel phenomena which are technologically important from the device point of view. [4.1-4.6]

The field dependence of the effective temperature of the electrons may be calculated from the solution of the energy balance equation. The solution however, depends upon the dominant type of interaction under the prevailing condition and the band structure of the material. The interaction with the optical and intervalley phonons may be dominant for lattice temperatures above some hundred degrees. On the other hand, the interaction with the intravalley acoustic phonons is intrinsic and may dominate along with the impurity scattering at the lower temperatures. However, the collision with impurities being elastic, the intravalley acoustic phonon scattering will dominate in determining the field dependence of the effective electron temperature in the lower temperature regime. Such field dependence has already been worked out for a non-degenerate material [4.1, 4.2, 4.6]. The dependence is of the simple form $T_n(T_n - 1) \sim E^2$ where $T_n = T_e/T_L$. Obviously such dependence is predicted for samples having lower carrier concentrations and at the higher lattice temperatures.

At lower temperatures, however, as a result of increasing the doping level the electron concentration in an n-type material increases, and when it eventually exceeds the effective density of states, the Fermi level ε_F moves into the conduction band. Under this condition and when ε_F is not much lower than $k_B T_L$ of the band edge, and the electron densities are beyond the insulator to metal transition, the electron ensemble turns out to be degenerate. A rough estimate of the critical donor concentration N_D for the onset of the degeneracy may be estimated from

$$\varepsilon_F = \left(\frac{\hbar^2}{2m^*}\right)(3\pi^2 N_D)^{2/3} > E_d$$

where $\hbar = h/2\pi$, h being Planck's constant, m^* is the effective mass of an electron and E_d is the donor ionisation energy. The degeneracy is said to be extreme when $\varepsilon_F \gg k_B T_L$ [4.7-4.9].

The purpose here is to obtain the electric field dependence of the effective electron temperature T_e for a degenerate ensemble of electrons which is subjected to a relatively high field, and under the condition when the interaction with the intravalley acoustic phonons dominate. Before solving the energy balance equation for the electron-phonon

system, it is first recast taking into account the degeneracy of the electron ensemble, the energy distribution of which is described by the F.D. statistics at the field dependent effective temperature T_e. Because of the complexity of the F.D distribution, the integrals that occur while solving the energy balance equation are not usually amenable to analytical evaluation. In the present analysis the alternative model of the F.D. distribution as described in Chapter II, has been used so that the integrals can indeed be carried out analytically without compromising with the validity of the final results. The numerical results obtained for Ge and InSb from the present analysis are then compared with other theoretical and experimental results. The agreement of the results from the present analysis with that from the experiments seems to be significantly better. The calculations have been carried out for any finite value of the degeneracy and the lattice temperature.

4.1.2. Development

The condition for energy conservation of the electron-phonon system may be expressed as [4.1, 4.2, 4.6]

$$\int \frac{\partial f(\vec{k})}{\partial t}\bigg|_{coll} \varepsilon d\vec{k} = \int \frac{\partial f(\vec{k})}{\partial t}\bigg|_{field} \varepsilon d\vec{k} \tag{4.1}$$

where $\frac{\partial f(\vec{k})}{\partial t}$ is the time rate of change of the distribution function $f(\vec{k})$, ε is the energy of an electron with wave vector $\vec{k}$. The distribution function in the diffusion approximation may be written as

$$f(\vec{k}) = f_0(\varepsilon) + k\cos\theta\, f_1(\varepsilon) \tag{4.2}$$

θ being the angle between the wave vector $\vec{k}$ and the electric field $\vec{E}$.

We consider a volume V of an isotropic, degenerate semiconductor material with a single, parabolic, spherically symmetric conduction band. Taking into account the four processes of absorption and emission involving a phonon of wave vector $\vec{q}$ that leads to the scattering of the electrons into and out of the state $|\vec{k}\rangle$ for transitions to and from the states $|\vec{k}+\vec{q}\rangle$ and $|\vec{k}-\vec{q}\rangle$, it follows from the perturbation theory that

$$\left.\frac{\partial f(\vec{k})}{\partial t}\right|_{coll} = \frac{2\pi}{\hbar}\sum_{\vec{q}}\left[\left|\langle \vec{k}, N_{\vec{q}} \pm 1 | H' | \vec{k} \pm \vec{q} \rangle\right|^2 \delta\left(\varepsilon_{\vec{k}} - \varepsilon_{\vec{k}\pm\vec{q}} \pm \hbar\omega_{\vec{q}}\right) f(\vec{k}+\vec{q}) f(\vec{k}) - \left|\langle \vec{k} \pm \vec{q}, N_{\vec{q}} \pm 1 | H' | \vec{k} \rangle\right|^2 \delta\left(\varepsilon_{\vec{k}\mp\vec{q}} - \varepsilon_{\vec{k}} \pm \hbar\omega_{\vec{q}}\right) f(\vec{k}) f(\vec{k} + \vec{q})\right] \quad (4.3)$$

where $N_{\vec{q}}$ is the equilibrium distribution function of the phonons, $\omega_{\vec{q}}$ is the angular frequency of a phonon with the wave vector $\vec{q}$. The upper or the lower sign in the first term must be taken for the processes of emission and absorption respectively, whereas those signs in the second term stand for the reverse processes. [4.1,4.2,4.10-4.14]

It is well known that when the band edge shift is linearly dependent upon the strain, one can neglect the spin exchange scattering [4.15], as such the matrix element for the transition remains unchanged for a degenerate ensemble, and hence it is given by [4.1,4.2,4.8]

$$\left|\langle \vec{k} \pm \vec{q}, N_{\vec{q}} \pm 1 | H' | \vec{k} \rangle\right|^2 = \frac{{E_1}^2 \hbar q}{2\rho u_l V}\begin{bmatrix} N_{\vec{q}} \\ N_{\vec{q}} + 1 \end{bmatrix} \quad (4.4)$$

where E_1 is the deformation potential constant, ρ is the density of the material and u_l is the average acoustic velocity. Now following the standard procedure [4.14.,2] one can obtain for a degenerate ensemble from (4.2) as

$$\left.\frac{\partial f_0(\vec{k})}{\partial t}\right|_{coll} = \frac{2}{\tau_{ace}}\left(\frac{\varepsilon}{k_B T_L}\right)^{1/2}\left[\varepsilon \frac{k_B T_L}{2}\frac{d^2 f_0}{d\varepsilon^2} + \left\{k_B T_L + \frac{\varepsilon}{2}(1 - 2f_0)\right\}\frac{df_0}{d\varepsilon} + (1 - f_0) f_0\right] \quad (4.5)$$

where

$$\tau_{ace} = \frac{\pi\rho\hbar^4}{2\sqrt{2}\, m^{*5/2} {E_1}^2 (k_B T_L)^{1/2}}$$

It may be noted that for a non-degenerate ensemble, when, $f_0 \ll 1$, (4.4) reduces to the form already known [4.1,4.2].

The rate of change due to field in given by [4.1,4.2]

$$\left.\frac{\partial f_0(\vec{k})}{\partial t}\right|_{field} = \frac{2}{3}\frac{eE}{\hbar}\mathcal{E}^{-1/2}\frac{d(\mathcal{E}^{3/2}f_1)}{d\mathcal{E}} \tag{4.6}$$

where $$f_1 = \frac{-e\hbar\tau_{acm}}{m^*}\left(\frac{\varepsilon}{k_B T_L}\right)^{-1/2} E\frac{\partial f_0}{\partial \mathcal{E}}$$

and $$\tau_{acm} = \frac{\pi\rho\hbar^4 u_l{}^2}{\sqrt{2}\, m^{*3/2} E_1{}^2 (k_B T_L)^{3/2}}$$

In the effective temperature approximation, f_0 for a degenerate ensemble is given by the Fermi Dirac function at an electron temperature T_e. Now, as already been pointed out, the integrations in (4.1) can hardly be evaluated analytically. To tide over this difficulty the energy domain is divided into three regions, demarcated on the two sides around $\varepsilon = \varepsilon_F$ and the F.D function is approximated for each regime in such a way as expressed in Chapter II, that the integrations in (4.1) can be evaluated analytically without incurring significant errors in the subsequent results.

The integrals in (4.1) for these three regions are now straight forward. Carrying out these integrals one can obtain the energy balance equation as

$$[I_{coll}]_{\mathbf{0}}^{\beta_1\varepsilon_F} + [I_{coll}]_{\beta_1\varepsilon_F}^{\beta_2\varepsilon_F} + [I_{coll}]_{\beta_2\varepsilon_F}^{\infty} = [I_{field}]_{\mathbf{0}}^{\beta_1\varepsilon_F} + [I_{field}]_{\beta_1\varepsilon_F}^{\beta_2\varepsilon_F} + [I_{field}]_{\beta_2\varepsilon_F}^{\infty} \tag{4.7}$$

where,

$$[I_{coll}]_0^{\beta_1\varepsilon_F} = c_1 \sum_{m=1}^{\infty} (-1)^m \left[\exp\left(m\eta(\beta_1 - 1)\frac{T_L}{T_e} \right) \left[(\beta_1 \eta T_L)^3 k_B{}^2 \left(\frac{m}{T_e} - \frac{1}{T_L} \right) - k_B{}^2 \left(1 - \frac{T_e}{mT_L} \right) \left((\beta_1 \eta T_L)^2 + 2\left(\frac{T_e}{m} \right)^2 \right) + 2\beta_1 \eta k_B{}^2 T_L T_e \left(1 - \frac{T_e}{m^2 T_L} \right) \right] + 2\exp\left(-m\eta \frac{T_L}{T_e} \right) \left(\frac{k_B T_e}{m} \right)^2 \left(1 - \frac{T_e}{mT_L} \right) - \sum_{n=1}^{\infty} (-1)^n \left[\exp\left((m+n)\eta(\beta_1 - 1)\frac{T_L}{T_e} \right) \left[(\beta_1 \eta)^3 (k_B T_L)^2 - \frac{T_e}{(m+n)T_L} \left\{ (\beta_1 \eta k_B T_L)^3 - \frac{2\beta_1 \eta k_B{}^2 T_e T_L}{m+n} + 2\left(\frac{k_B T_e}{m+n} \right)^2 \right\} \right] + 2\frac{k_B{}^2}{T_L} \left(\frac{T_e}{m+n} \right)^3 \exp\left(-(m+n)\eta \frac{T_L}{T_e} \right) \right] \right]$$

$$[I_{coll}]_{\beta_1\varepsilon_F}^{\beta_2\varepsilon_F} = c_1 \left[\frac{2}{3} c(\beta_2{}^3 - \beta_1{}^3)(\eta k_B T_L)^3 + \frac{3}{2} c^2 \eta (\beta_2{}^4 - \beta_1{}^4)(\eta k_B T_L)^4 - \frac{4}{5} c^2 \eta^5 (\beta_2{}^5 - \beta_1{}^5)(k_B T_L)^4 + \frac{1}{3} \eta^3 (\beta_2{}^3 - \beta_1{}^3)(k_B T_L)^2 (1 - 2c\eta k_B T_L) \left(\frac{1}{2} + c\eta k_B T_L \right) \right]$$

$$[I_{coll}]_{\beta_2\varepsilon_F}^{\infty} = c_1 \sum_{m=1}^{\infty} (-1)^m \left[\exp\left(-m\eta(\beta_2 - 1)\frac{T_L}{T_e} \right) \left[\left(\frac{T_e}{mT_L} - 1 \right) \left((\beta_2 \eta k_B T_L)^2 + \frac{2\beta_2 \eta k_B{}^2 T_L T_e}{m} + 2\left(\frac{k_B T_e}{m} \right)^2 \right) + (\beta_2 \eta)^3 (k_B T_L)^2 \left(1 - \frac{mT_L}{T_e} \right) \right] \right] + \sum_{m=1}^{\infty} \sum_{n=1}^{\infty} (-1)^{m+1} (-1)^{n+1} \exp\left(-(m+n)\eta(\beta_2 - 1)\frac{T_L}{T_e} \right) \left[(\beta_2 \eta)^3 (k_B T_L)^2 + \frac{T_e}{(m+n)T_L} \left((\beta_2 \eta k_B T_L)^2 + \frac{2\beta_2 \eta k_B{}^2 T_L T_e}{m+n} + 2\left(\frac{k_B T_e}{m+n} \right)^2 \right) \right]$$

$$[I_{field}]_0^{\beta_1\varepsilon_F} = c_2 \sum_{m=1}^{\infty} (-1)^m \left[\exp\left(m\eta(\beta_1 - 1)\frac{T_L}{T_e}\right)\left((\beta_1\eta k_B T_L)^2 m - \beta_1\eta k_B{}^2 T_L T_e + \frac{(k_B T_e)^2}{m}\right) - \exp\left(-m\eta\frac{T_L}{T_e}\right)\frac{(k_B T_e)^2}{m}\right]$$

$$[I_{field}]_{\beta_1\varepsilon_F}^{\beta_2\varepsilon_F} = c_2\left[\left(\frac{ck_B T_e}{2}\right)(\beta_2{}^2 - \beta_1{}^2)(\eta k_B T_L)^2\right]$$

$$[I_{field}]_{\beta_2\varepsilon_F}^{\infty} = c_2 \sum_{m=1}^{\infty} (-1)^m m \exp\left(-m\eta(\beta_2 - 1)\frac{T_L}{T_e}\right)\left((\beta_2\eta k_B T_L)^2 + \frac{\beta_2\eta k_B{}^2 T_L T_e}{m} + \left(\frac{k_B T_e}{m}\right)^2\right)$$

$$c_1 = \frac{2\pi(2m^*)^{\frac{3}{2}}(k_B T_L)^{\frac{1}{2}}}{\hbar^3\tau_{ace}}$$

$$c_2 = -\frac{8\pi}{3}\frac{(e\varepsilon)^2}{\hbar^3}\frac{(2m^* k_B T_L)^{1/2}}{k_B T_e}\tau_{acm}$$

From (4.7) one can obtain the dependence of the effective electron temperature T_e on the electric field E at any lattice temperature T_L and for any value of its degeneracy parameter $\eta = \frac{\varepsilon_F}{k_B T_L}$.

4.1.3. Comparison of Results and Discussion

It may be noted from (4.7) that the dependence of effective electron temperature on the electric field E for a degenerate ensemble is quite complex and significantly differs from the simple quadratic law which follows for a non-degenerate ensemble.

To make a comparison of the effective electron temperature characteristics with the available experimental and theoretical results, numerical values of T_e for different E as obtained from the present analysis for Ge and InSb are plotted in Figures 4.1 and 4.2 respectively. Some available experimental data [4.6] and the well known results for the non-degenerate material [4.2] are also plotted in the same figures for a ready comparison. The material parameters used for the numerical calculations are given in Table 4.1.

Table 4.1 : Material Parameters

Material	E_1 (eV)	m^*/m_0	u_l (cm/s)	ρ (gm/cc)
Ge	20.29	0.12	5.4×10^{-5}	5.32
InSb	30	0.0145	3.7×10^{-5}	5.77

The characteristics for Ge at lattice temperature of 2,4,10 and 85K and for two values of the degeneracy parameter $\eta = 1$ and 10 are shown in Fig.4.1. In Fig.4.2, the same dependence is plotted for InSb at lattice temperature of 1.35 and 4.2K and for $\eta = 1$ and 5.39.

The Figures 4.1 and 4.2, each drawn in a semi log scale, show that the electron ensemble may be significantly perturbed from the state of thermodynamic equilibrium, starting from lower and lower fields, the lower is the lattice temperature. This is distinctly more so, the lower is the level of degeneracy. A field of the order of just a Vcm^{-1} for Ge and, for InSb, because of the lower effective mass, a much lesser field of the order of a few hundredth of a Vcm^{-1} may appear to be high enough to significantly perturb the electron ensemble at lower lattice temperatures.

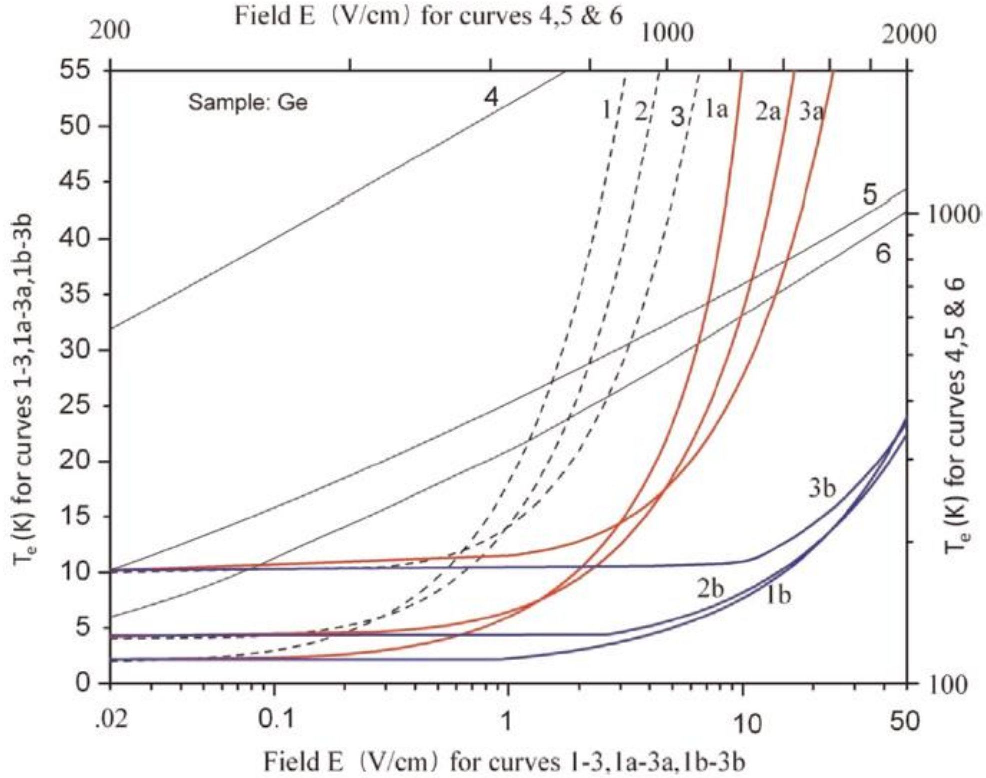

Fig. 4.1.1 : Dependence of the effective electron temperature upon the electric field in Ge at different lattice temperatures and for different values of the degeneracy parameter. The curves 1–3 may be obtained for a non-degenerate ensemble at the lattice temperatures of 2, 4 and 10 K respectively. The curves 1a–3a for $\eta = 5$ and 1b–3b for $\eta = 10$ are obtained from the present theory at the same lattice temperatures respectively. Curves 4–6 are drawn for $T_L = 85$ K; 4 represents the result that follows for a non-degenerate material, 5 is the result obtainable form the present analysis with $\eta = 1.4$, and 6 depicts the experimental data [4.6] for the hot valley till there is no intervalley carrier transfer.

The degeneracy of the material brings in appreciable changes in both the qualitative as well as the quantitative aspects of the electron temperature characteristics. At any lattice temperature the electron temperature assumes lower values for the same field compared to what follows had the degeneracy not been taken into account. As the electric field is increased, the electrons in the degenerate material initially get heated up at a slow rate compared to that in a non-degenerate material. But with the further increase of the field the rate gradually picks up and eventually at higher fields, the temperature of the ensemble tends to increase almost at the same rate, whatever may be the level of the degeneracy.

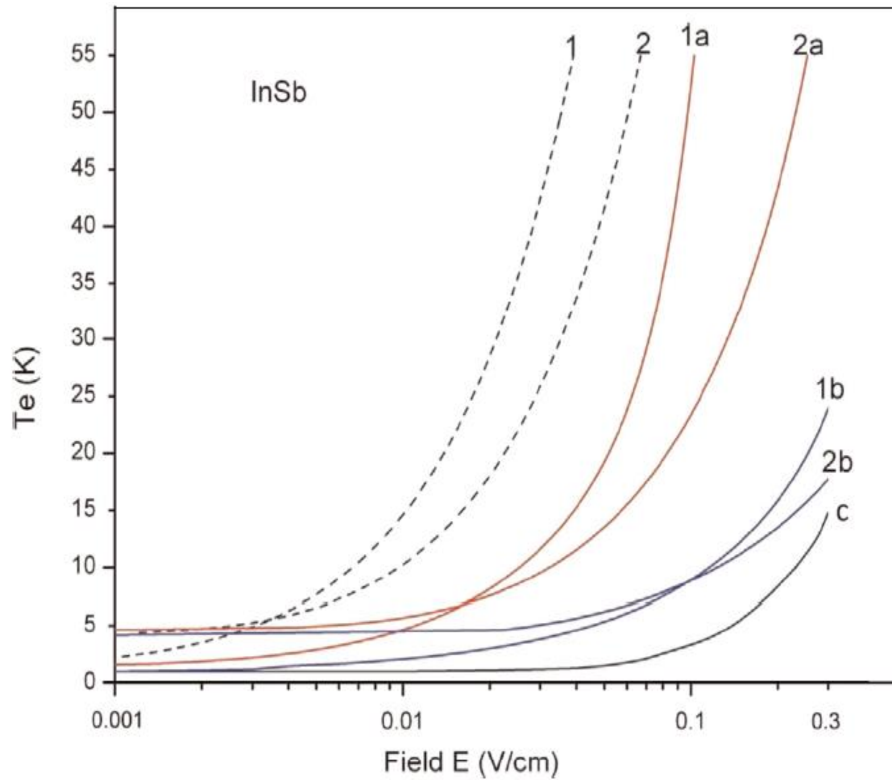

Fig. 4.1.2 : Dependence of the effective electron temperature upon the electric field in InSb at different lattice temperatures and for different values of the degeneracy parameter. Curves 1 and 2 may be obtained for a non-degenerate ensemble at lattice temperatures of 1.35 and 4.2 K respectively. The present theory describes the curves 1a and 2a for η=1 and the curves 1b and 2b for η=5.39, at the same lattice temperatures of 1.35 and 4.2 K respectively. The curve C is the experimental curve [4.6] for T_L = 1.35K and η = 5.39

Further, it may be noted that the same value for the degeneracy parameter η demands greater concentration of the carriers, the greater is the lattice temperature. As the concentration increases the semiconductor tends to be more and more like a metal and hence for higher temperatures the ensemble begins to be heated up at higher fields.

The sample of Ge for which experimental data are available seems to be lightly-degenerate as the effective density of states does not largely exceed the carrier concentration [4.9]. Here $E_d \approx 10^{-2}$eV and the average thermal energy at 85K, the lattice temperature for which the experimental data are available $\approx 7\text{x}10^{-3}$eV. This yields $\eta =$ 1.4. On the other hand, the sample of InSb chosen for the experiment at the lattice temperature of 1.35K is quite degenerate with $\eta = 5.39$. It may be seen that, for both the

materials, the agreement of the electron temperature characteristics which are obtained from the present analysis with the experimental observations is significantly better than that of what follows from the earlier theory where the degeneracy has not been taken into account.

InSb, though not a Wurzite material, shows some piezoelectric effect with a rather small value of the corresponding coupling constant [4.8]. It is well known that the piezoelectric interaction produces cooling of the electron ensemble instead of heating, in the presence of a high field [4.1, 4.2, 4.8]. Hence consideration of the interaction with the piezoelectric phonons along with that with the acoustic phonons, would somewhat bring down the electron temperature at any field, compared to what has been obtained from the present analysis. Hence inclusion of the piezoelectric interaction in the present analysis would result in some more improvement in the agreement with the experimental characteristics. Apart from that, at low lattice temperatures of interest here, the average thermal energy of the electrons may become comparable with the energy of the intravalley acoustic phonons. As such, the electron-phonon interaction becomes inelastic. Again, the equipartition approximation for the phonon distribution is hardly valid under the similar conditions of the low temperature. Moreover, for fields that make the electron temperature exceed the lattice temperature by one order so, the energy losses by $1s \rightarrow 2p$ excitation and ionisation of the neutral impurity atoms need to be taken into account. All these factors may be taken into consideration for further refinement of the present theory [,4.1,4.2, 4.16-4.18].

4.1.4. Conclusion

The transport characteristics of a degenerate semiconductor material in the presence of a relatively high electric field provide data which are useful from the device point of view. For a theoretical analysis of the characteristics one should know the energy distribution function of the degenerate ensemble of carriers in the presence of the high field. In principle, the distribution function can be known from a solution of the transport equation under the prevalent conditions. But in arriving at an analytical solution, one encounters much mathematical difficulties. However, under some physically realistic conditions, the distribution function for a degenerate ensemble in the presence of a relatively high field may be approximated by the Fermi Dirac function at an effective temperature of the electrons. But in that case, the field dependence of the effective temperature of the non-equilibrium carriers in the degenerate material should be made known under the specific conditions of interest.

The aim of the present work has been to make a theoretical study of the effects of degeneracy of the non-equilibrium ensemble of free electrons on the electrical field dependence of the effective electron temperature in a semiconductor, under the condition, when the electrons interact with intravalley acoustic phonons at low lattice temperatures. The methodology has been to arrive at an analytical solution of the energy balance equation of the electron phonon system. The balance equation has been recast taking the finite degeneracy of the ensemble into account. The resultant equation is apparently quite different from what may follow had the degeneracy not been taken into account. In solving the equation, the isotropic part of the non-equilibrium energy distribution of the degenerate ensemble of electrons, in the diffusion approximation, is taken to be the Fermi Dirac function with the effective electron temperature. But, because of the complex nature of the assumed distribution function, the integrations, which occur in the balance equation, could hardly be carried out analytically. As such, the total energy domain is divided in to three regions, demarcated on the two sides of the Fermi energy. The Fermi function for each region is simply approximated in a way that has made it possible to carry out the integrations in closed forms, and thus to arrive at an analytical solution of the energy balance equation. The validity of such simple approximations has been tested to be quite reasonable. It appears that, on using the approximations over the three regions, one can reach at the analytical solution of the balance equation for the degenerate ensemble of non-equilibrium carriers without incurring much error. Obviously, the field dependence of the effective electron temperature, thus obtained, seems to be quite complex and is largely different from what may yield, had the degeneracy factor not been taken into account. The effective electron temperature characteristics thus obtained for Ge and InSb are compared with the available experimental and other theoretical results. The effects of degeneracy of the ensemble on the characteristics are seen to quite significant even for just moderately doped materials. Moreover, for both the materials the agreement of the results which one obtains from the present analysis with the experimental data is significantly better than the same of what follows from the other theory where the finite degeneracy factor has not been taken into consideration. All these results inspire further studies of the transport characteristics of degenerate materials in the presence of relatively high fields, under the condition of low temperature making use of the approximated Fermi function, as has been done here.

4.2. Effective temperature of the non-equilibrium electrons for the combined interaction with the acoustic and the piezoelectric phonons.

4.2.1. Introduction

The results of the effects of degeneracy on the field dependence of the effective temperature T_e of the non-equilibrium electrons under the condition of low lattice temperature T_L ($T_L \leq 20K$) taking into account only the intrinsic interaction of the electrons with deformation potential acoustic phonons are reported in the early section [4.19]. The results which have been reported in [4.19] demonstrate that the consideration of the degeneracy makes the field dependence of T_e, significantly different from what one obtains for a non-degenerate material. Satisfactory agreement of the numerical results for Ge and InSb with the available experimental data has been observed.

However, the III-V compounds, which lack inversion symmetry, are piezoelectric in nature. Such materials, like InSb, InAs, GaN etc are now widely used to fabricate infrared detectors, galvanomagnetic devices, light emitting diodes respectively. The collision (coll) of the electrons with the piezoelectric phonons also makes significant contribution in controlling the electron transport in these materials at relatively lower temperatures. The interaction with high energy phonons like polar optical or intervalley phonons, do not come into consideration at low lattice temperatures of interest here [4.2, 4.19, 4.20]. The importance of piezoelectric interaction in controlling the ohmic transport has already been studied [4.21, 4.22]. The purpose of the present communication is to carry out an analysis of the field dependence of T_e in some degenerate III-V compounds, as controlled by the combined interaction with the acoustic and piezoelectric phonons, at low lattice temperatures. The analysis has been made in the same framework as that in [4.19]. The numerical results obtained for InSb and InAs are compared with other theoretical and available experimental data [4.19-4.20,4.23]. The results reveal the importance of the piezoelectric interaction in controlling the characteristics of the

effective electron temperature in degenerate materials, under the conditions of the low lattice temperature. The results for InSb seem to be in reasonable agreement with the experimental data. Moreover it is also seen, how important is the piezoelectric interaction, in deciding the field dependence of the effective temperature of the electrons.

GaN is also a III-V compound, which has recently been an important material, for the opto-electronic devices. We shall see shortly that the analysis developed here, taking the features of low lattice temperature duly into account are also applicable for higher temperatures. But, this is not true, for the theories developed under the high temperature conditions, that they are also applicable under the condition of low temperature. Hence we have also obtained numerical results for GaN using the theory developed here. It is seen that, in spite of the quite higher values of the piezoelectric coupling constant for GaN, the onset of the electrical non-linearity in the material starts from a higher field, since the effective mass of the material is at least one order higher than that of Indium compounds.

4.2.2. Development

The electric field dependence of the electron temperature $T_e(E)$ for the material, under the prevailing conditions can be determined from a solution of the equation that describes the condition of conservation of the energy of the electron-phonon system. The rate of gain of energy of the electron from the field, balances the rate of loss of energy of the energy of the electrons through collision with the lattice imperfections. The equation is symbolically write as [4.2]

$$\int \frac{\partial f(\vec{k})}{\partial t}\bigg|_{field} \varepsilon d\vec{k} = \sum_j \int \frac{\partial f(\vec{k})}{\partial t}\bigg|_j \varepsilon d\vec{k} \tag{4.8}$$

For the mixed interaction under consideration here, we can write [4.1, 4.2]

$$\sum_j \frac{\partial f(\vec{k})}{\partial t}\bigg|_{j^{th}coll} = \frac{\partial f}{\partial t}\bigg|_{ac} + \frac{\partial f}{\partial t}\bigg|_{pz}$$

where $f(\vec{k})$is the high field distribution function of the electron in the sample of a degenerate III-V compound semiconductor under the condition of low lattice temperature, when the electron simultaneously interact with the intravalley acoustic (ac) and piezoelectric (pz) phonons, $\vec{k}$ is the electron wave vector, $\frac{\partial f(\vec{k})}{\partial t}\Big|_{j^{th}coll}$ is the rate of change of the distribution function due to the jth interaction mechanism, ε , the carrier energy, is assumed to be $\varepsilon = \frac{\hbar^2 k^2}{2m^*}$ and m* is the isotropic effective mass of the electrons. The distribution function, in the diffusion approximation may be written as (4.2).

In order to calculate $\frac{\partial f(\vec{k})}{\partial t}\Big|_{coll}$, for either of the interactions, acoustic or piezoelectric, we consider the four process of absorption and emission of a phonon of wave vector $\vec{q}$, corresponding to the scattering of the electrons into and out of the state $|\vec{k}\rangle$, which results in transition to and from the states $|\vec{k}+\vec{q}\rangle$ and $|\vec{k}-\vec{q}\rangle$. Using the perturbation theory one can write [4.1]

$$\frac{\partial f(\vec{k})}{\partial t}\bigg|_{coll} = \frac{2\pi}{\hbar}\sum_{\vec{q}}\Big[\left|\langle\vec{k}, N_{\vec{q}} \pm 1|H'|\vec{k} \pm \vec{q}, N_{\vec{q}}\rangle\right|^2 \delta\left(\varepsilon_{\vec{k}} - \varepsilon_{\vec{k}\pm\vec{q}} \pm \hbar\omega_{\vec{q}}\right) f(\vec{k} \pm \vec{q})[1 - f(\vec{k})]$$
$$- \left|\langle\vec{k} \pm \vec{q}, N_{\vec{q}} \pm 1|H'|\vec{k}, N_{\vec{q}}\rangle\right|^2 \delta\left(\varepsilon_{\vec{k}\mp\vec{q}} - \varepsilon_{\vec{k}} \pm \hbar\omega_{\vec{q}}\right) f(\vec{k})[1 - f(\vec{k} \pm \vec{q})]\Big]$$

(4.9)

As has already been said, $N_{\vec{q}}$ is the equilibrium distribution function of the phonons, $\omega_{\vec{q}}$ is the angular frequency of the phonon. The upper or the lower sign in the

first term should be taken for the processes of emission and absorption respectively. But the same sign in the second term corresponds to the reverse process [4.1,4.2,4.10-4.14].

When the band edge shifts is linearly dependent upon the strain, one can neglect the spin exchange scattering [4.15]. Hence the matrix elements for the above transitions in the degenerate material remain the same as that of the non-degenerate materials**.**

Thus one can use [4.1, 4.2] for the acoustic interaction

$$\left|\langle\vec{k}, N_{\vec{q}} \pm 1|H'|\vec{k} \pm \vec{q}, N_{\vec{q}}\rangle\right|^2_{ac} = \frac{E_1{}^2\hbar q}{2\rho u_l V}\begin{bmatrix} N_{\vec{q}} \\ N_{\vec{q}} + 1 \end{bmatrix} \tag{4.10}$$

And for the piezoelectric interaction

$$\left|\langle\vec{k}, N_{\vec{q}} \pm 1|H'|\vec{k} \pm \vec{q}, N_{\vec{q}}\rangle\right|^2_{pz} = \frac{e^2\hbar q u_l k_m{}^2}{4Vk^2\epsilon_{sc}}\begin{bmatrix} N_{\vec{q}} \\ N_{\vec{q}} + 1 \end{bmatrix} \tag{4.11}$$

where E_1 is the deformation potential constant, ρ is the density of the material. u_l is the average acoustic velocity, V is the volume of material, e is the electronic charge, k_m is the piezoelectric coupling constant, ϵ_{sc} is the is the static dielectric constant.

Using (4.10) and (4.11) and proceeding in the usual way [4.1, 4.2] one can obtain under the condition when the electrons in the degenerate material are simultaneously scattered by both deformation acoustic and piezoelectric phonons

$$\sum_j \frac{\partial f_0(\vec{k})}{\partial t}\bigg|_j = \left(\frac{W}{\tau_{ace}} + \frac{1}{\tau_{pze}}\right) W^{\frac{1}{2}} \frac{d^2 f_0}{dW^2} + \left[\frac{W^{\frac{1}{2}}(2+W(1-2f_0))}{\tau_{ace}} + \frac{W^{-\frac{1}{2}}(1+W(1-2f_0))}{\tau_{pze}}\right]\frac{\partial f_0}{\partial W} + \left(\frac{2W^{\frac{1}{2}}}{\tau_{ace}} + \frac{W^{-\frac{1}{2}}}{\tau_{pze}}\right)(1-f_0)f_0 \tag{4.12}$$

where $W = \frac{\mathcal{E}}{K_B T_L}$; $\tau_{ace} = \frac{\pi\rho\hbar^4}{2\sqrt{2}\, m^{*5/2} E_1{}^2 (k_B T_L)^{1/2}}$; $\tau_{pze} = \frac{\sqrt{2}\pi\hbar^2\epsilon_{sc}{}^2(k_B T_L)^{1/2}}{m^{*3/2} e^2 k_m{}^2 u_l{}^2}$

It may be noted that for a non-degenerate material, since $f_0 \ll 1$, (4.12) reduces to the well known form given in [4.2].

The rate of change of the distribution function due to the field is given by [4.1,4.2]

$$\left.\frac{\partial f_0(\vec{k})}{\partial t}\right|_{field} = \frac{2}{3}\frac{eE}{\hbar}\mathcal{E}^{-1/2}\frac{d(\mathcal{E}^{3/2}f_1)}{d\mathcal{E}} \quad (4.13)$$

where $$f_1 = \frac{-e\hbar\tau_{eff}}{m^*}\left(\frac{\mathcal{E}}{k_B T_L}\right)^{-1/2} E\frac{\partial f_0}{\partial \mathcal{E}}$$

$$\tau_{eff} = \frac{\tau_{acm}\tau_{pzm}W^{1/2}}{\tau_{pzm}+\tau_{acm}} = \frac{\tau_{acm}W^{1/2}}{1+P}$$

$$P = \frac{\tau_{acm}}{\tau_{pzm}}$$

$$\tau_{acm} = \frac{\pi\rho\hbar^4 u_l^{\,2}}{\sqrt{2}\, m^{*3/2} E_1^{\,2}(k_B T_L)^{3/2}}$$

$$\tau_{pzm} = \frac{2\sqrt{2}\pi\hbar^2\epsilon_{sc}}{e^2\, m^{*1/2}(k_B T_L)^{1/2} k_m^{\,2}}$$

Again, to tide over the difficulty in evaluating the integrations, we use the well tested approximated model of F.D. distribution as has already been done in the previous section of this chapter. The integrals in (4.8) are carried out individually for the three different regions in the limits as specified in the distribution function. The results can be symbolically represented as

$$[I_{coll}]_0^{\beta_1\varepsilon_F} + [I_{coll}]_{\beta_1\varepsilon_F}^{\beta_2\varepsilon_F} + [I_{coll}]_{\beta_2\varepsilon_F}^{\infty} = [I_{field}]_0^{\beta_1\varepsilon_F} + [I_{field}]_{\beta_1\varepsilon_F}^{\beta_2\varepsilon_F} + [I_{field}]_{\beta_2\varepsilon_F}^{\infty} \quad (4.14)$$

where,

$$(I_{coll})_0^{\beta_1 \varepsilon_F} = \sum_{m=1}^{\infty} (-1)^m m^2 \left[\frac{(k_B T_L)^{0.5}}{\tau_{ace} (k_B T_e)^2} \left[Z_1 \exp(X_1) + \frac{6(k_B T_e)^3}{m^4} \exp(-X_2) \right] \right.$$

$$+ \frac{(k_B T_L)^{1.5}}{\tau_{pze} (k_B T_e)^2} \left[Z_2 \exp(X_1) - \frac{2(k_B T_e)^2}{m^3} \exp(-X_2) \right] \Bigg]$$

$$+ \frac{(k_B T_L)^{0.5}}{\tau_{ace} k_B T_e} \left[2 \sum_{m=1}^{\infty} (-1)^m m \left[\left[Z_2 \exp(X_1) - \frac{2(k_B T_e)^2}{m^3} \exp(-X_2) \right] \right. \right.$$

$$- \frac{1}{2 k_B T_L} \left[\left[Z_1 \exp(X_1) + \frac{6(k_B T_e)^3}{m^4} \exp(-X_2) \right] \right.$$

$$+ 2 \sum_{n=1}^{\infty} (-1)^n n \left[Z_3 \exp(X_3) + \frac{6(k_B T_e)^3}{(m+n)^4} \exp(-X_4) \right] \Bigg] \Bigg] \Bigg]$$

$$+ \frac{(k_B T_L)^{1.5}}{\tau_{pze} k_B T_e} \left[\sum_{m=1}^{\infty} (-1)^m m \left[\left[\left[\frac{\beta_1 \varepsilon_F}{m} - \frac{k_B T_e}{m^2} \right] \exp(X_1) + \frac{k_B T_e}{m^2} \exp(-X_2) \right] \right. \right.$$

$$- \frac{1}{k_B T_L} \left[\left[Z_2 \exp(X_1) - \frac{2(k_B T_e)^2}{m^2} \exp(-X_2) \right] \right.$$

$$+ 2 \sum_{n=1}^{\infty} \frac{(-1)^n n}{m} \left[Z_4 \exp(X_3) - \frac{2(k_B T_e)^2}{(m+n)^3} \exp(-X_4) \right] \Bigg] \Bigg] \Bigg]$$

$$- \frac{2}{\tau_{ace} (k_B T_L)^{0.5}} \left[\sum_{m=1}^{\infty} (-1)^m \left[\left[Z_2 \exp(X_1) - \frac{2(k_B T_e)^2}{m^3} \exp(-X_2) \right] \right. \right.$$

$$+ \sum_{n=1}^{\infty} (-1)^n \left[Z_4 \exp(X_3) - \frac{2(k_B T_e)^2}{(m+n)^3} \exp(-X_4) \right] \Bigg] \Bigg]$$

$$- \frac{(k_B T_L)^{0.5}}{\tau_{pze}} \left[\sum_{m=1}^{\infty} (-1)^m m \left[\left[\left[\frac{\beta_1 \varepsilon_F}{m} - \frac{k_B T_e}{m^2} \right] \exp(X_1) + \frac{k_B T_e}{m^2} \exp(-X_2) \right] \right. \right.$$

$$+\sum_{n=1}^{\infty}\left[\frac{\beta_1\varepsilon_F}{m+n}-\frac{k_BT_e}{(m+n)^2}\right]\exp(X_1)+\frac{k_BT_e}{(m+n)^2}\exp(-X_4)\Bigg]\Bigg]$$

$$Z_1=\frac{\left(\beta_1\varepsilon_F\right)^3}{m}-\frac{3k_BT_e\left(\beta_1\varepsilon_F\right)^2}{m^2}+\frac{6\beta_1\varepsilon_F(k_BT_e)^2}{m^3}-\frac{6(k_BT_e)^3}{m^4}$$

$$Z_2=\frac{\left(\beta_1\varepsilon_F\right)^2}{m}-\frac{2k_BT_e\beta_1\varepsilon_F}{m^2}+\frac{2(k_BT_e)^2}{m^3}$$

$$Z_3=\frac{\left(\beta_1\varepsilon_F\right)^3}{(m+n)}-\frac{3k_BT_e\left(\beta_1\varepsilon_F\right)^2}{(m+n)^2}+\frac{6\beta_1\varepsilon_F(k_BT_e)^2}{(m+n)^3}-\frac{6(k_BT_e)^3}{(m+n)^4}$$

$$Z_4=\frac{\left(\beta_1\varepsilon_F\right)^2}{(m+n)}-\frac{2k_BT_e\beta_1\varepsilon_F}{(m+n)^2}+\frac{2(k_BT_e)^2}{(m+n)^3}$$

$$X_1=\frac{m(\beta_1-1)\varepsilon_F}{k_BT_e}$$

$$X_2=\frac{m\varepsilon_F}{k_BT_e}$$

$$X_3=\frac{(m+n)(\beta_1-1)\varepsilon_F}{k_BT_e}$$

$$X_4=\frac{(m+n)\varepsilon_F}{k_BT_e}$$

$$(I_{coll})_{\beta_1\varepsilon_F}^{\beta_2\varepsilon_F} = \frac{(k_BT_L)^{0.5}D}{\tau_{ace}k_BT_e}\left[\frac{2}{3}\left(\beta_2^3-\beta_1^3\right)\varepsilon_F{}^3 - \frac{2D}{5k_BT_L}\left(\beta_2^5-\beta_1^5\right)\varepsilon_F{}^5 + \frac{D\varepsilon_F}{2k_BT_L}\left(\beta_2^4-\beta_1^4\right)\varepsilon_F{}^4\right]$$

$$+\frac{(k_BT_L)^{1.5}D}{\tau_{pze}k_BT_e}\left[0.5\left(\beta_2^2-\beta_1^2\right)\varepsilon_F{}^2 - \frac{D}{2k_BT_L}\left(\beta_2^4-\beta_1^4\right)\varepsilon_F{}^4\right.$$

$$\left.+\frac{2D\varepsilon_F}{3k_BT_L}\left(\beta_2^3-\beta_1^3\right)\varepsilon_F{}^3\right]$$

$$+\frac{2}{\tau_{ace}(k_BT_L)^{0.5}k_BT_e}\left[\frac{1}{12}\left(\beta_2^3-\beta_1^3\right)\varepsilon_F{}^3 - \frac{D^2}{5}\left(\beta_2^5-\beta_1^5\right)\varepsilon_F{}^5\right.$$

$$\left.+\frac{1}{2}D^2\left(\beta_2^4-\beta_1^4\right)\varepsilon_F{}^5 - \frac{D^2}{3}\left(\beta_2^3-\beta_1^3\right)\varepsilon_F{}^5\right]$$

$$+\frac{(k_BT_L)^{0.5}}{\tau_{pze}k_BT_e}\left[\frac{\left(\beta_2^2-\beta_1^2\right)\varepsilon_F{}^2}{8} - \frac{D^2}{4}\left(\beta_2^4-\beta_1^4\right)\varepsilon_F{}^4 + \frac{2D^2}{3}\left(\beta_2^3-\beta_1^3\right)\varepsilon_F{}^4\right.$$

$$\left.-0.5D^2\left(\beta_2^2-\beta_1^2\right)\varepsilon_F{}^4\right]$$

$$(I_{coll})^{\infty}_{\beta_2\varepsilon_F} = \sum_{m=1}^{\infty}(-1)^{m+1}m^2\left[\left[\frac{(k_BT_L)^{0.5}}{\tau_{ace}(k_BT_e)^2}[Z_5\exp(X_5)] + \frac{(k_BT_L)^{1.5}}{\tau_{pze}(k_BT_e)^2}[Z_6\exp(X_5)]\right]\right.$$

$$-\frac{(k_BT_L)^{0.5}}{\tau_{ace}k_BT_e}\left[\left[\frac{2}{m}Z_6\exp(X_5)\right]\right.$$

$$\left.\left.+\frac{1}{k_BT_L}\left[\frac{Z_5\exp(X_5)}{m} + \frac{2}{m^2}\sum_{n=1}^{\infty}(-1)^n n[Z_7\exp(X_6)]\right]\right]\right]$$

$$-\frac{(k_BT_L)^{1.5}}{\tau_{pze}k_BT_e}\left[\frac{1}{m}\left[\frac{\beta_2\varepsilon_F}{m} + \frac{k_BT_e}{m^2}\right]\exp(X_5)\right.$$

$$\left.+\frac{1}{k_BT_L}\left[\frac{Z_6\exp(X_5)}{m} + \frac{2}{m^2}\sum_{n=1}^{\infty}(-1)^n n[Z_7\exp(X_6)]\right]\right]$$

$$+\frac{2}{(k_BT_L)^{0.5}\tau_{ace}}\left[\frac{Z_6\exp(X_5)}{m^2} + \frac{1}{m^2}\sum_{n=1}^{\infty}(-1)^n[Z_7\exp(X_6)]\right]$$

$$+\frac{(k_BT_L)^{0.5}}{\tau_{pze}}\left[\frac{1}{m^2}\left[\frac{\beta_2\varepsilon_F}{m} + \frac{k_BT_e}{m^2}\right]\exp(X_5)\right.$$

$$\left.\left.+\frac{1}{m^2}\sum_{n=1}^{\infty}(-1)^n\left[\frac{\beta_2\varepsilon_F}{m+n} + \frac{k_BT_e}{(m+n)^2}\right]\exp(X_6)\right]\right]$$

$$Z_5 = \frac{(\beta_2\varepsilon_F)^3}{m} + \frac{3k_BT_e(\beta_2\varepsilon_F)^2}{m^2} + \frac{6\beta_2\varepsilon_F(k_BT_e)^2}{m^3} + \frac{6(k_BT_e)^3}{m^4}$$

$$Z_6 = \frac{(\beta_2\varepsilon_F)^2}{m} + \frac{2k_BT_e\beta_2\varepsilon_F}{m^2} + \frac{2(k_BT_e)^2}{m^3}$$

$$Z_7 = \frac{(\beta_2\varepsilon_F)^3}{(m+n)} + \frac{3k_BT_e(\beta_2\varepsilon_F)^2}{(m+n)^2} + \frac{6\beta_2\varepsilon_F(k_BT_e)^2}{(m+n)^3} + \frac{6(k_BT_e)^3}{(m+n)^4}$$

$$X_5 = \frac{-m(\beta_2 - 1)\varepsilon_F}{k_B T_e}$$

$$X_6 = \frac{-(m+n)(\beta_2 - 1)\varepsilon_F}{k_B T_e}$$

$$D = \frac{\exp\left[\frac{(\beta_1 - 1)\varepsilon_F}{k_B T_e}\right] - \exp\left[\frac{(\beta_2 - 1)\varepsilon_F}{k_B T_e}\right]}{(\beta_2 - \beta_1)\varepsilon_F\left[1 + \exp\left[\frac{(\beta_1 - 1)\varepsilon_F}{k_B T_e}\right]\right]\left[1 + \exp\left[\frac{(\beta_2 - 1)\varepsilon_F}{k_B T_e}\right]\right]}$$

$$\begin{aligned}
(I_{field})_0^{\beta_1\varepsilon_F} = \sum_{m=1}^{\infty}(-1)^m m \Bigg[\Bigg[\frac{(\beta_1\varepsilon_F)^3}{Y_{21}}\exp(X_1) \\
&- \exp\left[\frac{-m}{k_B T_e}(Y_{11} + \varepsilon_F)\right]\Bigg[[Y_{21} - Y_{11}]^2\left[\ln Y_{21} + \sum_{k=1}^{\infty}\left(\frac{m}{k_B T_e}\right)^k \frac{{Y_{21}}^k}{k.k!}\right] \\
&- {Y_{21}}^2[\ln Y_{21} - 0.5] + 2Y_{11}Y_{21}[\ln Y_{21} - 1] \\
&- 2\sum_{k=1}^{\infty}\left(\frac{m}{k_B T_e}\right)^k\left[\frac{{Y_{21}}^{k+2}}{k(k+2)k!} - \frac{Y_{11}{Y_{21}}^{k+1}}{k(k+1)k!}\right]\Bigg]\Bigg] \\
&+ \exp\left[\frac{-m}{k_B T_e}(Y_{11} + \varepsilon_F)\right]\Bigg[-{Y_{11}}^2[\ln Y_{11} - 0.5] + 2{Y_{11}}^2[\ln Y_{11} - 1] \\
&- 2\sum_{k=1}^{\infty}\left(\frac{m}{k_B T_e}\right)^k\left[\frac{{Y_{11}}^{k+2}}{k(k+2)k!} - \frac{{Y_{11}}^{k+2}}{k(k+1)k!}\right]\Bigg]\Bigg]
\end{aligned}$$

$Y_{11} = Pk_B T_L$; $Y_{21} = \beta_1\varepsilon_F + Y_{11}$

$$(I_{field})_{\beta_1\varepsilon_F}^{\beta_2\varepsilon_F} = D\,k_BT_e\left[\left[\frac{(\beta_2\varepsilon_F)^3}{\beta_2\varepsilon_F+Y_{11}} - \frac{(\beta_1\varepsilon_F)^3}{\beta_1\varepsilon_F+Y_{11}}\right] - 0.5\left[(\beta_2\varepsilon_F+Y_{11})^2 - (\beta_1\varepsilon_F+Y_{11})^2\right]\right.$$

$$\left. + 2Y_{11}\varepsilon_F(\beta_2-\beta_1) - {Y_{11}}^2\left[\ln(\beta_2\varepsilon_F+Y_{11}) - \ln(\beta_1\varepsilon_F+Y_{11})\right]\right]$$

$$(I_{field})_{\beta_2\varepsilon_F}^{\infty} = \sum_{m=1}^{\infty}(-1)^m m\left[\frac{(\beta_2\varepsilon_F + n\,k_BT_e)^3}{\beta_2\varepsilon_F + n\,k_BT_e + Y_{11}}\exp(X_8)\right.$$

$$- \exp\left[\frac{-m}{k_BT_e}(Y_{11}+\varepsilon_F)\right]\left[[Y_{23}-Y_{11}]^2\left[\ln Y_{23} + \sum_{k=1}^{\infty}\left(\frac{m}{k_BT_e}\right)^k\frac{{Y_{23}}^k}{k.\,k!}\right]\right.$$

$$- {Y_{23}}^2[\ln Y_{23} - 0.5] + 2Y_{11}Y_{23}[\ln Y_{23} - 1]$$

$$\left.\left. - 2\sum_{k=1}^{\infty}\left(\frac{m}{k_BT_e}\right)^k\left[\frac{{Y_{23}}^{k+2}}{k(k+2)k!} - \frac{Y_{11}{Y_{23}}^{k+1}}{k(k+1)k!}\right]\right]\right]$$

$$- \frac{(\beta_2\varepsilon_F)^3}{\beta_2\varepsilon_F+Y_{11}}\exp[-m(\beta_2-1)\,{}^{\varepsilon_F}/_{k_BT_e}]$$

$$+ \exp\left[\frac{-m}{k_BT_e}(Y_{11}+\varepsilon_F)\right]\left[-{Y_{13}}^2[\ln Y_{13} - 0.5] + 2Y_{11}Y_{13}[\ln Y_{13} - 1]\right.$$

$$- 2\sum_{k=1}^{\infty}\left(\frac{m}{k_BT_e}\right)^k\left[\frac{{Y_{13}}^{k+2}}{k(k+2)k!} - \frac{Y_{11}{Y_{13}}^{k+1}}{k(k+1)k!}\right]$$

$$\left.\left. + [Y_{13}-Y_{11}]^2\left[\ln Y_{13} + \sum_{k=1}^{\infty}\left(\frac{m}{k_BT_e}\right)^k\frac{{Y_{13}}^k}{k.\,k!}\right]\right]\right]$$

$$Y_{13} = \beta_2\varepsilon_F + Y_{11}\,;\ \ Y_{23} = \beta_2\varepsilon_F + n\,k_BT_e + Y_{11}\ \ ;\ \ X_8 = -m(\beta_2-1)\,\varepsilon_F/\,k_BT_e + n$$

From (4.14) one can obtain the dependence of the effective electron temperature T_e on the electric field E at any lattice temperature $T_L$and for any value of the degeneracy

parameter $\eta = \frac{\varepsilon_F}{k_B T_L}$, taking into account the combined interaction of the electrons with the acoustic and the piezoelectric phonons.

4.2.3. Results

By solving the energy balance equation for the electron-phonon system in a moderately degenerate compound semiconductor, we have obtained the electric field dependence of the effective electron temperature, under the conditions of low lattice temperatures. At the low temperatures, the electrons are dominantly scattered simultaneously by the acoustic and the piezoelectric phonons, and the electrons may get heated up at relatively low fields. The Fermi function at the effective electron temperature has been approximated in a way, that facilitates the analytical solution of the problem without any serious loss of accuracy.

It appears from the results that the field dependence of the effective temperature is quite complex if the degeneracy of the ensemble is taken into account. To make a comparison of the field dependence which is obtained here, with the available theoretical and experimental results we have numerically calculated the values of T_e for different values of E, considering various samples of InSb, InAs and GaN with the material parameters given in Table 4.2. The results are plotted in figures 4.2.1, 4.2.2 and 4.2.3 respectively. To facilitate a ready comparison we have also plotted in each figure, the same field dependence at different lattice temperatures for (a) a non-degenerate material, (b) a degenerate material when the electrons are scattered only by acoustic phonons, (c) a degenerate material when the electrons suffer mixed scattering with the acoustic and the piezoelectric phonons. Different levels of degeneracy have been considered. Moreover, the figures are supplemented by the experimental results, wherever, they are available for the prevalent conditions of our interest here.

Table 4.2 : Material Parameters

Materials	m*/m	u_l(m/sec)	ρ(kg/m^3)	K_m^2	ϵ_r	E_1 (eV)	$P\vert_{4.2K}$
InSb	0.014	3.7×10^3	5.78×10^3	7.29×10^3	17.54	20	3.55
InAs	0.022	3.09×10^3	5.61×10^3	2.882×10^3	14.54	5.8	8.36
GaN	0.2	5×10^3	6.1×10^3	3.2×10^3	9.5	8	242.01

4.2.4. Discussion

On comparing the curves 1(a) with 3(a) and 3(b), and 1(b) with 3(c) and 3(d), it may be seen that the consideration of the degeneracy of the ensemble brings in significant qualitative, as well as quantitative changes in the field dependence of the effective electron temperature. As the degeneracy is increased, the ensemble requires higher fields to attain the same electron temperature. Moreover, for the non-degenerate ensemble, the rise in the electron temperature with the electric field is quite slow initially, and then the rate of increase picks up fast. Whereas, for the degenerate ensembles, the rate of increase of the electron temperature with the electric field is much regular, following almost like a power law, from the beginning.

On comparing the curves 2(a) with 3(a), 2(b) with 3(b), 2(c) with 3(c) and 2(d) with 3(d), one can also see, how important is it to consider the contribution of the piezoelectric interaction, which brings in even more significant changes in the field dependence characteristics, compared to what is brought about by the degeneracy, particularly for the lower fields. For InSb, comparing the curve 3(d) with the available experimental curve, marked Exp [4.23] one can see that, for lower fields, the agreement

of the results obtained from our analysis with the experimental values seems to be quite satisfactory. At high fields however, the experimental curve gives lower values of the electron temperature. This is possibly, due to the fact that the interaction with the optical phonons starts contributing more and more to determine the field dependence of the effective electron temperature, as the field increases. It has already been said that such contribution has not been taken into account in our analysis, which has been developed here under the condition of low lattice temperature.

For InAs however, the experimental results that are available in the literature [4.23], are for highly degenerate ensembles. But, our theory assumes that the materials are only moderately degenerate. For the case of highly degeneracy, the theory, which has been developed here need to be modified accordingly. Hence, in the absence of suitable experimental data under the prevalent conditions of interest here, the results for InAs could not be compared with the experimental data.

It can be seen from Table 4.2, that the piezoelectric coupling constant for GaN is nearly two orders of magnitude higher and the effective mass of the electrons is one order higher than those of the Indium compounds. Hence, this makes it difficult to get a convergent result for GaN unless the temperature is increased accordingly, say around 77K or more, so as to reduce the influence of the piezoelectric interaction in determining the field dependence of the electron temperature. As such, the filed dependence characteristics for GaN has been calculated for T_L=77K and 300K. It may also be seen that due to the higher values of the lattice temperature and the effective mass, the electron ensemble in GaN requires higher fields to be sufficiently heated up. There being absence of any experimental data of the field dependence of the effective electron temperature under the conditions of interest here, we could not compare the theoretical results for GaN with the experimental data. However, comparing Fig. 4.2.3 with Fig. 4.2.1 and Fig. 4.2.2, it may be seen that the qualitative nature of the characteristics of field dependence of the electron temperature in GaN remains almost the same as that for the Indium compounds.

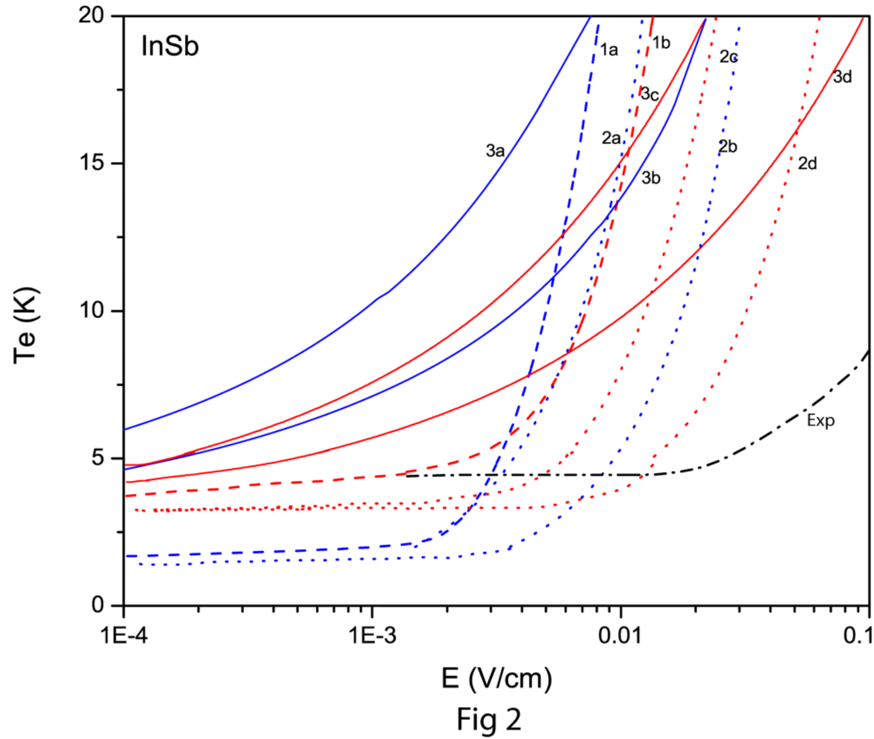

Fig. 4.2.1 : Dependence of effective electron temperature upon electric field in InSb. Curves 1a and 1b show the dependence when the electrons are simultaneously scattered by acoustic and piezoelectric phonons in a non-degenerate sample at 1.35K and 4.2K respectively. Curves 2a-2b and 2c-2d show the dependence when the electrons are scattered by only acoustic phonons in a degenerate sample at 1.35K and 4.2K respectively. Curves 3a-3b and 3c-3d show the dependence when the electrons are simultaneously scattered by acoustic and piezoelectric phonons in a degenerate sample at 1.35K and 4.2K respectively. Curves marked a and b, and c and d are the results when the degeneracy factor η=1.35 and 5.39 respectively. The curve marked 'Exp' represents the available experimental data [4.24].

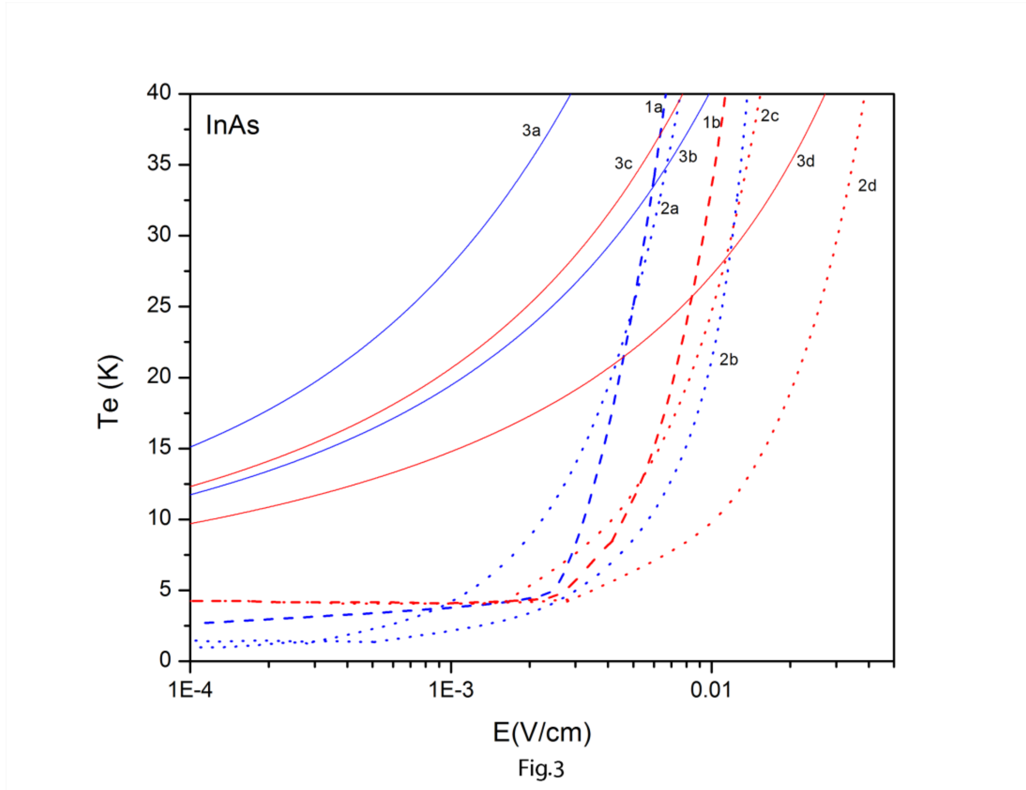

Fig. 4.2.2 : Dependence of effective electron temperature upon electric field in InAs. Curves 1a and 1b show the dependence when the electrons are simultaneously scattered by acoustic and piezoelectric phonons in a non-degenerate sample at 1.35K and 4.2K respectively. Curves 2a-2b and 2c-2d show the dependence when the electrons are scattered by only acoustic phonons in a degenerate sample at 1.35K and 4.2K respectively. Curves 3a-3b and 3c-3d show the dependence when the electrons are simultaneously scattered by acoustic and piezoelectric phonons in a degenerate sample at 1.35K and 4.2K respectively. Curves marked a and b, and c and d are the results when the degeneracy factor η=1.35 and 5.39 respectively.

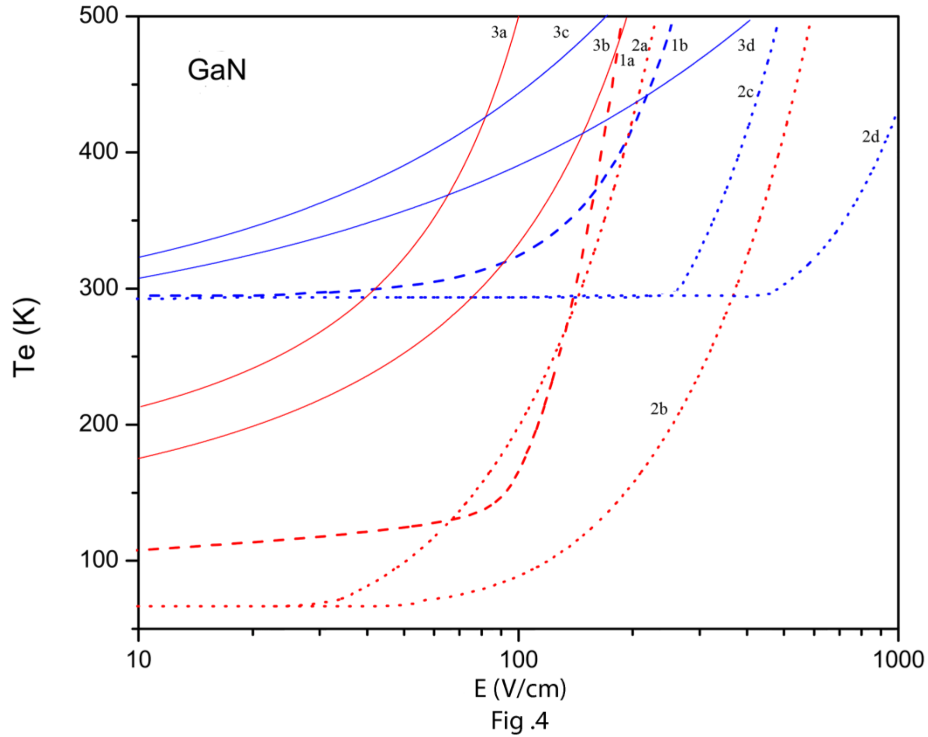

Fig. 4.2.3 : Dependence of effective electron temperature upon electric field in GaN. Curves 1a and 1b show the dependence when the electrons are simultaneously scattered by acoustic and piezoelectric phonons in a non-degenerate sample at 77K and 300K respectively. Curves 2a-2b and 2c-2d show the dependence when the electrons are scattered by only acoustic phonons in a degenerate sample at 77K and 300K respectively. Curves 3a-3b and 3c-3d show the dependence when the electrons are simultaneously scattered by acoustic and piezoelectric phonons in a degenerate sample at 77K and 300K respectively. Curves marked a and b, and c and d are the results when the degeneracy factor η=1.35 and 5.39 respectively.

4.2.5. Conclusion

This present communication is an analytical study of the effects of degeneracy on the electrical field dependence characteristics of the effective electron temperature of some III-V compound semiconductors under the condition when the lattice temperature is

low and the electrons interact simultaneously with both the intravalley acoustic and the piezoelectric phonons. The energy balance equation has been recast to incorporate the effects of degeneracy using Pauli's exclusion principle. Traditionally the high field energy distribution function of the electrons in the degenerate materials is assumed to be given by the FD distribution function at the field dependent effective temperature of the electrons. Due to the intrinsic complexity of the FD distribution, the integrals that one encounters in solving the energy balance equation for the degenerate ensemble of electrons, are hardly amenable to analytical evaluation. So they are usually evaluated taking recourse to some oversimplified approximations. These approximations do hardly hold good for the degenerate ensembles, and so compromise with the physical validity of the results. To tide over such difficulties, an effective, and well tested, approximate model of FD distribution has been chosen. This choice makes it possible to carry out the integrals easily, without taking recourse to such undue approximations which one has to make when dealing with actual FD function. Thus the analytical solution of the energy balance equation is obtained quite easily for the degenerate ensemble of non-equilibrium carriers without incurring much error.

The field dependence of the effective electron temperature in degenerate semiconductors thus obtained under the conditions of low lattice temperature seems to be quite complex, and is largely different from what may yield, had the degeneracy factor not been taken into account. It may also be seen from the figures that, when the interaction with the piezoelectric phonons is also considered apart from that with the deformation acoustic phonons, significant qualitative as well as quantitative changes in the electron temperature characteristics are effected over the lower ranges of the electric field and of the lattice temperature. The degenerate ensemble of electrons now interacting simultaneously with both the intravalley acoustic and the piezoelectric phonons at low lattice temperatures, gets heated up for even smaller values of the electric field due to the intrinsic unstable feature of the piezoelectric interaction. However at higher fields, the characteristics for the combined interaction tend to that due to the acoustic interaction

only, as the importance of the piezoelectric interaction reduces more and more. This picture continues till the lattice temperature and the field is high enough so that the interaction with the polar optical phonons begins to be more and more important. Thus the effects of the piezoelectric scattering of electrons under the condition of low lattice temperature in controlling the field dependent effective temperature characteristics are revealed.

It is well known that the piezoelectric interaction of the electrons is more important at lower lattice temperatures. Similarly, the degeneracy of the ensemble is also a low-temperature feature. Both of these features have been considered in the present analysis. But under the conditions of low temperature other low temperature features should also come into play.

At low temperature, the average thermal energy of the electrons may become comparable with the phonon energy. As such, the electron-phonon collision becomes inelastic. Moreover, the equipartition approximation for the phonon distribution is hardly valid at low temperatures where the true phonon distribution needs to be taken into account. Since the materials which we have considered here, are assumed to be degenerate, the electron concentration is quite high. So the electrostatic screening of the scattering potential should also be taken into account to develop the theory of electrical transport in degenerate materials, under the condition of low lattice temperature. All this factors should be given due consideration for the refinement of the present theory. It is hardly possible to account for each and every aspects of low temperature at a time. Each factor needs to be considered separately. However, the results obtained here being quite interesting, it encourages one to proceed with further work in the same field.

Moreover, the database resulting from such theoretical studies on the hot electron characteristics in degenerate compound semiconductors under the condition of low lattice temperature would be of importance for the device technologist.

References:

[4.1] E. M. Conwell, High Field Transport in Semiconductors ,Academic Press, New York (1967).

[4.2] B. R. Nag, Theory of Electrical Transport in Semiconductors, Pergamon Press, Oxford (1972).

[4.3] S. H. Koenig, R. D. Brown and W. Schillinger, Phys. Rev. 128 1668 (1962).

[4.4] A. Zylbersztjn, Phys. Rev. 127 744 (1962).

[4.5] Z. S. Kachlishvili, Phys. Stat. Sol. (a) 33 15 (1976).

[4.6] G.Bauer, Springer Tracts in Modern Physics 74 ,Springer, Berlin, Heidelberg, New York (1974).

[4.7] J. S. Blackemore, Semiconductor Statistics ,Pergamon Press, Oxford (1962).

[4.8] B. R. Nag, Electron Transport in Compound Semiconductors ,Springer, Berlin, Heidelberg, New York (1980).

[4.9] S.M. Sze, Physics of Semiconductors Devices, Wiley Eastern Limited, New Delhi, (1983).

[4.10] M. S. Sodha and B. M. Gupta, Phys Rev. B 1 3993 (1970).

[4.11] S.Midday, D.P. Bhattacharya, Physica B 458 18 (2015).

[4.12] S.Midday, D.P. Bhattacharya, Phys. Scr. 83 025702 (2011).

[4.13] S.N.Patra, D.P. Bhattacharya, Physica B 325 17 (2003).

[4.14] S.N.Patra, D.P. Bhattacharya, Physical Review B 52 4651 (1995).

[4.15] W. Shockley, Electrons and Holes in Semiconductors ,Van Nostrand, Princeton, N.J (1950).

[4.16] Jaroslav Karlovsky, Phys. Rev. 127 419 (1962).

[4.17] C.Kittel, Elementary Statistical Physics ,John Wiley & Sons, Inc., New York, (1958.

[4.18] Z.S. Kachhlishvili , Phys. Stat. Sol. (b) 43 6 (1971).

[4.19] B. Das, A. Basu, J. Das, D.P. Bhattacharya, Phys. B 474 21 (2015).

[4.20] G. Bauer, Springer Tracts in Modern Physics Springer, Berlin, Heidelberg, New York (1974).
[4.21] P.K. Basu, B.R. Nag, Phys. Rev. B 22 4849 (1980).
[4.22] P.K. Basu, B.R. Nag, J. Phys. C: Solid State Phys. 14 1519 (1981).
[4.23] B. Das, A. Basu, J. Das, D.P. Bhattacharya, Can. J. Phys. 95 167 (2017).
[4.24] J.P. Maneval, A. Zylbersztein, H.F. Budd, Phys. Rev. Letters 23 848 (1969).
[4.25] G. Bauer, H.Kahlert, Phys.Rev. B 5 566 (1972).

CHAPTER V

Phonon growth characteristics in a degenerate semiconductor at low lattice temperatures

5.1. Phonon growth rate for the interaction of the electrons with the acoustic phonons.

5.1.1. Introduction

In the presence of a relatively high electric field, the electron ensemble in a semiconductor may be significantly perturbed from the state of thermodynamic equilibrium with the lattice atoms. In such a perturbed state, the non equilibrium electrons attain a field dependant effective temperature $T_e$that exceeds the lattice temperature T_L. As a result, the electrical non-linearity may set in and the prevalent experimental conditions determine the required field [5.1-5.2]. For example, n-Ge or InSb may exhibit such non-linearity even for a field of a fraction of V/cm or less, under the conditions of low lattice temperature $T_L \leq 20K$.

When the lattice temperature is low, the electrons predominantly interact with the acoustic mode lattice vibrations. The scattering of the electrons with the impurities being elastic, it would hardly effect on the energy balance of the electron-phonon system [5.1]. Under the condition when the electrons become hot ($T_e > T_L$), they emit more phonons

than what they absorb in an interval, thereby making a finite growth of the phonon number $N_{\vec{q}}$ ($\vec{q}$ being the phonon wave vector) with the time [5.3-5.4].

The purpose of this analysis is to obtain the phonon-growth characteristics in the degenerate materials under the condition of low lattice temperatures, taking due account of the inelasticity of the interactions of the electrons with the acoustic phonons, and the true phonon distribution. The calculations have been carried out in the light of the model F.D. distribution function [5.2,5.5], as has been discussed in Chapter-III. The results thus obtained are then compared with the rough estimation of the same characteristics that uses the exact form of the F.D distribution but takes recourse to oversimplified approximations [5.6]. The numerical results have been obtained for the various degenerate samples of Si.

5.1.2. Development

Let, the non-equilibrium electrons in a volume V of a degenerate material interact with the intravalley acoustic phonons and there be electronic transition between the wave vector states $|\vec{k}\rangle$ and $|\vec{k}+\vec{q}\rangle$ with attendant emission and absorption of a phonon. On using the model F.D. distribution one can evaluate the phonon growth rate $\left(\frac{\partial N_{\vec{q}}}{\partial t}\right)$ from the time dependent perturbation theory [5.3]

$$\frac{\partial N_{\vec{q}}}{\partial t} = \frac{2\pi}{\hbar}\sum_{\vec{k}}\left|M(\vec{k},\vec{k}+\vec{q})\right|^2 \delta\left(\varepsilon_{\vec{k}}, N_{\vec{q}}+1-\varepsilon_{\vec{k}+\vec{q}}, N_{\vec{q}}\right) f(\vec{k}+\vec{q})\left[1-f(\vec{k})\right] - \left|M(\vec{k}+\vec{q},\vec{k})\right|^2 \delta\left(\varepsilon_{\vec{k}+\vec{q}}, N_{\vec{q}}-1-\varepsilon_{\vec{k}}, N_{\vec{q}}\right) f(\vec{k})\left[1-f(\vec{k}+\vec{q})\right] \tag{5.1}$$

The square of the matrix element for the transition is given by [5.3]

$$\left|M(\vec{k},\vec{k}+\vec{q})\right|^2 = \frac{E_1^2\hbar q}{2V\rho u_l}\begin{bmatrix} N_{\vec{q}} \\ N_{\vec{q}}+1 \end{bmatrix} \tag{5.2}$$

where, E_1 is the deformation potential constant, ρ is the density of the material, $\hbar = \frac{h}{2\pi}$; h being the Planck's constant and u_l is the acoustic velocity of the electrons. To account for

the contributions from all the electrons of the ensemble, one needs to sum up over the wave vector states $\vec{k}$. The non-equilibrium distribution function $f(\vec{k})$ can usually be expressed as a sum of the spherically symmetric term $f_0(\varepsilon)$ and a negligibly small additional term which gives the asymmetry in the field direction [5.3].

Now the wave vector $\vec{k}$ may be expressed in terms of the spherical polar coordinates k, θ and ∅ with the phonon wave vector $\vec{q}$ aligned along the z-axis. Taking the spin degeneracy into account, and integrating over the polar and azimuthal angles, and converting the summation over k into an integration over energy ε one can obtain for the degenerate ensemble

$$\frac{\partial N_{\vec{q}}}{\partial t} = \frac{E_1^2 m^{*2}}{2\pi\rho\hbar^4 u_l}\int_{\varepsilon_0}^{\infty}\left[\left(N_{\vec{q}}+1\right)f_0\left(\vec{k}+\vec{q}\right)\left\{1-f_0\left(\vec{k}\right)\right\}-N_{\vec{q}}f_0\left(\vec{k}\right)\left\{1-f_0\left(\vec{k}+\vec{q}\right)\right\}\right]d\varepsilon \qquad (5.3)$$

With due regard to the prevalent features of low temperature, $N_{\vec{q}}$ is given by the true phonon distribution without truncation to the equipartition approximation : $N_{\vec{q}} = (e^x - 1)^{-1}$ where $x = \frac{\hbar u_l q}{k_B T_L}$, and ε_0 may be obtained from the energy and momentum balance equations for the electron-phonon system as $\varepsilon_0 = \frac{\hbar^2}{2m^*}\left(\frac{q}{2} - \frac{m^* u_l}{\hbar}\right)^2$. Now using the approximated F.D. distribution, the integrals in eq.(5.3) giving the contribution of each region to $\left(\frac{\partial N_{\vec{q}}}{\partial t}\right)$ can be evaluated easily without making any approximation. Thus one may obtain

$$\left(\frac{\partial N_x}{\partial t}\right)_{deg} = \frac{E_1^2 m^{*2}}{2\pi\rho\hbar^4 u_l}\sum_{i=1}^{3} I_{Reg.i} \qquad (5.4)$$

where

$I_{Reg.1} = I_1 - I_2 - I_3$ and

$$I_1 = (N_x + 1)\left[\varepsilon_0' + (\beta_2 - \beta_1)\varepsilon_F\left\{\frac{1}{2} + \frac{c}{2}(\beta_2 + \beta_1)\varepsilon_F - ck_BT_L(\eta - x)\right\} + k_BT_e\left\{\sum_{m=1}^{\infty}\frac{(-1)^m}{m}(A - B) + \sum_{m=1}^{\infty}\sum_{n=1}^{\infty}\frac{(-1)^m}{n!}\left(\frac{mx}{T_n}\right)^n(A - (-1)^n B)\right\}\right]$$

$$I_2 = N_x\left[\varepsilon_0' + (\beta_2 - \beta_1)\{1 + c\varepsilon_F(\beta_2 - 1)\}\frac{\varepsilon_F}{2} + k_BT_e\sum_{m=1}^{\infty}\frac{(-1)^m}{m}(A - B)\right]$$

$$I_3 = \varepsilon_0' + k_BT_e\left[2\sum_{m=1}^{\infty}\frac{(-1)^m}{m}A + \sum_{l=1}^{\infty}\sum_{n=1}^{\infty}\frac{(-1)^l}{n!}l^{(n-1)}\left(\frac{x}{T_n}\right)^n A + \sum_{m=1}^{\infty}\sum_{l=1}^{\infty}\frac{(-1)^{(m+l)}}{(m+l)}\left\{1 + \sum_{n=1}^{\infty}\frac{1}{n!}\left(\frac{lx}{T_n}\right)^n\right\}(D + G)\right] + \frac{1}{3c}(F_1^3 - F_2^3) + \frac{1}{2}xk_BT_Lc(\beta_2 - \beta_1)\varepsilon_F\{1 + (\beta_2 + \beta_1 - 2)c\varepsilon_F\}$$

$I_{Reg.2} = I_4 - I_5 - I_6$ and

$$I_4 = (N_x + 1)\left[\varepsilon_0''\left\{\frac{c}{2}(\beta_2\varepsilon_F + \varepsilon_{02}) + \frac{1}{2} - ck_BT_L(\eta - x)\right\} + k_BT_e\sum_{m=1}^{\infty}\frac{(-1)^{(m+1)}}{m}\left\{1 + \sum_{n=1}^{\infty}\frac{(-1)^n}{n!}\left(\frac{mx}{T_n}\right)^n\right\}B\right]$$

$$I_5 = N_x\left[\varepsilon_0''\left\{\frac{c}{2}(\beta_2\varepsilon_F + \varepsilon_{02}) + \frac{1}{2} - c\varepsilon_F\right\} + k_BT_e\sum_{m=1}^{\infty}\frac{(-1)^{(m+1)}}{m}B\right]$$

$$I_6 = \frac{1}{3c}\left(H_1{}^3 - H_2{}^3\right) + xk_BT_Lc\varepsilon_0'' \left[\frac{1}{2} - c\varepsilon_F + \frac{c}{2}(\beta_2\varepsilon_F + \varepsilon_{02})\right] + k_BT_e \sum_{m=1}^{\infty}\sum_{l=1}^{\infty} \frac{(-1)^{(m+l)}}{(m+l)}\left[1 + \sum_{n=1}^{\infty}\frac{1}{n!}\left(\frac{lx}{T_n}\right)^n\right] G$$

$I_{Reg.3} = I_7 - I_8 - I_9$ and

$$I_7 = (N_x + 1)k_BT_e \sum_{m=1}^{\infty} \frac{(-1)^{(m+1)}}{m}\left[1 + \sum_{n=1}^{\infty}\frac{(-1)^n}{n!}\left(\frac{mx}{T_n}\right)^n\right] J$$

$$I_8 = N_xk_BT_e \sum_{m=1}^{\infty} \frac{(-1)^{(m+1)}}{m} J$$

$$I_9 = k_BT_e \sum_{m=1}^{\infty}\sum_{l=1}^{\infty} \frac{(-1)^{(m+l)}}{(m+l)}\left[1 + \sum_{n=1}^{\infty}\frac{1}{n!}\left(\frac{lx}{T_n}\right)^n\right] L$$

where,

$\varepsilon_0{}' = \beta_1\varepsilon_F - \varepsilon_{01}$; $\varepsilon_0{}'' = \beta_2\varepsilon_F - \varepsilon_{02}$

$A = e^{m(\beta_1-1)\eta/T_n} - e^{m(\varepsilon_{01}-\varepsilon_F)/k_BT_e}$; $\varepsilon_{01} < \varepsilon_F$

$B = e^{-m(\beta_1-1)\eta/T_n}$

$$C = \frac{e^{\frac{(\beta_1-1)\eta}{T_n}} - e^{\frac{(\beta_2-1)\eta}{T_n}}}{\left[1+e^{\frac{(\beta_2-1)\eta}{T_n}}\right]\left[1+e^{\frac{(\beta_1-1)\eta}{T_n}}\right][\beta_2-\beta_1]\varepsilon_F}$$ [5.2,5.5]

$D = e^{(m+l)(\beta_1-1)\eta/T_n} - e^{(m+l)(\varepsilon_{01}-\varepsilon_F)/k_BT_e}$; $\varepsilon_{01} < \beta_1\varepsilon_F$

$F_1 = \frac{1}{2} - c\varepsilon_F(1-\beta_2)$; $F_2 = \frac{1}{2} - c\varepsilon_F(1-\beta_1)$

$G = e^{-(m+l)(\beta_2-1)\eta/T_n}$

$H_1 = \frac{1}{2} - c\varepsilon_F(1-\beta_2)$; $H_2 = \frac{1}{2} - c(\varepsilon_F - \varepsilon_{02})$; $\beta_1\varepsilon_F \lesssim \varepsilon_{02} \lesssim \beta_2\varepsilon_F$

$J = e^{-m(\varepsilon_{03}-\varepsilon_F)/k_B T_e}$; $\varepsilon_{03} > \beta_2\varepsilon_F$

$L = e^{-(m+l)(\varepsilon_{03}-\varepsilon_F)/k_B T_e}$; $\varepsilon_{03} > \beta_2\varepsilon_F$

The limiting value of the energy ε_0 for the three regimes are designated respectively as ε_{01}, ε_{02} and ε_{03}.

$\eta = \frac{\varepsilon_F}{k_B T_e}$ and $\frac{T_e}{T_L} = T_n$

It may be noted that the integrals that occurred could easily be carried out analytically, and the resultant series in each case are fast converging.

The results of the theoretical analysis on the effects of the finite energy of the deformation acoustic phonons and the true phonon distribution on the phonon growth rate obtained earlier for the non-degenerate materials under the similar conditions of low temperature may be quoted here for a ready reference [5.3].

$$\left(\frac{\partial N_x}{\partial t}\right)_{non-deg} = \frac{E_1^2 m^{*2}}{2\pi\rho\hbar^4 u_l} k_B T_e e^{\eta}\left[1 + \left(N_q + 1\right)\sum_{j=1}^{\infty}\frac{\left(-\frac{x}{T_n}\right)^j}{j!}\right]\exp[-a(x-b)^2] \qquad (5.5)$$

where $a = \frac{k_B T_L}{8m^* {u_l}^2 T_L}$; $b = \frac{2m^* {u_l}^2}{k_B T_L}$

The rate of increase of the number of phonons for the non-degenerate materials seems to be quite smoothly varying with the phonon wave vector x, actually decreasing with the increase of the same. The effect is more pronounced the lower the value of T_n.

5.1.3. Results and Discussions

The phonon growth characteristics as obtained in eq.(5.4) calculated here for the degenerate materials in the framework of the proposed $f_0(\varepsilon)$, the symmetric part of the non-equilibrium distribution function as given in Chapter III, and without making oversimplified assumptions, may now be normalized to eq.(5.5) giving $\left(\frac{\partial N_x}{\partial t}\right)_{norm}$.

For numerical results, we consider Si with the following parameters: $E_1 = 9.0\text{eV}$; $\rho = 2.329 \times 10^3\ \text{kgm}^{-3}$; u_l=9.037$\times 10^3\ \text{ms}^{-1}$; $m^* = 0.32m_0$; m_0 being the free electron mass. The dependence of $\left(\frac{\partial N_x}{\partial t}\right)_{norm}$ upon x thus obtained here for different values of the lattice temperature T_L and normalized electron temperature T_n are plotted in Figures 5.1 and 5.2 for the degeneracy parameter $\frac{\varepsilon_F}{k_B T_L}$ = 5 and 15 respectively. The same results as obtained earlier in [5.6] are also reproduced in the same figures to facilitate a ready comparison.

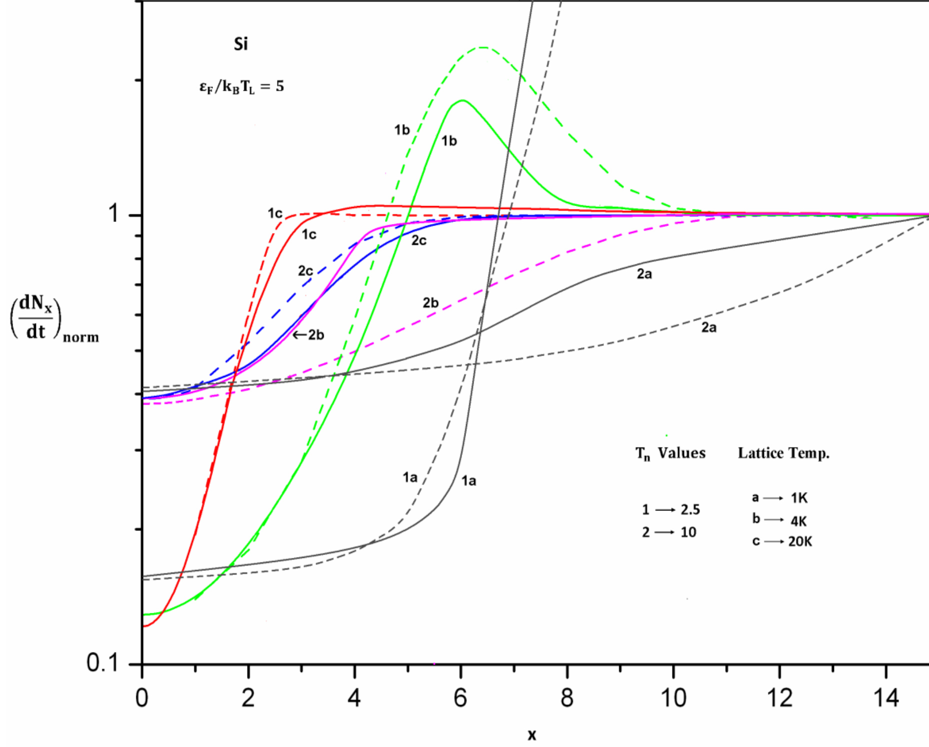

Fig. 5.1 : For the degeneracy parameter $\frac{\varepsilon_F}{k_B T_L} = 5$ the dependence of the phonon growth rate $\left(\frac{\partial N_x}{\partial t}\right)_{deg}$ as normalized to the rate $\left(\frac{\partial N_x}{\partial t}\right)_{non-deg}$, upon the phonon wave vector x, in a sample of Si for different values of the lattice temperature T_L and the normalized electron temperature T_n. The curves 1 and 2 are for T_n= 2.5 and 10 respectively, and those marked a, b and c correspond to the lattice temperature of 1, 4 and 20K respectively. The continuous curves represent the results obtained from the present analysis and the dotted curves are the estimated results of [5.6].

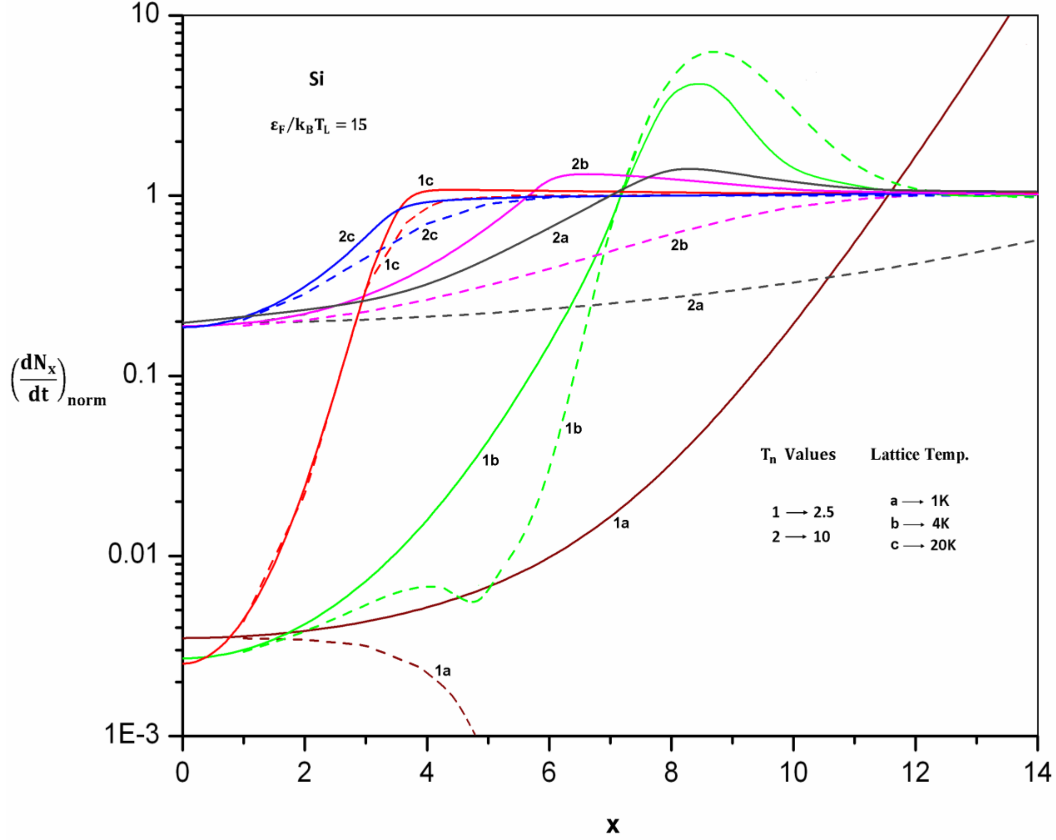

Fig. 5.2 : For the degeneracy parameter $\frac{\varepsilon_F}{k_B T_L} = 15$ the dependence of the phonon growth rate $\left(\frac{\partial N_x}{\partial t}\right)_{deg}$ as normalized to the rate $\left(\frac{\partial N_x}{\partial t}\right)_{non-deg}$, upon the phonon wave vector x, in a sample of Si for different values of the lattice temperature T_L and the normalized electron temperature T_n. The curves 1 and 2 are for T_n= 2.5 and 10 respectively, and those marked a, b and c correspond to the lattice temperature of 1, 4 and 20K respectively. The continuous curves represent the results obtained from the present analysis and the dotted curves are the estimated results of [5.6].

From the figures, one can notice that the present analysis made in the light of the proposed form of $f_0(\varepsilon)$ and without having to take recourse to oversimplified approximations, predicts phonon growth characteristics which are significantly different from what has been obtained earlier in [5.6]. The present analysis brings in both qualitative and quantitative change in $\left(\frac{\partial N_x}{\partial t}\right)_{norm}$. The effective changes are more pronounced, the lower the lattice temperature or higher the degeneracy parameter $\frac{\varepsilon_F}{k_B T_L}$,

particularly for the long wavelength phonons, i.e. over the lower range of x. For the lower values of x, the relative changes in the $\left(\frac{\partial N_x}{\partial t}\right)$ characteristics are mainly brought about by the degeneracy factor. However, as x increases the effects of inelasticity of the interaction and true phonon distribution are exhibited more and more.

The phonon growth characteristics for the degenerate materials, which have been obtained here from the proposed model of $f_0(\varepsilon)$, are also significantly different from what has been observed earlier for the non-degenerate materials under the same low temperature conditions [5.3]. However, as expected, the dependence of the phonon growth rate upon x, that follows from present analysis still remains quite smooth, unlike what the earlier approximated analysis [5.6] which is based on the F.D. distribution predicts. There is hardly any physical reason why should such under shoot immediately followed by overshoot in the growth characteristics occur at low temperatures for lower values of x. Obviously they are exhibited due to the use of the oversimplified approximations in [6]. Hence the results of the phonon growth rate as obtained here with the help of the proposed model for the distribution function $f_0(\varepsilon)$ seem to be more realistic and prompt its further use for the development of the low temperature transport theory in the degenerate materials.

In the regime of low temperature of interest here ($T_L \lesssim 20K$) the thermal energy available to excite optical mode lattice vibrations is quite limited since the optical phonons have characteristic temperature higher than 300K [5.3,5.7,5.8]. Hence we have neglected the interaction of the electrons with the optical phonons in the present analysis. However, at higher temperatures the interaction with the optical phonons needs to be taken into account to study the electron cooling due to the coupling of electrons to the optical phonons. For such interaction $\left(\frac{\partial N_q}{\partial t}\right)$ is to be calculated afresh, obviously after replacing the expression (5.2) for the matrix elements. Moreover, the vibrational dispersion curve for the acoustic mode has been assumed to be linear here and we have put $\hbar\omega_q = \hbar u_l q$. But in case of optical mode, the dispersion can be neglected and one should put $\hbar\omega_q = \hbar\omega_0$, where ω_0 is the angular frequency for optical phonons and is supposed to be a constant independent of q. However, the results obtained here being realistic stimulate for further development of the theory.

5.2. Phonon growth rate for the combined interaction of the electrons with the acoustic and the piezoelectric phonons.

5.2.1. Introduction

Under the experimental conditions, there may be mixed scattering of the carriers in a semiconductor. For example, in the compound semiconductors, which lack inversion symmetry, the carriers are scattered simultaneously by the intravalley acoustic (ac.) and the piezoelectric (pz.) phonons under the condition when the lattice temperature is low. It is well known that the interaction with the piezoelectric phonons makes significant contribution to the process of electrical transport when the lattice temperature is low [5.1]. Though such semiconductor compounds are polar in nature, the interaction with the polar optical phonons may contribute in the transport process only when the lattice temperature is high and a sufficiently large number of polar optical phonons may be generated.

There are a number of devices like infrared detectors, galvanomagnetic devices, light emitting diodes etc which make use of piezoelectric semiconductors [5.7]. The importance of the piezoelectric interaction relative to that of the deformation potential scattering of electrons in controlling the ohmic transport characteristics has already been studied [5.3,5.9,5.10]. The purpose of the present theory is to make an analysis of the effects of piezoelectric interaction of the non-equilibrium electrons on the phonon growth characteristics in a degenerate compound semiconductor under the condition of low lattice temperature. The analysis uses the same model distribution function of the non-equilibrium electrons, as that used in [5.2,5.5] and described in Chapter III and takes due account of the inelasticity of the electron-phonon collisions and of the true phonon distribution. The similar analysis for a non-degenerate semiconductor is also added here as a special case. Numerical results are obtained for InSb. The results clearly demonstrate the importance of the piezoelectric scattering in determining the phonon growth characteristics under the condition of low lattice temperature.

5.2.2. Development

Let us consider a degenerate (deg.) ensemble of non-equilibrium electrons in a volume V of a compound semiconductor. When the lattice temperature is low, the electrons are simultaneously scattered by the acoustic and the piezoelectric phonons. In the process of scattering due to interaction with any of the phonons, an electron makes transition between the wave vectors states $|\vec{k}\rangle$ and $|\vec{k}+\vec{q}\rangle$ through either emission or absorption of a phonon of wave vector $\vec{q}$.

From the time-dependent perturbation theory it follows that the phonon growth rate $\left(\frac{\partial N_{\vec{q}}}{\partial t}\right)$, when the degeneracy is taken into consideration, may be expressed symbolically as eq.(5.1) [3]. Here $\left|M\left(\vec{k},\vec{k}+\vec{q}\right)\right|^2$, the square of the matrix element for the piezoelectric interaction is given by [5.3,5.7,5.9,5.10]

$$\left|M\left(\vec{k},\vec{k}+\vec{q}\right)\right|^2 = \frac{e^2 {k_m}^2 \hbar u_l}{2V\epsilon_{sc} q}\frac{q^2}{2k^2}\begin{bmatrix} N_{\vec{q}} \\ N_{\vec{q}}+1 \end{bmatrix} \tag{5.6}$$

where e is the electronic charge, k_m is the piezoelectric coupling constant, ϵ_{sc} is the permittivity of the material.

Since the electrons under the conditions of interest here, are mainly confined to a short segment of the energy dispersion curve near the minima of the conduction band, the nature of the curve around there, can be regarded as parabolic. Thus the analysis is carried out using a parabolic, spherically symmetric, conduction band without any serious loss of accuracy [5.11].

The summation over $\vec{k}$ in eq.(5.1) when converted to an integral taking the spin degeneracy into account, and integrating over the polar and azimuthal angles [5.3] one obtains for piezoelectric scattering of the electrons

$$\left[\left(\frac{\partial N_{\vec{q}}}{\partial t}\right)_{pz.}\right]_{deg.} = \frac{e^2 {k_m}^2 m^* u_l}{8\pi\epsilon_{sc}\hbar^2}\int_{\varepsilon_0}^{\varepsilon'}\frac{1}{\varepsilon}\left[\left(N_{\vec{q}}+1\right)f_0\left(\vec{k}+\vec{q}\right) - N_{\vec{q}}f_0\left(\vec{k}\right) - f_0\left(\vec{k}\right)f_0\left(\vec{k}+\vec{q}\right)\right]d\varepsilon \tag{5.7}$$

The limits of the integration may be established from the energy and momentum balance conditions with due regard to the inelasticity of the collisions of the electron-phonon system. Thus the lower limit $\varepsilon_0 = \frac{\hbar^2}{2m^*}\left(\frac{q}{2} - \frac{m^* u_l}{\hbar}\right)^2$. To obtain a convergent result, the upper limit ε' may be set to a quite high value of energy, say $\varepsilon' = pk_B T_e$ where p may be chosen to be $p \geq 15$ or so, instead of infinity. This will not incur much error, as there will be an insignificant number of electrons which have energies higher than ε'[5.12].

Moreover, as has already been said, under the conditions of low lattice temperature, the full phonon distribution should be taken for $N_{\vec{q}}$ as its truncation to the equipartition law is no longer possible. Thus, $N_{\vec{q}} = (e^x - 1)^{-1}$, where $x\left(= \frac{\hbar u_l q}{k_B T_L}\right)$ is the normalized phonon wave vector.

Now, making use of the model distribution as proposed in [5.5] one can carry out the integration in eq.(5.7) in a closed form without making any oversimplified approximations. For the representation of the model distribution, the energy axis is divided into three domains : $0 < \varepsilon < \beta_1 \varepsilon_F$; $\beta_1 \varepsilon_F < \varepsilon < \beta_2 \varepsilon_F$ and $\beta_2 \varepsilon_F < \varepsilon < \infty$. The parameters $\beta_1 \lesssim 1$ and $\beta_2 \gtrsim 1$ which may be chosen as $\beta_1 = 1 - \frac{k_B T_L}{\varepsilon_F}$ and $\beta_2 = 1 + \frac{k_B T_L}{\varepsilon_F}$ [5.12]. For the first and third domains, $f_0(\varepsilon)$ has been approximated with the help of some exponential function [5.2,5.5]. For the second narrow domain, $f_0(\varepsilon)$ is, however, approximated by some linear function as done by Karlovsky [5.13].

Obviously the value of $q\left(= \frac{x\, k_B T_L}{\hbar u_l}\right)$ determines the domain to which the lower limit ε_0 belongs. The position of ε_0 on the energy axis, again determines the contributions of the domains to the value of $\left[\left(\frac{\partial N_{\vec{q}}}{\partial t}\right)_{pz.}\right]_{deg.}$. Thus one obtains from eq.(5.7)

$$\left[\left(\frac{\partial N_{\vec{q}}}{\partial t}\right)_{pz.}\right]_{deg.} = A_{pz} \mathcal{J}(x) \tag{5.8}$$

where, $A_{pz} = \frac{e^2 {k_m}^2 m^* u_l}{8\pi \epsilon_{sc} \hbar^2}$. Depending upon the position of ε_0 on the energy axis, the function $\mathcal{J}(x)$ assumes different forms over different ranges of x.

For $0 < x < x_1$: $\mathcal{J}(x) = I_{10}(x) - I_{11}(x) - I_{12}(x)$

where $x_1 = \frac{2u_l}{k_B T_L}\left[m^* u_l + \sqrt{2m^*(\eta - 1)k_B T_L}\right]$; and

$$I_{10}(x) = \left(N_q + 1\right)\left[\ln\left(\frac{\beta_1 \varepsilon_F}{\varepsilon_{01}}\right) + \sum_{m=1}^{\infty}(-1)^m \left\{1 + \sum_{n=1}^{\infty}\frac{1}{n!}\left(\frac{mx}{T_n}\right)^n\right\} A' e^{-\frac{m\eta}{T_n}} + \{0.5 - C(\varepsilon_F - x k_B T_L)\}\ln\left(\frac{\beta_2}{\beta_1}\right) + C\varepsilon_F(\beta_2 - \beta_1) + \sum_{m=1}^{\infty}(-1)^{m+1} e^{\frac{m\eta}{T_n}}\left\{1 + \sum_{n=1}^{\infty}\frac{1}{n!}\left(-\frac{mx}{T_n}\right)^n\right\} B'\right]$$

$$I_{11}(x) = N_q\left[\ln\left(\frac{\beta_1 \varepsilon_F}{\varepsilon_{01}}\right) + \sum_{m=1}^{\infty}(-1)^m A' e^{-\frac{m\eta}{T_n}} + (0.5 - C\varepsilon_F)\ln\left(\frac{\beta_2}{\beta_1}\right) + C\varepsilon_F(\beta_2 - \beta_1)\sum_{m=1}^{\infty}(-1)^{m+1} e^{\frac{m\eta}{T_n}} B'\right]$$

$$I_{12}(x) = \ln\left(\frac{\beta_1 \varepsilon_F}{\varepsilon_{01}}\right) + \sum_{m=1}^{\infty}(-1)^m e^{-\frac{m\eta}{T_n}}\left\{2 + \sum_{n=1}^{\infty}\frac{1}{n!}\left(\frac{mx}{T_n}\right)^n\right\} A' + \sum_{m=1}^{\infty}\sum_{n=1}^{\infty}(-1)^{m+n} e^{-\frac{(m+n)\eta}{T_n}}\left\{1 + \sum_{l=1}^{\infty}\frac{1}{l!}\left(-\frac{nx}{T_n}\right)^l\right\} A'' + \left\{\frac{1}{4} - C\varepsilon_F(C\varepsilon_F - 1)\right\}\ln\left(\frac{\beta_2}{\beta_1}\right) + C\varepsilon_F(\beta_2 - \beta_1)\{0.5C\varepsilon_F(\beta_2 + \beta_1) + 2 - 2C\varepsilon_F\} + \sum_{n=1}^{\infty}\frac{(x k_B T_L)^n}{n!}\frac{C}{2}(1 + 2\varepsilon_F)\ln\left(\frac{\beta_2}{\beta_1}\right) + \sum_{m=1}^{\infty}\sum_{n=1}^{\infty}(-1)^{m+n} e^{\frac{(m+n)\eta}{T_n}}\left\{1 + \sum_{l=1}^{\infty}\frac{1}{l!}\left(-\frac{nx}{T_n}\right)^l\right\} B''$$

For $x_1 < x < x_2$: $\mathcal{I}(x) = I_{13}(x) - I_{14}(x) - I_{15}(x)$

where $x_2 = \frac{2u_l}{k_B T_L}\left[m^* u_l + \sqrt{2m^*(\eta+1)k_B T_L}\right]$; and

$$I_{13}(x) = \left(N_q + 1\right)\left[\{0.5 - C(\varepsilon_F - x k_B T_L)\}\ln\left(\frac{\beta_2\varepsilon_F}{\varepsilon_{02}}\right) + C(\beta_2\varepsilon_F - \varepsilon_{02}) + \sum_{m=1}^{\infty}(-1)^{m+1}e^{\frac{m\eta}{T_n}}\left\{1 + \sum_{n=1}^{\infty}\frac{1}{n!}\left(-\frac{mx}{T_n}\right)^n\right\}B'\right]$$

$$I_{14}(x) = N_q\left[(0.5 - C\varepsilon_F)\ln\left(\frac{\beta_2\varepsilon_F}{\varepsilon_{02}}\right) + C(\beta_2\varepsilon_F - \varepsilon_{02}) + \sum_{m=1}^{\infty}(-1)^{m+1}\,e^{\frac{m\eta}{T_n}}B'\right]$$

$$I_{15}(x) = \left\{\frac{1}{4} + C\varepsilon_F(C\varepsilon_F - 1)\right\}\ln\left(\frac{\beta_2\varepsilon_F}{\varepsilon_{02}}\right) + C(\beta_2\varepsilon_F - \varepsilon_{02})\{0.5C(\beta_2\varepsilon_F + \varepsilon_{02}) + 2 - 2C\varepsilon_F\} + \sum_{n=1}^{\infty}\frac{(x k_B T_L)^n}{n!}\frac{C}{2}(1 + 2\varepsilon_F)\ln\left(\frac{\beta_2\varepsilon_F}{\varepsilon_{02}}\right) + \sum_{m=1}^{\infty}\sum_{n=1}^{\infty}(-1)^{m+n}\,e^{\frac{(m+n)\eta}{T_n}}\left\{1 + \sum_{l=1}^{\infty}\frac{1}{l!}\left(-\frac{nx}{T_n}\right)^l\right\}B''$$

and for $x_2 < x < \infty$: $\mathcal{I}(x) = I_{16}(x) - I_{17}(x) - I_{18}(x)$

where

$$I_{16}(x) = \left(N_q + 1\right)D'\left[1 + \sum_{n=1}^{\infty}\frac{1}{n!}\left(-\frac{mx}{T_n}\right)^n\right]$$

$$I_{17}(x) = N_q D'$$

$$I_{18}(x) = \sum_{m=1}^{\infty}\sum_{n=1}^{\infty}(-1)^{m+n}\,e^{\frac{(m+n)\eta}{T_n}}\left[1 + \sum_{l=1}^{\infty}\frac{1}{l!}\left(-\frac{nx}{T_n}\right)^l\right]E$$

Here,

$$A' = \ln\left(\frac{\beta_1 \varepsilon_F}{\varepsilon_{01}}\right) + \sum_{k=1}^{\infty} \frac{\left(\frac{m\beta_1\eta}{T_n}\right)^k - \left(\frac{m\varepsilon_{01}}{k_B T_e}\right)^k}{k.k!}$$

$$A'' = \ln\left(\frac{\beta_1 \varepsilon_F}{\varepsilon_{01}}\right) + \sum_{k=1}^{\infty} \frac{\left\{\frac{(m+n)\beta_1\eta}{T_n}\right\}^k - \left\{\frac{(m+n)\varepsilon_{01}}{k_B T_e}\right\}^k}{k.k!}$$

$$B' = \ln\left(1 + \frac{\alpha T_n}{\beta_2 \eta}\right) + \sum_{k=1}^{\infty} \frac{\left\{-\frac{m(\beta_2\varepsilon_F + \varepsilon')}{k_B T_e}\right\}^k - \left\{-\frac{m\beta_2\eta}{T_n}\right\}^k}{k.k!}$$

$$B'' = \ln\left(1 + \frac{\alpha T_n}{\beta_2 \eta}\right) + \sum_{k=1}^{\infty} \frac{\left\{-\frac{(m+n)(\beta_2\varepsilon_F + \varepsilon')}{k_B T_e}\right\}^k - \left\{-\frac{(m+n)\beta_2\eta}{T_n}\right\}^k}{k.k!}$$

$$D' = \sum_{m=1}^{\infty} (-1)^{m+1} e^{\frac{m\eta}{T_n}} \left[\ln\left(1 + \frac{\varepsilon'}{\varepsilon_{03}}\right) + \sum_{k=1}^{\infty} \frac{\left\{-\frac{m(\varepsilon_{03} + \varepsilon')}{k_B T_e}\right\}^k - \left\{-\frac{m\varepsilon_{03}}{k_B T_e}\right\}^k}{k.k!}\right]$$

$$E = \left[\ln\left(1 + \frac{\varepsilon'}{\varepsilon_{03}}\right) + \sum_{k=1}^{\infty} \frac{\left\{-\frac{(m+n)(\varepsilon_{03} + \varepsilon')}{k_B T_e}\right\}^k - \left\{-\frac{(m+n)\varepsilon_{03}}{k_B T_e}\right\}^k}{k.k!}\right]$$

and the constant C is given by [4.2,4.55]

$$C = \frac{e^{\frac{(\beta_1 - 1)\eta}{T_n}} - e^{\frac{(\beta_2 - 1)\eta}{T_n}}}{\left[1 + e^{\frac{(\beta_2 - 1)\eta}{T_n}}\right]\left[1 + e^{\frac{(\beta_1 - 1)\eta}{T_n}}\right][\beta_2 - \beta_1]\varepsilon_F}$$

The phonon growth rate in a degenerate semiconductor under the condition when the electrons interact only with the acoustic phonons, has already been analyzed in the same framework under the similar conditions of low temperature elsewhere [5.2]. Putting

these two rates together, one can obtain the effective growth rate characteristics as controlled by the combined interaction of the non-equilibrium electrons with the acoustic and piezoelectric phonons in a degenerate semiconductor at the low lattice temperature.

As a special case one can consider a non-degenerate (n-deg.) semiconductor, for which $f_0(\vec{k})$ may be assumed to be Maxwellian function with the effective electron temperature T_e. Since $f_0(\vec{k})$ is now much smaller than 1 [5.1], the third term of the integrand in eq.(5.7) may be neglected. Thus carrying out the integration in eq.(5.7) one can obtain the phonon growth rate for the non-degenerate ensemble of carriers for interaction only with piezoelectric phonons.

$$\left[\left(\frac{\partial N_{\vec{q}}}{\partial t}\right)_{pz.}\right]_{n-deg.} = A_{pz}\left(\frac{n_0}{N_c}\right)\left[1+\left(N_q+1\right)\sum_{m=1}^{\infty}\frac{(-1)^m}{m!}\left(\frac{x}{T_n}\right)^m\right]\left[\ln\left(\frac{\varepsilon'}{\varepsilon_0}\right)+\sum_{n=1}^{\infty}\frac{(-1)^n}{n.n!}(k_B T_e)^{-n}\{(\varepsilon')^n-(\varepsilon_0)^n\}\right] \quad (5.9)$$

where, n_0 is the concentration of electrons in the non-degenerate material and $N_c(T_e) = \frac{2(2\pi m^* k_B T_e)^{3/2}}{8\pi^3\hbar^3}$.

Similar analysis for the phonon growth characteristics of a non-degenerate ensemble of electrons, under the condition when the electrons interact only with the acoustic phonons, has already been made [5.14]. Putting together the rates given by eq.(5.9) and that reported in [5.14], one can obtain the effective phonon growth rate characteristics in a non-degenerate ensemble for the combined interaction of the electrons at low lattice temperatures.

Still again, under the condition of high lattice temperature, when the electron-phonon collisions become elastic, one can indeed neglect the phonon energy in comparison to the average thermal energy of the carriers. Apart from that, the phonon distribution can now be truncated to the equipartition (eq.) law. Taking these high temperature features into account, one can obtain the phonon growth rate for piezoelectric interaction of the electrons in the non-degenerate material by carrying out the integral in eq.(5.7), after neglecting the third, product term, and assuming $f_0(\varepsilon)$ to be Maxwellian at effective electron temperature T_e. It is given by

$$\left[\left(\frac{\partial N_{\vec{q}}}{\partial t}\right)_{pz.}\right]_{n-deg.,eq.} = A_{pz}\left(\frac{n_0}{N_c}\right)\left(1-\frac{1}{T_n}\right)\left[\ln\left\{\frac{8m^* u_l^2 \varepsilon'}{(xk_B T_L)^2}\right\} + \sum_{n=1}^{\infty}\frac{(-1)^n}{n.n!}(k_B T_e)^{-n}\left\{(\varepsilon')^n - \left\{\frac{(xk_B T_L)^2}{8m^* u_l^2 \varepsilon'}\right\}^n\right\}\right] \tag{5.10}$$

It is easy to see that the same result also follows from eq.(5.9) as one makes use of the approximations which are valid for high lattice temperatures.

Under the same condition of high temperature, the phonon growth rate for interaction with the acoustic phonons in a non-degenerate semiconductor viz. $\left[\left(\frac{\partial N_{\vec{q}}}{\partial t}\right)_{ac.}\right]_{n-deg.,eq.}$ has already been analysed in [5.3]. Hence adding them up, one can obtain the effective phonon growth characteristic for the combined interaction of the electrons in a non-degenerate semiconductor under the condition of high lattice temperature.

5.2.3. Results and Discussions

In the case of degenerate materials, one can get the effective phonon growth rate for the combined interaction by adding eq.(5.8) with the similar expression for $\left[\left(\frac{\partial N_{\vec{q}}}{\partial t}\right)_{ac.}\right]_{deg.}$ as reported in [5.2]. Likewise, by adding eq.(5.9) with the expression for $\left[\left(\frac{\partial N_{\vec{q}}}{\partial t}\right)_{ac.}\right]_{n-deg.}$ as reported in [5.14], one can obtain the effective growth rate for the combined interaction in a non-degenerate material. Each of the expressions has been obtained with the identical tenets of development. Since the expressions are apparently quite complex, it is hardly possible to decipher the salient features of the dependence of the effective rate of phonon growth upon x, under different conditions in respect of the lattice temperature, the effective electron temperature (which is determined by the applied electric field), and the level of degeneracy. Hence the numerical results are calculated for degenerate samples of InSb at the lattice temperatures T_L of 4K and 20K and for the normalized electron temperature T_n of 2.5 and 10 for each lattice temperature. We have chosen only moderately doped samples having η = 5 and 15. However, for the non-degenerate samples, the numerical results are calculated at the lattice temperatures T_L of 300K, 77K and also 4K, and for the same values of T_n of 2.5 and 10, as that have been chosen for the degenerate samples.

The results are represented by the Figures 5.3, 5.4 and 5.5, each drawn on a semi-log scale. The horizontal axis of the figures is customarily taken to represent $x\left(=\frac{\hbar u_l q}{k_B T_L}\right)$. Hence any point on this axis corresponds to a value of q, that is directly proportional to T_L . It is well known that the electrons strongly interact only with long wavelength phonons for which one can assume a linear lattice dispersion law i.e. $\omega_q = u_l q$ [5.3]. It is easy to see that the chosen range of x and the lattice temperatures ensures that our figures here, comfortably covers the long wavelength range of the phonons, and also sufficient number of such phonons are generated [5.15]. To assess the effects of piezoelectric interaction on the effective growth rate characteristics, each figure has been supplemented with the characteristics that have been obtained under the condition when the electrons are scattered only by the acoustic phonons. The semiconductor compound InSb has been chosen for the numerical computations, because it has a quite low effective mass. So, the electrons in the material, get heated up even for an apparently lower electric field. Moreover, other parameters like ${k_m}^2, u_l,\ \rho, \epsilon_{sc}$ and the deformation potential constant E_1 of the compound are of such values, that, over the low temperature range of interest here, the piezoelectric interaction is expected to contribute significantly in controlling the phonon emission. Apart from that, InSb is an important material in as much as it is commonly used for devices, like infrared detectors etc. The values of the material parameters which have been used for InSb are :$m^* = 0.014 m_0$; m_0 being the free electron mass, $u_l = 3.7 \times 10^3 ms^{-1}$, $\rho = 5.78 \times 10^3 kgm^{-3}$, ${k_m}^2 = 7.29 \times 10^{-4}$, $\in_r = 17.54$, $E_1 = 20$ eV. The figures here reveal the effectiveness of the degeneracy and of the piezoelectric interaction in controlling the characteristics of the phonon growth rate under the prevalent conditions of interest here. Let us first consider Figs.5.3 and 5.4. From a comparison of the solid curves (1a) with (3a), (2a) with (4b), (1b) with (3b) and (2b) with (4b) one can see that the degeneracy always reduces the phonon growth rate significantly, and as a whole, changes the growth rate, both qualitatively and quantitatively, particularly for the lower range of x. For higher values of x, however, the effects of degeneracy gradually reduce. Obviously, for the same values of T_n, the effective changes which are brought about by the degeneracy, are seem to be more pronounced, the higher the value of the degeneracy level $\frac{\varepsilon_F}{k_B T_L}$ is. It may also be seen that, for the same value of η, the degeneracy of the material effects greater changes in the phonon growth rate, the higher the effective electron temperature T_n is.

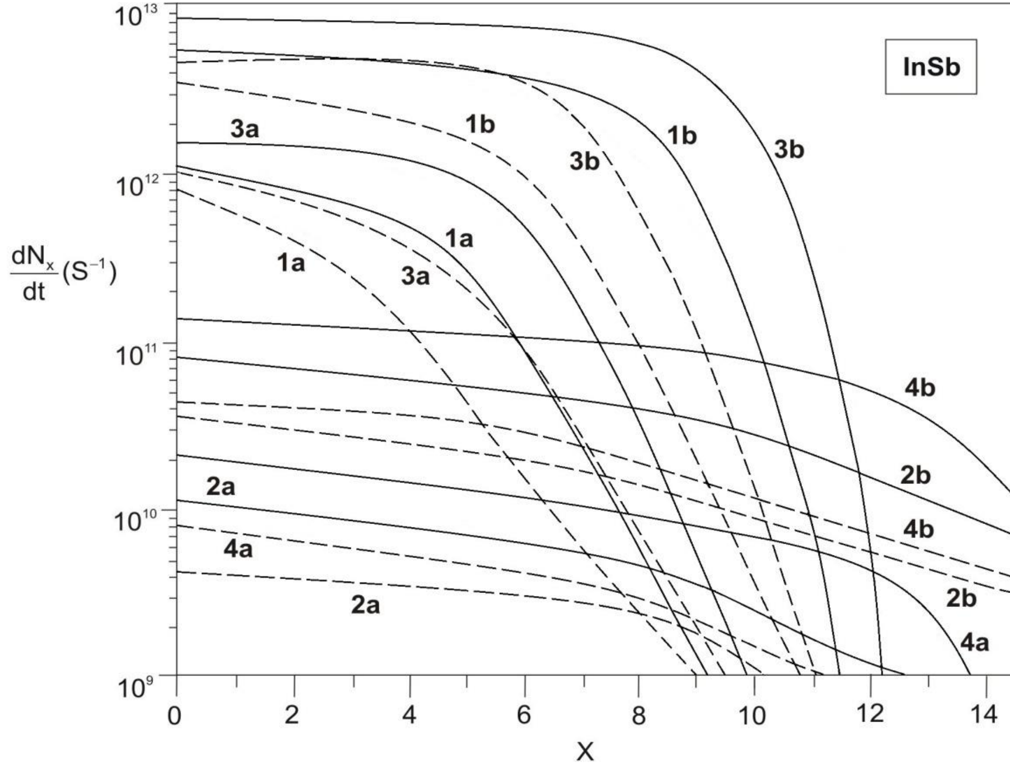

Fig. 5.3 : The dependence of the phonon growth rate $\left(\frac{\partial N_x}{\partial t}\right)$ upon the normalized phonon wave vector x $\left(=\frac{\hbar u_l q}{k_B T_L}\right)$ in a sample of InSb, for different values of the lattice temperature T_L and the normalized effective electron temperature $T_n\left(=\frac{T_e}{T_L}\right)$. The curves 1 and 2 which follow from eq.(5.8) after combining the results which have been reported in Ref.[5.2], are for a degenerate sample with $\frac{\varepsilon_F}{k_B T_L} = 5$; whereas curves 3 and 4 which follow from eq.(5.9) after combining the results which have been reported in Ref.[5.14], are for non-degenerate sample. Curves 1 and 3 are for $T_L = 20$, whereas curves 2 and 4 are for $T_L = 4K$. The curves marked a and b correspond to$T_n = 2.5$ and 10 respectively. The solid curves represent the results one obtains for the combined interaction of the electrons with the acoustic and piezoelectric phonons and the dashed curves follow when the electrons interact only with the acoustic phonons.

To assess the contribution of the piezoelectric interaction on the phonon growth characteristics, one can compare the identically labeled sets of two curves, one of which is a solid curve and the other is dashed, for the same values of $T_L$and T_n ; like the two (1a) curves or the two (3a) curves etc. Thus it seems that, the piezoelectric interaction

makes the growth characteristics quite sensitive to the changes of T_L, particularly for the lower values of x. For the higher values of x, however, the contribution of the piezoelectric interaction in shaping the growth characteristics gradually diminishes. This trend of the characteristics continues to the higher values of x, the lower the lattice temperature is. In general, under the prevalent conditions of interest here, the piezoelectric interaction effects almost equally significant changes in the growth characteristics, irrespective of the values of the degeneracy level of the sample.

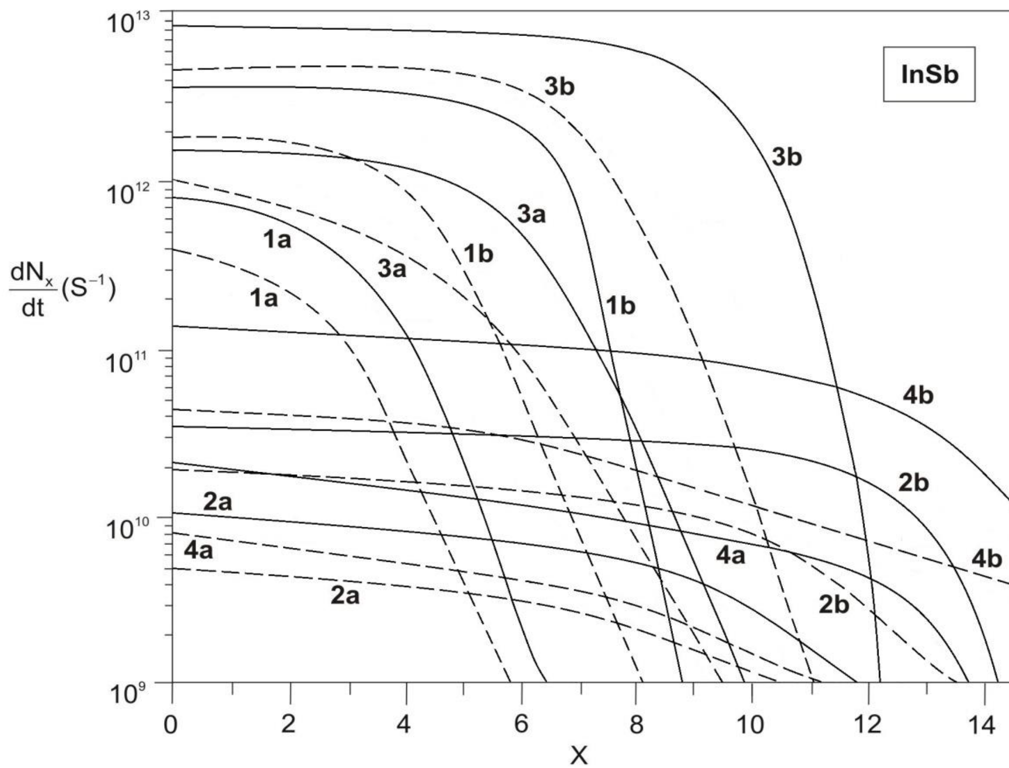

Fig. 5.4 : The dependence of the phonon growth rate $\left(\frac{\partial N_x}{\partial t}\right)$ upon the normalized phonon wave vector x $\left(=\frac{\hbar u_l q}{k_B T_L}\right)$ in a sample of InSb, for different values of the lattice temperature T_L and the normalized effective electron temperature $T_n \left(=\frac{T_e}{T_L}\right)$. The curves 1 and 2 which follow from eq.(4.8) after combining the results which have been reported in Ref.[5.2], are for a degenerate sample with $\frac{\varepsilon_F}{k_B T_L} = 15$; whereas curves 3 and 4 which follow from eq.(5.9) after combining the results which have been reported in Ref.[5.14], are for non-degenerate sample. Curves 1 and 3 are for $T_L = 20$, whereas curves 2 and 4

are for $T_L = 4K$. The curves marked a and b correspond to$T_n = 2.5$ and 10 respectively. The solid curves represent the results one obtains for the combined interaction of the electrons with the acoustic and piezoelectric phonons and the dashed curves follow when the electrons interact only with the acoustic phonons.

The contribution of the piezoelectric scattering in effecting changes in the growth characteristics at any lattice temperature is greater, the higher the T_n is. It is obvious that, unlike the degeneracy of the sample, the consideration of the piezoelectric scattering tends to increase the growth rate.

As T_L changes, different values of x will correspond to the same value of q, which is consistent with the normalization constant of the phonon wave vector. Comparing the discrepancy in the values of the phonon growth rate around the same value of q, for the acoustic and combined interaction of the electrons, one can note that the piezoelectric interaction is more dominant, the lower the T_L is. Moreover, the effects of piezoelectric interaction are manifested more prominently for degenerate materials compared to that in the non-degenerate materials. Thus, it may be concluded that both the low temperature features, viz. the piezoelectric interaction and the degeneracy of the material, which have been considered here, bring about equally significant changes in the growth rate characteristics of the phonons.

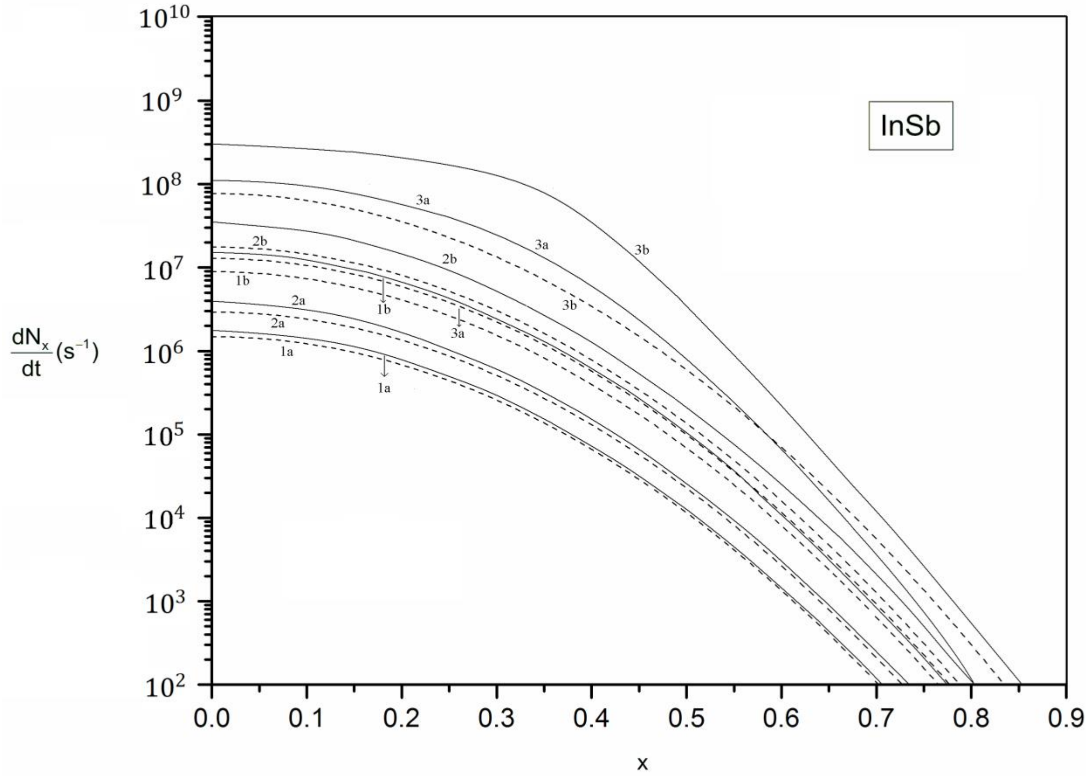

Fig. 5.5 : The dependence of the phonon growth rate $\left(\frac{\partial N_x}{\partial t}\right)$ upon the normalized phonon wave vector x $\left(=\frac{\hbar u_l q}{k_B T_L}\right)$ in a non-degenerate sample of InSb, for different values of the lattice temperature T_L and the normalized effective electron temperature T_n. The solid curves represent the results one obtains for the combined interaction of the electrons with the acoustic and the piezoelectric phonons. They follow from eq.(5.10) in combination with the results which have been reported in Ref.[5.3]. Curves 1, 2 and 3 are for $T_L = 300\text{K}, 77\text{K}$ and 4K respectively. Curves marked a and b correspond to$T_n = 2.5$ and 10 respectively. The results under the condition when the electrons interact only with the acoustic phonons follow from Ref.[5.3] and are here represented by the dashed curves. All curves are drawn for $n_0 \approx 10^{20}/\text{m}^3$.

Fig.5.5 depicts the effectiveness of the piezoelectric interaction in controlling the phonon growth characteristics in the non-degenerate sample of InSb under the condition of high lattice temperature.

It is seen that, unlike the characteristics that are obtained under the conditions of low lattice temperature, now the characteristics are quite simple at higher temperatures.

The rate almost monotonically falls with the increase of x. Moreover, as expected, the effectiveness of the piezoelectric interaction in controlling the growth rate is now hardly perceptible. However, to obtain the complete picture of the characteristics, the interaction with the polar optical phonons, which could be neglected for the analysis under the conditions of low temperature ($T_L \leq 20$ K), should now be duly taken into account when T_L is high and a sufficient number of optical phonons are generated.

Four of the important low temperature features have been taken into account here in developing the analysis of phonon growth characteristics. However, other low temperature features, like the band tailing in the degenerate materials due to high doping, and the electrostatic screening of the scattering potential due to higher concentration of the electrons, should also be taken into consideration for further refinement of the present analysis.

The prevalent conditions of interest here may be easily realized in suitably designed experiments. Since there is a dearth of the experimental data, the growth characteristics of the phonons for the combined interaction of the electrons in a degenerate material at the low lattice temperatures, as obtained here, could not be compared with the experiment. However, the results that are obtained here, seem to be quite realistic and hence encourage further studies in the non-ohmic transport in degenerate semiconductors at low lattice temperatures.

References:

[5.1] B.R.Nag, Theory of Electrical Transport in Semiconductors, Pergemon Press, Oxford, (1972).

[5.2] A.Basu, B.Das, T.R.Middya, D.P.Bhattacharya, J.Phys.Chem. Solids 10 9 (2017).

[5.3] E.M.Conwell, High Field Transport in Semiconductors, Academic Press, New York, (1967).

[5.4] G.Bauer, Springer Tracts in Modern Physics, Springer, Berlin, Heidelberg, New York, (1974).

[5.5] B.Das, A.Basu, J.Das, D.P.Bhattacharya, Physica B 474 21 (2015).

[5.6] S.Midday, S.Nag, D.P.Bhattacharya, Physica B 458 18 (2015).

[5.7] B.R.Nag, Electron Transport In Compound Semiconductors, Springer, Berlin, Heidelberg, New York, (1980).

[5.8] S.M.Sze, Physics of Semiconductor Devices, Wiley Eastern Limited, New Delhi, (1983).

[5.9] P.K.Basu, B.R.Nag, Phys. Rev. B 22 4849 (1980).

[5.10] P.K.Basu, B.R.Nag, J. Phys. C: Solid State Phys. 14 1519 (1981).

[5.11] Z.S.Kachlishvili, Phys. Status Solidi A33 15 (1976).

[5.12] J.S.Blackmore, Semiconductor Statistics, Pergamon Press, Oxford, (1962).

[5.13] JaroslavKarlovsky, Phys. Rev. 127 419 (1962).

[5.14] N.Chakrabarti and D.P.Bhattacharya, J.Phys.Chem. Solids 57 653 (1995).

[5.15] Canali C., Jacoboni C, Nava F., Ottaviani G. and AlberigiQuaranta A., Phys. Rev. B 12 2265 (1975).

CHAPTER VI

Energy loss rate and the high field mobility characteristics in a degenerate semiconductor at low lattice temperatures

6.1. Calculation of the energy loss rate and the high field mobility for the interaction of the electrons with the acoustic phonons using the Fermi – Dirac distribution function.

6.1.1. Introduction

Under different experimental conditions, the electrical transport characteristics of a semiconductor are determined by the dominant interactions of the electrons with the lattice imperfections. When the lattice temperature T_L is low ($T_L \leq 20$ K), the free electrons in a high purity elemental semiconductor interact dominantly only with intravalley acoustic phonons. Under this Condition, the electrons may be Significantly perturbed from the state of thermodynamic equilibrium for a field of only a few V/cm or even less [6.1,6.2]. The non-equilibrium electrons then attain an effective temperature T_e which exceeds the lattice temperature and the material exhibits electrical non-linearity. The electrons then emit more phonons per unit time, compared to how much they absorb in the same interval. This leads to a finite rate of phonon growth, which results in a finite energy loss rate (ELR) of the ensemble of electrons.

In calculating the Phonon growth and the energy loss rate characteristics under the condition when the non-equilibrium electrons interact only with intravalley acoustic phonons, one traditionally neglects the Phonon energy ε_{ph} compared to the carrier energy

$\varepsilon_{\vec{k}}$, i.e. assumes the electron-phonon interactions to be elastic and also approximates the phonon distribution by the equipartition law. For this long wave length acoustic phonon, it may be seen that $\varepsilon_{ph}/\varepsilon_{\vec{k}} \approx u_l/u_T$, where u_l is the acoustic velocity and the u_T is the average thermal velocity of the carriers [6.1]. Hence, though the traditional simplifications can be made at higher temperature, the same simplifications can hardly be made if the temperature is low, where $u_T \approx u_l$. Hence under the condition of low temperature, the electron-phonon interaction can neither be assumed to be elastic, nor the phonon distribution be truncated to the equipartition form. It has been shown in [6.3,6.4] how the approximations like the elastic interaction and the equipartition law for the phonon distribution lead to significant errors in the phonon growth and the energy loss characteristics in a non-degenerate (non-deg) semiconductor at low lattice temperatures.

For the low lattice temperatures, if the Fermi energy ε_F is not much lower than the $k_B T_L$ of the conduction band edge (k_B being the Boltzmann constant), and the electron densities are beyond the insulator to metal transitions, the free electrons ensemble in the semiconductor should be treated as degenerate (deg). With the increase of the doping level, as the electron concentration of an n-type material exceeds the effective density of states, the Fermi level ε_F then moves into the conduction band and the material behaves as a degenerate one. The critical concentration of the donors N_D which is required for the degeneracy, may be roughly estimated from

$$\varepsilon_F = \left(\frac{\hbar^2}{2m^*}\right)(3\pi^2 N_D)^{2/3} > E_d$$

where m* is the effective mass of an electron and E_d is the donor ionisation energy [6.5-6.7]. It may be kept in mind, though with the increase doping the interaction with the impurity atoms may be important, but such interaction being elastic, hardly takes part in the energy balance equation.

The purpose of the present study is to calculate the energy loss rate characteristic, and then, from the loss-rate, to get the non-ohmic mobility characteristics in a degenerate sample of semiconductor at the low temperatures. The calculations have been carried out taking due account of the inelasticity of the electron-phonon interaction and also the true phonon distribution thereby not truncating the same to the equipartition law. The numerical results which are obtained from the present theory for some degenerate samples of Si and Ge, are then compared with the results reported earlier for the non-degenerate materials in the same framework satisfying the low temperature conditions

[6.3]. From the Comparison, the effects of degeneracy on the ELR and non-ohmic mobility characteristics are analyzed.

6.1.2. Development

The average rate of energy loss of a carrier due to interaction with the intravalley acoustic phonons can be calculated from [6.1]

$$\langle \frac{d\varepsilon_{\vec{k}}}{dt} \rangle = -\frac{1}{nV} \sum_{\vec{q}} \hbar u_l q \left(\frac{\partial N_q}{\partial t} \right) \tag{6.1}$$

where n is the concentration of the free carriers, V is the volume of the semiconductor material, $\hbar = \frac{h}{2\pi}$, h being the Plank's Constant, $\vec{q}$ is the phonon wave vector, N_q is the number of phonons with wave vector $\vec{q}$ and $\left(\frac{\partial N_q}{\partial t} \right)$ is the phonon growth rate. Now transforming the summation over $\vec{q}$ to an integration over the spherical coordinates q,θ, φ and integrating over θ and φ one obtains

$$\langle \frac{d\varepsilon_{\vec{k}}}{dt} \rangle = -\frac{\hbar u_l}{2\pi^2 n} \int_{q=0}^{q_0} q^3 \left(\frac{\partial N_q}{\partial t} \right) dq \tag{6.2}$$

Where q_0 is the upper limit of q. So, in order to carry out the integration in (6.2), apart from assigning a proper value of q_0, the expression for the phonon growth rate should be obtained for a degenerate semiconductor under the identical conditions of low temperature of our interest, where the effects of the inelasticity of the electron-phonon interaction and the true phonon distribution have been duly incorporated. One of the present authors, with some others have recently obtained such an expression for the phonon growth rate [6.8]. Making use of the expression for $\left(\frac{\partial N_q}{\partial t} \right)$ from [6.8] one can obtain

$$\langle \frac{d\varepsilon_{\vec{k}}}{dt} \rangle = -\frac{(E_1 m^*)^2 k_B{}^8 T_L{}^4 T_e}{4\pi^3 n\rho \hbar^7 u_l{}^4} (I_1 - I_2 - I_3) \tag{6.3}$$

Where E_1 is the deformation potential constant, ρ is the density and n, the electron concentration for the degenerate material is given by

$$n = \frac{2(2\pi m^* k_B T_e)^{3/2}}{8\pi^3 \hbar^3} F_{\frac{1}{2}}(\eta_e)$$

$F_{\frac{1}{2}}(\eta_e)$ being the Fermi integral, $\eta_e = \frac{\varepsilon_F}{k_B T_e}$ and

$$I_1 = \int_0^{x_c} x^3 (N_q + 1) \ln\left[1 + \exp\left\{\eta_e - a(x-b)^2 - \frac{x}{T_n}\right\}\right] dx \qquad (6.4)$$

$$I_2 = \int_0^{x_c} x^3 N_q \ln[1 + \exp\{\eta_e - a(x-b)^2\}] dx \qquad (6.5)$$

$$I_3 = \int_0^{x_c} x^3 \left[\frac{1}{\lambda} + \ln\lambda - 1 + \frac{x}{T_n}\left(\frac{1}{\lambda} - \frac{1}{2\lambda^2} - \frac{1}{2}\right)\right] dx \qquad (6.6)$$

x being the normalised phonon wave vector given by $x = \frac{\hbar u_l q}{k_B T_L}$, $N_q = (e^x - 1)^{-1}$, $a = \frac{k_B T_L}{8 m^* u_l^2 T_n}$, $b = \frac{2 m^* u_l^2}{k_B T_L}$, $T_n = \frac{T_e}{T_L}$, $\lambda = 1 + \exp[\eta_e - a(x-b)^2]$.

The integrals (6.4)-(6.6) can be carried out analytically under the condition $\eta_e > \left[a(x-b)^2 + \frac{x_c}{T_n}\right]$

where x_c, the upper limit of the normalised phonon wave vector can be set at

$$x_c = \frac{2 m^* u_l}{k_B T_L}\left[\sqrt{\frac{2 k_B T_e \eta_e}{m^*}} - u_l\right]$$

Thus one can obtain as follows:

$$I_1 = (\eta - ab^2)\left[\frac{{x_c}^4}{4} - \sum_{m=1}^{\infty}\left\{\sum_{r=0}^{3} P(3,r)\frac{{x_c}^{(3-r)}}{m^{(r+1)}}e^{-mx_c} - \frac{6}{m^4}\right\}\right]$$
$$- \left(2ab - \frac{1}{T_n}\right)\left[\frac{{x_c}^5}{5} - \sum_{m=1}^{\infty}\left\{\sum_{r=0}^{4} P(4,r)\frac{{x_c}^{(4-r)}}{m^{(r+1)}}e^{-mx_c} - \frac{24}{m^5}\right\}\right]$$
$$- a\left[\frac{{x_c}^6}{6} - \sum_{m=1}^{\infty}\left\{\sum_{r=0}^{5} P(5,r)\frac{{x_c}^{(5-r)}}{m^{(r+1)}}e^{-mx_c} - \frac{120}{m^6}\right\}\right]$$

$$I_2 = (ab^2 - \eta)\left[\sum_{r=0}^{3} P(3,r)\,{x_c}^{(3-r)}e^{-x_c} - 6\right.$$
$$\left. + \sum_{m=1}^{\infty}\left\{\sum_{r=0}^{3} P(3,r)\frac{{x_c}^{(3-r)}}{(m+1)^{(r+1)}}e^{-(m+1)x_c} - \frac{6}{(m+1)^4}\right\}\right]$$
$$- 2ab\left[\sum_{r=0}^{4} P(4,r)\,{x_c}^{(4-r)}e^{-x_c} - 24\right.$$
$$\left. + \sum_{m=1}^{\infty}\left\{\sum_{r=0}^{4} P(4,r)\frac{{x_c}^{(4-r)}}{(m+1)^{(r+1)}}e^{-(m+1)x_c} - \frac{24}{(m+1)^5}\right\}\right]$$
$$+ a\left[\sum_{r=0}^{5} P(5,r)\,{x_c}^{(5-r)}e^{-x_c} - 120\right.$$
$$\left. + \sum_{m=1}^{\infty}\left\{\sum_{r=0}^{5} P(3,r)\frac{{x_c}^{(5-r)}}{(m+1)^{(r+1)}}e^{-(m+1)x_c} - \frac{120}{(m+1)^4}\right\}\right]$$

$$I_3 = e^{-\eta}\sum_{m=0}^{\infty}\frac{a^m}{m!}\left[\frac{1}{m_4}\{x_c'^{m_4} - (-b)^{m_4}\} + \frac{3b}{m_3}\{x_c'^{m_3} - (-b)^{m_3}\} + \frac{3b^2}{m_2}\{x_c'^{m_2} - (-b)^{m_2}\}\right.$$
$$\left. + \frac{b^3}{m_1}\{x_c'^{m_1} - (-b)^{m_1}\}\right] + \frac{e^{-\eta}}{T_n}\sum_{m=0}^{\infty}(1 - 2^m e^{-\eta})\frac{a^m}{m!}H$$
$$+ \frac{1}{4}(\eta - ab^2 - 1)x_c^{\,4} + \frac{2}{5}\left(ab - \frac{1}{4T_n}\right)x_c^{\,5} - \frac{a}{6}x_c^{\,6}$$

where, $m_i = 2m + 1$; i is a positive integer which ranges from 1 to 5

$$x_c' = x_c - b$$
$$H = \frac{1}{m_5}\{x_c'^{m_5} - (-b)^{m_5}\} + \frac{4b}{m_4}\{x_c'^{m_4} - (-b)^{m_4}\} + \frac{6b^2}{m_3}\{x_c'^{m_3} - (-b)^{m_3}\}$$
$$+ \frac{4b^3}{m_2}\{x_c'^{m_2} - (-b)^{m_2}\} + \frac{b^4}{m_1}\{x_c'^{m_1} - (-b)^{m_1}\}$$
$$P(n,k) = \frac{n!}{k!(n-k)!}$$

Now $\langle\frac{d\varepsilon_{\vec{k}}}{dt}\rangle_{deg}$, the average energy loss rate of the electrons in the degenerate material due to the phonon emission being known, one can obtain the non-ohmic mobility μ.

In the presence of an electric field E, the energy supplied to the carriers is at the rate $e\mu E^2$. A steady state is reached when the average energy loss rate due to phonon emission, balances the rate of gain of energy from the field [6.1]

$$\langle\frac{d\varepsilon_{\vec{k}}}{dt}\rangle = e\mu E^2 \qquad (6.7)$$

Thus the non-ohmic mobility of the degenerate semiconductors under the prevalent conditions of low temperature when the inelastic interaction of the electrons with the intravalley acoustic phonons and the full form of the Bose-Einstein distribution for the phonons are duly taken into account, takes the form

$$\mu_{deg} = -\frac{1}{eE^2}\frac{E_1^2 m^{*1/2} k_B{}^{7/2} T_L{}^4}{(2\pi)^{3/2}\rho\hbar^4 u_l^4 T_e^{1/2}}\frac{1}{F_{\frac{1}{2}}(\eta_e)}(I_1 - I_2 - I_3) \tag{6.8}$$

6.1.3. Results and Discussions

In the frame work of the diffusion approximation, the average energy of a carrier in a degenerate ensemble is known to be $\langle\varepsilon_{\vec{k}}\rangle_{deg} = k_B T_e \frac{F_{3/2}(\eta_e)}{F_{1/2}(\eta_e)}$. For relatively lower concentration of the carriers, when $\varepsilon_F < 0$ and $|\varepsilon_F|$ is not much larger than $k_B T_e$, the material seems to be non-degenerate and the energy distribution that has been taken to be the Fermi Dirac distribution at an effective electron temperature T_e, then simplifies to the Maxwellian function. The average energy under this condition $\langle\varepsilon_{\vec{k}}\rangle_{non-deg}$ reduces to $\frac{3}{2}k_B T_e$. Thus, $T_n (= \frac{T_e}{T_L})$ at any lattice temperature T_L is a measure of the average energy of a carrier of the ensemble [6.9]. The degeneracy of a material can be assessed on taking into account the temperature T_L as well as the concentration of the carriers. That is why the level of degeneracy is indicated by the value of the factor $\frac{\varepsilon_F}{k_B T_L}$. Thus for a particular concentration of the electron ensemble which sets the value of ε_F, the ensemble behaves more and more like a degenerate one as the temperature is lowered [6.5,6.10].

Hence it follows from eq.(6.3) that the dependence of $\langle\frac{d\varepsilon_{\vec{k}}}{dt}\rangle_{deg}$ on the average energy of a carrier at any lattice temperature turns out to be more involved in comparison to that of $\langle\frac{d\varepsilon_{\vec{k}}}{dt}\rangle_{non-deg}$, which has been already calculated under the similar conditions of low temperature and reported in [6.3,6.4]. However, from a comparison of the characteristics of $\langle\frac{d\varepsilon_{\vec{k}}}{dt}\rangle_{deg}$ which follows from eq.(6.3), with that of $\langle\frac{d\varepsilon_{\vec{k}}}{dt}\rangle_{non-deg}$, which has been reported in [6.3], one can assess the effects of degeneracy on the energy loss rate of the electrons at any lattice temperature. Hence to make such a comparison $\langle\frac{d\varepsilon_{\vec{k}}}{dt}\rangle_{deg}$ is calculated using eq.(6.3), considering the samples of Si and Ge for different values of T_n, with the material parameters given in Table 6.1. The similar data for $\langle\frac{d\varepsilon_{\vec{k}}}{dt}\rangle_{non-deg}$ are then collected from eq.(6.3), and the normalised loss rate $\langle\frac{d\varepsilon_{\vec{k}}}{dt}\rangle_{norm} = \frac{\langle\frac{d\varepsilon_{\vec{k}}}{dt}\rangle_{deg}}{\langle\frac{d\varepsilon_{\vec{k}}}{dt}\rangle_{non-deg}}$ is plotted against T_n in Figures 6.1 and 6.2 for different values of the lattice temperature (T_L= 1, 4

and 20K) and for different levels of the degeneracy ($\frac{\varepsilon_F}{k_B T_L}$ = 5 and 10). While comparing the figures, it is to be kept in mind that, since $T_e = T_n T_L$, the same value of T_e occurs earlier on T_n axis, the higher the lattice temperature is. Thus one can see from Figures 6.1 and 6.2 that significant qualitative and quantitative changes in the energy loss characteristics are effected as one takes into account the degeneracy of the electron ensemble. The changes are more for the lower values of the energy for any value of the level of degeneracy ($\frac{\varepsilon_F}{k_B T_L}$). Moreover, the changes for any lattice temperature are again seem to be more, the higher the level of degeneracy is. For higher energies, however, the electron ensemble in the material tends to obey Maxwellian distribution, and hence the effects of degeneracy on the energy loss rate characteristic is hardly observed. Hence the $\langle\frac{d\varepsilon_{\vec{k}}}{dt}\rangle_{deg}$ characteristic asymptotically follows the $\langle\frac{d\varepsilon_{\vec{k}}}{dt}\rangle_{non-deg}$ characteristic, this makes $\langle\frac{d\varepsilon_{\vec{k}}}{dt}\rangle_{norm}$ tending to unity.

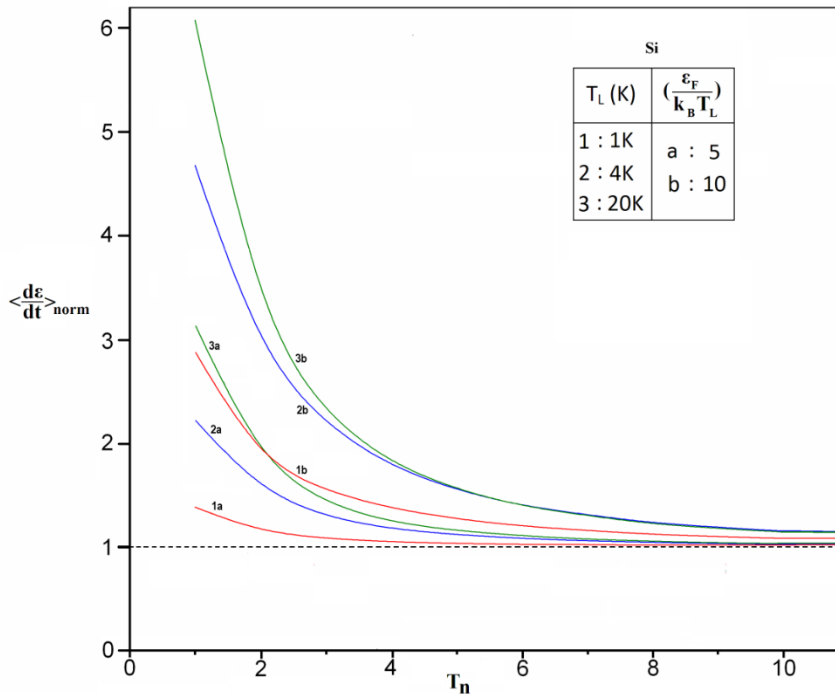

Fig. 6.1 : Dependence of the $\langle\frac{d\varepsilon_{\vec{k}}}{dt}\rangle_{norm}$, the rate of energy loss of the non-equilibrium electrons in a degenerate sample of Si, normalised to the same rate in the non-degenerate sample of the same material upon T_n. The curves 1, 2 and 3 are for the lattice temperatures of 1K, 4K and 20K respectively. The curves marked a and b correspond to the degeneracy parameter $\frac{\varepsilon_F}{k_B T_L}$ = 5 and 10 respectively.

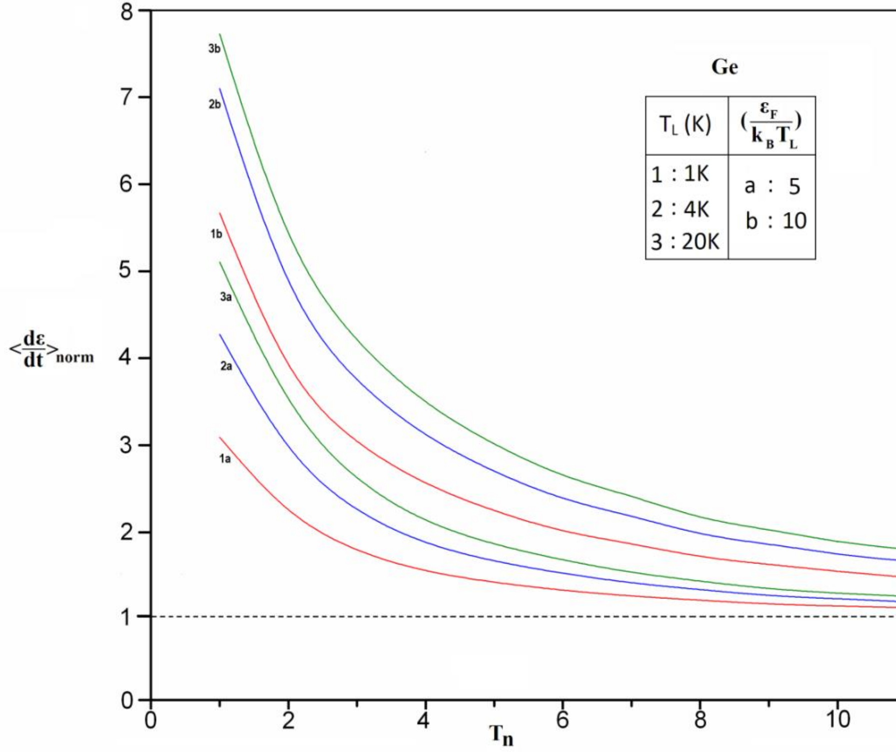

Fig. 6.2 : Dependence of the $\langle\frac{d\varepsilon_{\vec{k}}}{dt}\rangle_{norm}$, the rate of energy loss of the non-equilibrium electrons in a degenerate sample of Ge, normalised to the same rate in the non-degenerate sample of the same material upon T_n. The curves 1, 2 and 3 are for the lattice temperatures of 1K, 4K and 20K respectively. The curves marked a and b correspond to the degeneracy parameter $\frac{\varepsilon_F}{k_B T_L}$ = 5 and 10 respectively.

Table 6.1. : Material parameters of Si and Ge. $m_0$is the free electron mass.

Physical Parameters	**Si**	**Ge**
Acoustic deformation potential constant E_1 (eV)	9.0	20.29
Longitudinal acoustic velocity $u_l(\times 10^5$ cm $s^{-1})$	9.073	5.4
Effective mass m^* (g)	$0.32m_0$	$0.12m_0$
Density (g cm^{-3})	2.329	5.32

Equation (6.8) is obtained here as the expression for the non-ohmic mobility of the electrons in a degenerate material under the condition of low temperature when the inelasticity of the electron-phonon interaction and the full form of the phonon distribution without truncation to the equipartition law, both are taken into account. The expression is quite complex, much more than what follows from [6.3] for a non-degenerate material under the identical conditions of low temperature. In order to obtain the dependence of the non-ohmic mobility on the electric field, one should know how does the effective electron temperature T_e depend upon the electric field. The problem of the field dependence of the effective electron temperature in a degenerate material under the condition of low temperature has been studied in [6.11]. The same field dependence of the electron temperature in a non-degenerate material is already well known [6.12]. Thus the dependence of the non-ohmic mobility on the electric field in a degenerate material is obtained from eq.(6.8) and using the data from [6.11]. Similarly the non-ohmic mobility characteristic for the non-degenerate material is obtained using the data from [6.3] and [6.12]. The dependence of the normalized non-ohmic mobility $(\frac{\mu_{deg}}{\mu_{non-deg}})$ upon the electric field, thus obtained for Si and Ge are plotted in Figures 3 and 4 for different lattice temperatures (T_L = 1, 4 and 20K) and degeneracy parameter ($\frac{\varepsilon_F}{k_B T_L}$ = 5 and 10).

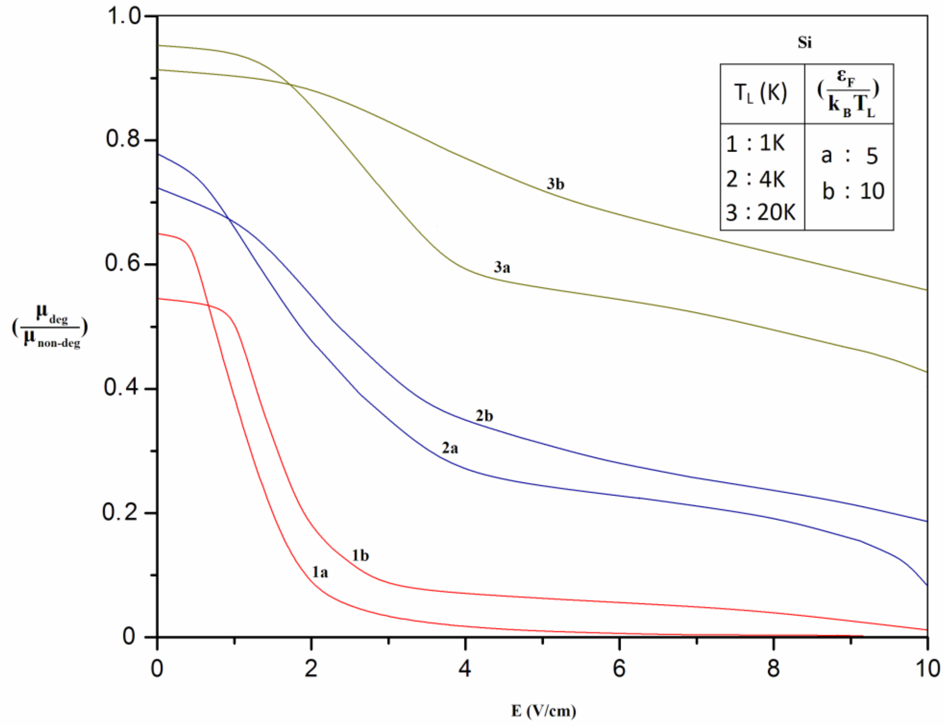

Fig. 6.3 : Dependence of $(\frac{\mu_{deg}}{\mu_{non-deg}})$, the non-ohmic mobility of the electrons in a degenerate sample of Si, normalised to the same mobility in the non-degenerate sample of the same material upon the electric field E. Curves 1, 2 and 3 are for the lattice temperatures of 1K, 4K and 20K respectively. Curves marked a and b correspond to the degeneracy parameter $\frac{\varepsilon_F}{k_B T_L} = 5$ and 10 respectively.

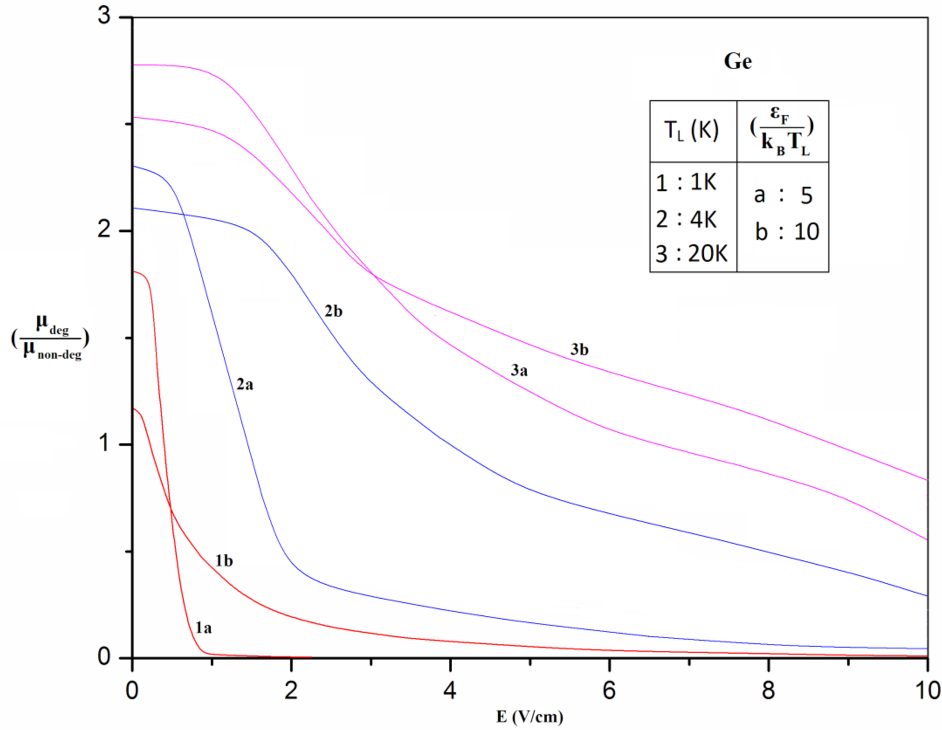

Fig. 6.4 : Dependence of $(\frac{\mu_{deg}}{\mu_{non-deg}})$, the non-ohmic mobility of the electrons in a degenerate sample of Ge, normalised to the same mobility in the non-degenerate sample of the same material upon the electric field E. Curves 1, 2 and 3 are for the lattice temperatures of 1K, 4K and 20K respectively. Curves marked a and b correspond to the degeneracy parameter $\frac{\varepsilon_F}{k_B T_L} = 5$ and 10 respectively.

It may be seen that the dependence of the non-ohmic mobility on the electric field significantly changes as one takes the degeneracy of the sample into account. The changes have been both qualitative and quantitative. Since the minimum concentration of electrons for the onset of degeneracy is higher for Si than that for Ge, the non-ohmic mobility in degenerate samples of Si is less than that of the non-degenerate sample, for any field. On the other hand, for the Ge samples the non-ohmic mobility is higher for the degenerate ensemble of the carriers compared to that of the non-degenerate ensemble. This trend for Ge continues up to higher fields, the higher is the lattice temperature. But,

for both Si and Ge, the rate of fall of the non-ohmic mobility with the electric field is higher for the degenerate samples compared to that for the non degenerate ones. Thus the results obtained here for the energy loss rate of the non-equilibrium electrons and the non-ohmic mobility in some moderately doped degenerate samples of the elemental semiconductors under the conditions of low lattice temperature seem to be interesting. So these results inspire for the studies of the non-ohmic transport in compound semiconductors under the conditions of low temperature where the contribution of the interaction with the piezoelectric phonon is also quite important. Moreover, the analysis made here is based only on some features of low temperature. Degeneracy can be taken to be one of such features, which has been taken to be one of such features, which has been taken into account first by assuming the energy distributed of the carrier ensemble to be given by the Fermi Dirac Function. However, when the material is highly doped the impurity levels degenerate into impurity band and also the Phenomenon like band tailing takes place, which effectively reduces the band gap. Apart from that as the electron concentration increases, the effects of electrostatic screening of the scattering potential due to lattice imperfections becomes more and more important [6.5,6.6]. All these factors may be duly taken into consideration for a further refinement of the present theory.

6.2. Calculation of the energy loss rate and the high field mobility for the interaction of the electrons with the acoustic phonons using the alternative model of heated Fermi – Dirac distribution function.

6.2.1. Introduction

Since degenerate semiconductors form the basis of a number of important bulk effect devices, the analysis of their ohmic and non-ohmic transport has been of interest [6.6].

In the presence of a relatively high electric field, the electron ensemble in a semiconductor may be perturbed significantly from the state of thermodynamic equilibrium with the host lattice atoms. The electrical transport under this condition exhibits some novel features which are hardly perceptible when the electric field is low. For example, when the electric field is high, the mobility of the electrons, and sometimes their concentration may become field dependent and that in turn leads to electrical non linearity. The electrons then emit more phonons than what they absorb per unit time. This leads to a finite rate of growth of the phonon number N_q with wave vector $\vec{q}$. Consequently, the rate of loss of energy of the electeons is also finite [6.1,6.5,6.9,6.12,6.13]. Under this condition, the mean energy of the electrons will usually higher than its thermal equilibrium value. Often, a field dependent electron temperature T_e of the electrons is associated with this mean energy. At any field, T_e exceeds the lattice temperature T_L. The electric field dependence of the effective temperature may be obtained from the solution of the energy balance equation of the electron phonon system.

The amount of field, which is required for the onset of these novelties in any material, depends upon the lattice temperature. For the materials in which the effective mass of the electrons is low, the high field effects may be observed for an apparently low field, of only a fraction of a Volt/cm or even less, under the condition when the lattice temperature is low ($T_L \leq 20K$). This is because, the apparently low field, now effectively turns out to be high enough to significantly perturb the electron ensemble from the state of thermodynamic equilibrium at the low lattice temperatures [6.1,6.5,6.9,6.12,6.13].

Apart from that, there are some specific features of low lattice temperature. These features, as elaborated next, are to be given due consideration for any theoretical

analysis of the electrons transport under the conditions of low lattice temperature. The interaction of the electrons with the impurities is elastic. Although, the interaction with the intravalley acoustic phonons can also be assumed elastic at the high lattice temperatures, but it is not so if the temperature is low. This is because, the average thermal energy of the electrons now turns out to be comparable with the phonon energy and such interaction becomes inelastic in nature. At such low temperatures ($T_L \leq 20K$), the optical mode lattice vibration is quite insignificant since the optical phonons have characteristic temperatures usually higher than 300K [6.5,6.12,6.13]. Hence the free electrons interact principally only with the intravalley acoustic phonons and thus lose energy [6.1,6.13]. Again, the energy distribution of the phonons, as given by the Bose-Einstein (BE) function can indeed be truncated to the simple equipartition law if the temperature is high. But at low temperatures, this is not possible, and one has to work with the full form of the BE function without any truncation. Moreover, for low lattice temperatures, a lower level of doping is required for the onset of degeneracy in the material [6.6,6.5].

The details of those features have already been discussed in [6.8,6.11,6.14]. Thus, under the condition of low temperature and in the presence of such an apparently low, but effectively high field, one can assume that the spherically symmetric part of the non equilibrium distribution function $f_0(\varepsilon)$ is given by the Fermi -Dirac (F.D) function with the effective electron temperature [6.9,6.13].

The knowledge of the phonon growth rate provides important data for development of some simulation softwares for the study of electronic devices. Some of the present authors along with others, have made an approximate analysis of the characteristics of phonon growth rate ($\frac{dN_q}{dt}$) in a degenerate semiconductor at low lattive temperatures, taking due account of the inelasticity of the interactions of the non equilibrium electrons with the intravalley acoustic phonons and also the full form of the phonon distribution function. The heated F.D function with the effective electron temperature has been used for the isotropic part of the distribution function of the non equilibrium electrons [6.8]. Later, in another work using the results of [6.8], the energy loss rate of the non equilibrium electrons and the corresponding non-ohmic mobility characteristics have been obtained [6.14]. Obviously, the approximate results of [6.8] and [6.14], though seem to be indicative of interesting, salient features of the characteristics, but in any case one can hardly take them to be much reliable. This is because, the problem of analytical integration of the functions that involve the Fermi function, has been somehow negotiated there, taking recourse to a number of

oversimplified approximations. Subsequently, the same group of authors, proposed a much convenient and well tested approximate model of the Fermi-Dirac distribution function [6.11] such that, on using this model, the integrations could be evaluated without making oversimplified approximations anymore and this not incurring any significant error. Using this proposed model, a much realistic analysis of the phonon growth rate in degenerate semiconductors has been made, and this time the results have been more realistic [6.15]. The purpose here is to use the same model distribution function, in place of complicated F.D function, in order to make a more realistic analysis of the effects of degeneracy on the energy loss rate of the non equilibrium electrons and on the non-ohmic mobility characteristics in semiconductors at low lattice temperatures, taking due account of the inelasticity of the electron phonon collisions and the full phonon distribution. The numerical results obtained for Si and InSb from the present analysis are compared with the other theoretical results which have been reported earlier for the degenerate and the non-degenerate materials [6.8,6.14].

6.2.2. Development

In the framework of the proposed model for $f_0(\varepsilon)$, the energy domain has been divided into three distinct ranges : $0 \leq \varepsilon \leq \beta_1\varepsilon_F$ $(\beta_1 \lesssim 1)$; $\beta_1\varepsilon_F \leq \varepsilon \leq \beta_2\varepsilon_F$ $(1 \lesssim \beta_2)$ and $\beta_2\varepsilon_F \leq \varepsilon \leq \infty$; where ε_F is the Fermi energy, β_1 and β_2 are chosen as $\beta_1 = 1 - \frac{k_B T_L}{\varepsilon_F}$ and $\beta_2 = 1 + \frac{k_B T_L}{\varepsilon_F}$; k_B being the Boltzmann constant. The proposed model distribution is represented by three different simple functions over three ranges. As has already been mentioned, the theory of phonon growth rate which is developed in [6.15] uses this model distribution in place of the true F.D. function. Using the same framework as that of [6.15] one can now calculate the average rate of loss of energy of the non-equilibrium carriers due to interaction with the intravalley acoustic phonons in a degenerate material under the condition of low lattice temperature.

Multiplying the phonon growth rate $\left(\frac{\partial N_q}{\partial t}\right)$ by $\hbar\omega_{\vec{q}}$, the energy of a phonon of wave vector q and summing up the product for all values of q, then by dividing the sum by the total number of electrons, one can get the average rate of loss of energy of the non-equilibrium electrons [6.1]. Thus symbolically,

$$\langle\frac{d\varepsilon_{\vec{k}}}{dt}\rangle = -\frac{1}{nV}\sum_{\vec{q}} \hbar\omega_{\vec{q}} \left(\frac{\partial N_q}{\partial t}\right) \qquad (6.9)$$

where $\vec{k}$ is the wave vector of an electron, n is the concentration of the electrons, V is the volume of the material, $\hbar = \frac{h}{2\pi}$; h being the Planck's constant, $\omega_{\vec{q}}$ is the angular frequency of a phonon. Since the electrons mostly interact with the long wavelength phonos [6.1], the lattice dispersion may be assumed to be linear i.e. $\omega_{\vec{q}} = u_l q$, where u_l is the longitudinal acoustic velocity. The concentration n of the electrons may be obtained by integrating [6.5]

$$dn = \frac{1}{4\pi^3} f_0(\vec{k})\overrightarrow{dk} \tag{6.10}$$

If the energy dispersion law of the electrons is assumed to be parabolic, then $\varepsilon_{\vec{k}} = \frac{\hbar^2 k^2}{2m^*}$, m^* being the effective mass of the electrons. When the F.D function at an effective temperature T_e is used for $f_0(\vec{k})$ one can obtain [6.13]

$$n = N_c\, F_{\frac{1}{2}}(\eta_e) \tag{6.11}$$

where, $N_c = 2\left(\frac{2\pi m^* k_B T_e}{h^2}\right)^{3/2}$, $\eta_e = \frac{\varepsilon_F}{k_B T_e}$ and $F_j(x)$ is the Fermi integral.

It has already been said that, the aim here is to develop the theory using an approximate and well tested model distribution in place of the F.D function. Hence calculating the concentration with the help of the model distribution one obtains

$$n = \frac{2}{\sqrt{\pi}} N_c\, [I_4 + I_5 + I_6] \tag{6.12}$$

where,

$$I_4 = \frac{2}{3}\sum_{m=1}^{\infty}\sum_{n=0}^{\infty}\frac{(-1)^m}{n!} m^n e^{-m\eta_e}\frac{(\beta_1\eta_e)^{(n+3)}}{\left(n+\frac{3}{2}\right)}$$

$$I_5 = \frac{2}{3}\left(\frac{1}{2} - C\eta_e k_B T_e\right)\left(\beta_2^{\,3/2} - \beta_1^{\,3/2}\right)\eta_e^{\,3/2} + \frac{2}{5}Ck_B T_e\left(\beta_2^{\,5/2} - \beta_1^{\,5/2}\right)\eta_e^{\,5/2}$$

$$I_6 = \sum_{m=1}^{\infty}\sum_{n=0}^{\infty} \frac{(-1)^{m+n+1}}{n!} \frac{m^n e^{m\eta_e}}{k_B T_e\left(n+\frac{3}{2}\right)}\left[\left(\beta_1\eta_e k_B T_e + P k_B T_e\right)^{\left(n+\frac{3}{2}\right)} - \left(\beta_1\eta_e k_B T_e\right)^{\left(n+\frac{3}{2}\right)}\right]$$

and $C = \frac{e^{(\beta_1-1)\eta_e} - e^{(\beta_2-1)\eta_e}}{\left[1+e^{(\beta_1-1)\eta_e}\right]\left[1+e^{(\beta_2-1)\eta_e}\right](\beta_2-\beta_1)\varepsilon_F}$

In arriving at (6.12), the upper limit of the energy of electrons has been taken as $P k_B T_e$ in place of ∞, where $P \geq 1$, since at a finite temperature the F.D function fuzzes out over a width of the order of $k_B T_e$ around $\varepsilon = \varepsilon_F$ [6.7,6.16].

In order to estimate once more, the validity of the model distribution, the variation of the carrier concentration with T_e as obtainable from (6.11) and (6.12) are compared in Fig 6.5. From the comparison one can again note that the approximate model distribution works quite satisfactorily and hence this distribution is used in the present analysis in place of the exact form of the F.D. function.

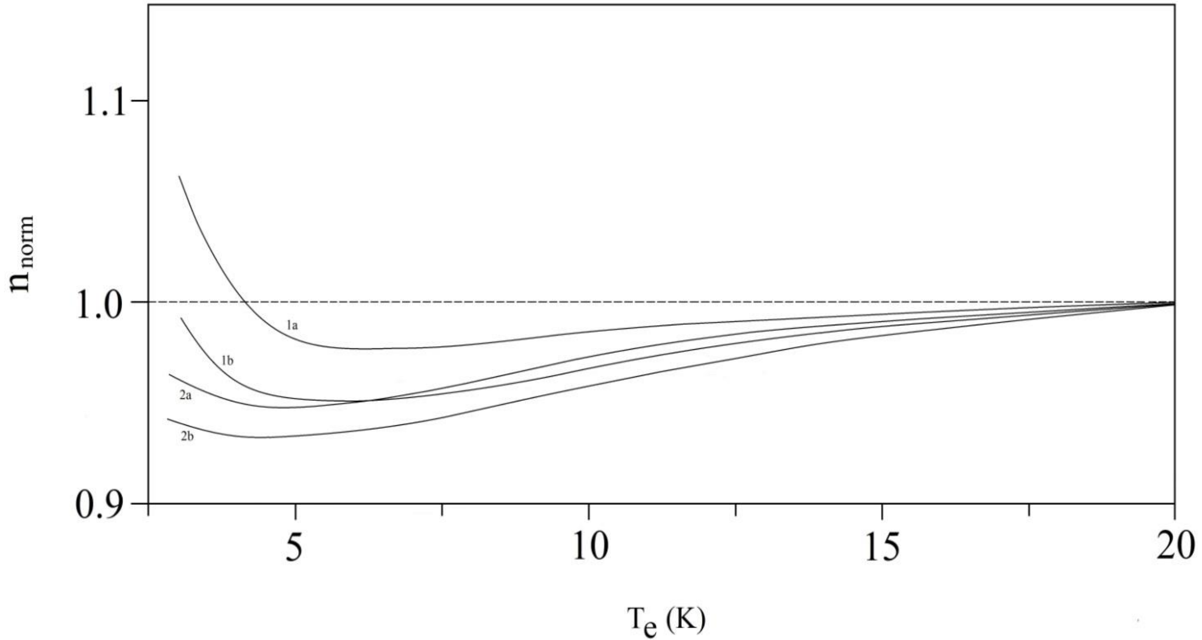

Fig. 6.5 : Dependence of normalised concentration $n_{norm}\left(=\frac{n_{\text{Model F.D.distribution}}}{n_{\text{Exact F.D distribution}}}\right)$ as a function of the effective electron temperature T_e. Curves marked '1' and those marked '2' are for Si and InSb respectively. Curves 'a' and 'b' respectively represent the characteristics for the degeneracy parameters $\frac{\varepsilon_F}{k_B T_L} = 15$ and 5.

The rate of phonon growth $\left(\frac{\partial N_q}{\partial t}\right)$ due to non-equilibrium electrons in a degenerate material is obtained from the time dependant perturbation theory. For interaction of the electrons with intravalley acoustic phonons one can obtain the phonon growth rate by integrating [6.1]

$$\left(\frac{\partial N_q}{\partial t}\right) = \frac{(E_l m^*)^2}{2\pi\rho\hbar^4 u_l} \int_{\varepsilon_0}^{\infty} \left[(N_q + 1) f_0(\vec{k} + \vec{q}) \{1 - f_0(\vec{k})\} - N_q f_0(\vec{k}) \{1 - f_0(\vec{k} + \vec{q})\} \right] d\varepsilon \quad (6.13)$$

where E_l is the deformation potential constant.

Over energy, ε_0 is the lower limit of energy as obtained from the energy and momentum conservation equation for the inelastic interaction of the electrons with the phonons, under the condition of low lattice temperature. It is given by $\varepsilon_0 = \frac{\hbar^2}{2m^*}\left(\frac{q}{2} - \frac{m^* u_l}{\hbar}\right)^2$. Since N_q, the phonon distribution cannot be truncated to the simple equipartition law at the low temperatures, one needs to work with full phonon distribution $N_q = (e^x - 1)^{-1}$, where $x = \frac{\hbar u_l q}{k_B T_L}$.

Now, if the heated F.D. function is taken for $f_0(\vec{k})$, the integrations in (6.13) can hardly be carried out analytically, particularly for the product terms like $f_0(\vec{k}) f_0(\vec{k} + \vec{q})$ unless some oversimplified approximations are made.

However, we now make use of the more realistic expression for the $\left(\frac{\partial N_q}{\partial t}\right)$, which has been obtained in [6.15] on using the well tested alternative model of F.D function in order to calculate the ELR characteristics from eq.(6.9). As has been explained in [6.15], the value of q $\left(= \frac{x k_B T_L}{\hbar u_l}\right)$ determines the location of the lower limit ε_0 on the energy axis, in the expression (6.13). As such, $\left(\frac{\partial N_q}{\partial t}\right)$ is represented by three different expressions over the three different ranges of the normalised phonon wave vector x, viz, over $0 < x < x_1$, $x_1 < x < x_2$ and $x_2 < x < \infty$;

where

$$x_1 = \frac{2u_l}{k_B T_L}\left[m^* u_l + \sqrt{2m^*(\varepsilon_F - k_B T_L)}\right] \text{ and } x_2 = \frac{2u_l}{k_B T_L}\left[m^* u_l + \sqrt{2m^*(\varepsilon_F + k_B T_L)}\right].$$

Now converting the summation over $\vec{q}$ in (6.9) by integrations in terms of spherical polar coordinates [6.1] and carrying out the integrations one can obtain

$$\langle \frac{d\varepsilon_{\vec{k}}}{dt} \rangle = -\frac{(E_1 m^*)^2 (k_B T_L)^4}{4\pi^3 \rho \hbar^7 u_l{}^4 n} [I_7 + I_8 + I_9] \quad (6.14)$$

where,

$$I_7 = \beta_1 \varepsilon_F \left(\frac{x_1{}^4}{4} - A_m^3\right) - b_8 \left[\frac{x_1{}^6}{6} - 2a\left(\frac{x_1{}^5}{5} + A_m^4\right) + a^2\left(\frac{x_1{}^4}{4} - A_m^3\right) - A_m^5\right] - k_B T_e \sum_{m=1}^{\infty} \frac{(-1)^m}{m} \left[b_1 \left(\frac{x_1{}^4}{4} - A_m^3\right)\right.$$
$$\left. - b_2 \sum_{k=0}^{\infty}\sum_{p=0}^{\infty} \frac{(-1)^p}{k!\,p!} (md)^k \frac{x_1{}^{2k+p+4}}{2k+p+4} b_6\right] + \sum_{m=1}^{\infty}\sum_{n=1}^{\infty} \frac{(-1)^m}{n!}\left(\frac{m}{T_n}\right)^{(n-1)} k_B T_L \left[b_1 Y - b_2 \sum_{k=0}^{\infty}\sum_{p=0}^{\infty} \frac{(-1)^p}{k!\,p!} (md)^k\right.$$
$$\left.\frac{x_1{}^{2k+p+n+4}}{2k+p+n+4} b_6\right] + (\beta_2 - \beta_1)\varepsilon_F \left[(0.5 + C\varepsilon_F)\left(\frac{x_1{}^4}{4} - A_m^3\right) + C k_B T_L \left(\frac{x_1{}^5}{5} - A_m^4\right)\right]$$
$$+ \frac{C}{2}(\beta_2{}^2 - \beta_1{}^2)\varepsilon_F{}^2 \left(\frac{x_1{}^4}{4} - A_m^3\right) + k_B T_e \sum_{m=1}^{\infty} \frac{(-1)^{m+1}}{m} b_3 \left(\frac{x_1{}^4}{4} - A_m^3\right) + \sum_{m=1}^{\infty}\sum_{n=1}^{\infty} \frac{(-1)^{m+n+1}}{n!}\left(\frac{m}{T_n}\right)^{(n-1)} b_3 X$$
$$+ \beta_1 \varepsilon_F (B_m^3 + Z) + b_8 \left[120 - B_m^5 + 2a(B_m^4 - 24) - a^2(B_m^3 - 6) - \sum_{r=1}^{\infty}\left\{D_m^5 - \frac{120}{(r+1)^6}\right\}\right.$$
$$\left. + 2a \sum_{r=1}^{\infty}\left\{D_m^4 - \frac{24}{(r+1)^5}\right\} - a^2 \sum_{r=1}^{\infty}\left\{D_m^3 - \frac{6}{(r+1)^4}\right\}\right] + k_B T_e \sum_{m=1}^{\infty} \frac{(-1)^{m+1}}{m}\left[(b_3 + Z) + b_2 \sum_{k=0}^{\infty}\sum_{p=0}^{\infty}\frac{(-1)^p}{k!\,p!}\right.$$
$$\left.(md)^k \frac{x_1{}^{2k+p+4}}{2k+p+4} \left\{\left(1 + \frac{m}{2T_n}\right)^p + \left(1 + r + \frac{m}{2T_n}\right)^p\right\}\right] + \left[b_7 + k_B T_e \sum_{m=1}^{\infty} \frac{(-1)^{m+1}}{m} b_3\right] Z - \frac{\beta_1 \varepsilon_F}{4} x_1{}^4$$
$$+ b_8 \left(\frac{x_1{}^6}{6} + \frac{2}{5} a x_1{}^5 + \frac{a^2}{4} x_1{}^4\right) - 2 k_B T_e \sum_{m=1}^{\infty} \frac{(-1)^m}{m}\left[\frac{x_1{}^4}{4} b_1 - b_2 X\right] - k_B T_e \sum_{m=1}^{\infty}\sum_{l=1}^{\infty} \frac{(-1)^{(m+l)}}{(m+l)}\left[\frac{x_1{}^4}{4} b_4 - b_5 X\right]$$
$$- \sum_{m=1}^{\infty}\sum_{n=1}^{\infty} \frac{(-1)^m}{n!}\left(\frac{m}{T_n}\right)^{(n-1)} k_B T_L \left[\frac{x_1{}^{n+4}}{n+4} b_1 - b_2 X\right] - \sum_{m=1}^{\infty}\sum_{n=1}^{\infty}\sum_{l=1}^{\infty} \frac{(-1)^{(m+l)}}{(m+l)n!} \frac{k_B T_L l^n}{T_n{}^{n-1}} \left[\frac{x_1{}^{n+4}}{n+4} b_4\right.$$
$$\left. - b_5 \sum_{k=0}^{\infty}\sum_{p=0}^{\infty} \frac{(-1)^p}{k!\,p!} (2a)^p \{m+l)d\}^{(k+p)} \frac{x_1{}^{2k+p+n+4}}{2k+p+n+4}\right]$$
$$- \frac{x_1{}^4}{12C}[\{0.5 - C\varepsilon_F(1-\beta_2)\}^3 - \{0.5 - C\varepsilon_F(1-\beta_1)\}^3] - \frac{C k_B T_L b_7 x_1{}^5}{5}$$
$$- \sum_{m=1}^{\infty}\sum_{l=1}^{\infty} \frac{(-1)^{(m+l)}}{(m+l)} b_4 k_B \left[\frac{x_1{}^4}{4} T_e + \sum_{n=1}^{\infty} \frac{(-1)^n}{n!} \frac{k_B T_L l^n}{T_n{}^{n-1}} \frac{x_1{}^{n+4}}{n+4}\right]$$

$$
\begin{aligned}
I_{8} = {} & \beta_2 C k_B T_L\left(\frac{{x_{21}}^5}{5}-F_m^3\right)+(0.5-C\varepsilon_F)\beta_2\varepsilon_F\left(\frac{{x_{21}}^4}{4}-F_m^3\right)-Cb_8\left[\frac{{x_{21}}^7}{7}-a\left(\frac{{x_{21}}^6}{3}-2F_m^5\right)+\ a^2\left(\frac{{x_{21}}^5}{5}-F_m^4\right)\right. \\
& \left.-F_m^6\right]-b_8(0.5-C\varepsilon_F)\left[\frac{{x_{21}}^6}{6}-a\left(\frac{{x_{21}}^5}{5}-2F_m^4\right)+a^2\left(\frac{{x_{21}}^4}{4}-F_m^3\right)-F_m^5\right]+\frac{C}{2}(\beta_2\varepsilon_F)^2\left(\frac{{x_{21}}^4}{4}-F_m^3\right) \\
& -\frac{C}{2}{b_8}^2\left[\frac{{x_{21}}^8}{8}-4a\left(\frac{{x_{21}}^7}{7}-F_m^6\right)+a^2({x_{21}}^6-6F_m^5)-4a^3\left(\frac{{x_{21}}^5}{5}-F_m^4\right)+a^4\left(\frac{{x_{21}}^4}{4}-F_m^3\right)\right] \\
& +k_B T_e\sum_{m=1}^{\infty}\frac{(-1)^{m+1}}{m}b_3\left(\frac{{x_{21}}^4}{4}-F_m^3\right)+\sum_{m=1}^{\infty}\sum_{n=1}^{\infty}\frac{(-1)^{m+n+1}}{n!}\left(\frac{m}{T_n}\right)^{(n-1)}k_B T_L b_1\left[\frac{{x_{21}}^{n+4}}{n+4}\right. \\
& \left.+\sum_{r=1}^{\infty}\sum_{k=0}^{\infty}\frac{(-r)^k}{k!}\frac{{x_{21}}^{n+k+4}}{n+k+4}\right]+(0.5-C\varepsilon_F)[\beta_2\varepsilon_F(G_m^3+H_m^3)-b_8\{-G_m^5-H_m^5+2a(G_m^4+H_m^4)-a^2(G_m^3+H_m^3)\}] \\
& +\frac{C}{2}(\beta_2\varepsilon_F)^2(G_m^3+H_m^3)-\frac{C}{2}(G_m^7-H_m^7)+2Ca(G_m^6+H_m^6)-3Ca^2(G_m^5+H_m^5)+2Ca^3(G_m^4+H_m^4) \\
& +\frac{C}{2}a^4(G_m^3+H_m^3)+k_B T_e\sum_{m=1}^{\infty}\frac{(-1)^{m+1}}{m}b_3\,(G_m^3+H_m^3)-\frac{1}{3C}\left[(0.5-C\varepsilon_F+C\beta_2\varepsilon_F)^3\frac{{x_{21}}^4}{4}(0.5-C\varepsilon_F)^3\frac{{x_{21}}^2}{4}\right. \\
& -3C(0.5-C\varepsilon_F)b_8\left(\frac{{x_{21}}^6}{6}-\frac{2}{5}a{x_{21}}^5+\frac{1}{4}a^2{x_{21}}^4\right)-3C^2(0.5-C\varepsilon_F){b_8}^2\left(\frac{{x_{21}}^8}{8}-\frac{4}{7}a{x_{21}}^7+a^2{x_{21}}^6\right. \\
& \left.\left.-\frac{4}{5}a^3{x_{21}}^5+\frac{1}{4}a^4{x_{21}}^4\right)-C^3{b_8}^3\left(\frac{{x_{21}}^{10}}{10}-\frac{2}{3}a{x_{21}}^9+\frac{15}{8}a^2{x_{21}}^8-\frac{20}{7}a^3{x_{21}}^7+\frac{5}{2}a^4{x_{21}}^6-\frac{6}{5}a^5{x_{21}}^5+\frac{a^6}{6}{x_{21}}^4\right)\right] \\
& -Ck_B T_L\left[(0.5-C\varepsilon_F)\left\{\frac{\beta_2\varepsilon_F}{5}{x_{21}}^5-b_8\left(\frac{{x_{21}}^7}{7}-\frac{a}{3}{x_{21}}^6+\frac{a^2}{5}{x_{21}}^5\right)\right\}+\frac{C}{2}\left\{\frac{(\beta_2\varepsilon_F)^2}{5}{x_{21}}^5\right.\right. \\
& \left.\left.-{b_8}^2\left(\frac{{x_{21}}^9}{9}-\frac{a}{2}{x_{21}}^8+\frac{6}{7}a^2{x_{21}}^7-\frac{2}{3}a^3{x_{21}}^6+\frac{1}{5}a^4{x_{21}}^5\right)\right\}\right] \\
& -\sum_{m=1}^{\infty}\sum_{l=1}^{\infty}\frac{(-1)^{m+l+2}}{(m+l)}e^{-\frac{(m+l)(\beta_2-1)\eta}{T_n}}k_B\left[\frac{T_e}{4}{x_{21}}^4+\sum_{n=1}^{\infty}\frac{T_L}{n!}\frac{l^n}{{T_n}^{n-1}}\frac{{x_{21}}^{n+4}}{(n+4)}\right]
\end{aligned}
$$

$$I_9 = k_B T_e \sum_{m=1}^{\infty}\sum_{r=0}^{\infty}\sum_{k=0}^{\infty}\sum_{p=0}^{\infty} \frac{(-1)^{(m+1)}}{k!\,p!}(-md)^k \left(\frac{m}{4T_n} - r\right)^p \left(\frac{1}{b_2}\right)\left[\frac{x_{c2}{}^{(2k+p+4)}}{(2k+p+4)} + \sum_{n=1}^{\infty}\frac{(-1)^n}{n!}\frac{m^{(n-1)}}{T_n{}^n}\frac{x_{c2}{}^{(2k+p+n+4)}}{(2k+p+n+4)}\right] - k_B T_e \sum_{m=1}^{\infty}\sum_{l=1}^{\infty}\sum_{k=0}^{\infty}\sum_{p=0}^{\infty}\frac{(-1)^{(m+1)}}{mk!\,p!}(-md)^k \left(\frac{m}{4T_n} - l\right)^p \left(\frac{1}{b_2}\right)\frac{x_{c2}{}^{(2k+p+4)}}{(2k+p+4)} - k_B T_e \sum_{m=1}^{\infty}\sum_{l=1}^{\infty}\sum_{k=0}^{\infty}\sum_{p=0}^{\infty}\frac{(-1)^{(m+l+2)}}{(m+l)k!\,p!}\{-(m+l)d\}^k \left(\frac{m+l}{4T_n}\right)^p \left(\frac{1}{b_5}\right)\left[\frac{x_{c2}{}^{(2k+p+4)}}{(2k+p+4)} - \sum_{n=1}^{\infty}\left(\frac{l}{T_n}\right)^n \frac{x_{c2}{}^{(2k+p+n+4)}}{(2k+p+n+4)}\right]$$

and

$a = \frac{2m^* u_l{}^2}{k_B T_L}$; $b_1 = e^{\frac{m(\beta_1 - 1)\eta}{T_n}}$; $b_2 = e^{\left(\frac{mm^* u_l{}^2}{2k_B T_e} - \frac{m\eta}{T_n}\right)}$; $b_3 = e^{-\frac{m(\beta_2 - 1)\eta}{T_n}}$;

$b_4 = e^{\frac{(m+l)(\beta_1 - 1)\eta}{T_n}}$;

$b_5 = e^{\left\{\frac{(m+l)m^* u_l{}^2}{2k_B T_e} - \frac{(m+l)\eta}{T_n}\right\}}$; $b_6 = (2mda)^p + \sum_{r=1}^{\infty}\left(r + \frac{m}{2T_n}\right)^p$;

$b_7 = (0.5 - C\varepsilon_F)(\beta_2 - \beta_1)\varepsilon_F + \frac{C}{2}(\beta_2{}^2 - \beta_1{}^2)\varepsilon_F{}^2$; $b_8 = \frac{1}{2m^*}\left(\frac{k_B T_L}{2u_l}\right)^2$;

$d = \frac{k_B T_L}{8m^* u_l{}^2 T_n}$;

$A_m^i = \sum_{r=1}^{\infty}\left[\sum_{m=0}^{i} P(i,m)\frac{x_1{}^{(i-m)}}{r^{(m+1)}} e^{-rx_1} - \frac{6}{r^4}\right]$; $B_m^i = \sum_{m=0}^{i} P(i,m) x_1{}^{(i-m)} e^{-x_1}$

$D_m^i = \sum_{m=0}^{i} P(i,m)\frac{x_1{}^{(i-m)}}{(r+1)^{(m+1)}} e^{-(r+1)x_1}$;

$F_m^i = \sum_{r=1}^{\infty}\sum_{m=0}^{i}\frac{P(i,m)}{r^{(m+1)}}\left[\{x_2{}^{(i-m)}e^{-rx_2}\} - \{x_1{}^{(i-m)}e^{-rx_1}\}\right]$;

$G_m^i = \sum_{r=1}^{\infty}\sum_{m=0}^{i} P(i,m)\left[\{x_2{}^{(i-m)}e^{-x_2}\} - \{x_1{}^{(i-m)}e^{-x_1}\}\right]$;

$H_m^i = \sum_{r=1}^{\infty}\sum_{m=0}^{i}\frac{P(i,m)}{(r+1)^{(m+1)}}\left[\{x_2{}^{(i-m)}e^{-(r+1)x_2}\} - \{x_1{}^{(i-m)}e^{-(r+1)x_1}\}\right]$;

$$X = \sum_{k=0}^{\infty}\sum_{p=0}^{\infty}(-2a)^p(md)^{(k+p)}\frac{{x_1}^{(2k+p+4)}}{(2k+p+4)};$$

$$Y = \frac{{x_1}^{(n+4)}}{(n+4)} - \sum_{r=1}^{\infty}\sum_{k=0}^{\infty}\frac{(-r)^k}{k!}\frac{{x_1}^{(n+k+4)}}{(n+k+4)};$$

$$Z = \sum_{r=1}^{\infty}\left[D_m^3 - 6 - \frac{6}{(r+1)^4}\right];$$

$$x_{ij}^k = x_i^k - x_j^k;$$

Thus, once the average rate of loss of energy by the non-equipartition electrons due to phonon emission being known, one can calculate the non-ohmic mobility μ by equating $\langle\frac{d\varepsilon_{\vec{k}}}{dt}\rangle$ to $eE\mu^2$, the rate of gain of energy from the field [6.1]. Since it is the usual practise to express the non-ohmic mobility after normalising the same with the ohmic mobility, one should get the expression for μ_0 in the degenerate semiconductor under the similar low temperature conditions of interest here.

The ohmic mobility can be obtained from the expression for the current density J under the condition when the electron ensemble is subjected to quite low field such that the ensemble may still be assumed to remain in equilibrium with the lattice atoms. Obviously, the electrons then process the same temperature as that of the lattice atoms, i.e. $T_e = T_L$ [6.12]. The current density may be calculated by evaluating the integral

$$J = -\frac{8\sqrt{2}}{3}\frac{e^2Em^{*\frac{1}{2}}}{\hbar^3}\int_0^{\infty}\tau_{ac}\varepsilon^{\frac{3}{2}}\frac{\partial f_0}{\partial\varepsilon}d\varepsilon \qquad (6.15)$$

where, τ_{ac} is the momentum relaxation time for interaction with the intravalley acoustic phonons and is given by $\tau_{ac} = \tau_{acm}\left(\frac{\varepsilon}{k_BT_L}\right)^{-\frac{1}{2}}$; where $\tau_{acm} = \frac{\pi\rho\hbar^4{u_l}^2}{\sqrt{2}m^{*\frac{3}{2}}{E_1}^2(k_BT_L)^{\frac{3}{2}}}$.

Now using the model distribution function in place of the F.D. function at the temperature T_L, one can carry out the integration in (6.15), and thus obtain.

$$(\mu_0)_{deg} = \frac{8\sqrt{2m^*}}{3}\frac{e}{n\hbar^3}[I_{10} + I_{11} + I_{12}] \qquad (6.16)$$

where,

$$I_{10} = \sum_{m=1}^{\infty} (-1)^m \tau_{acm} (k_B T_L)^{1/2} \left[\left(\beta_1 \varepsilon_F + \frac{k_B T_L}{m} \right) e^{-\frac{m\beta_1 \varepsilon_F}{k_B T_L}} - \frac{k_B T_L}{m} \right]$$

$$I_{11} = \tau_{acm} (k_B T_L)^{1/2} \left(\frac{C}{2} \right) ({\beta_2}^2 - {\beta_1}^2) {\varepsilon_F}^2$$

$$I_{12} = \sum_{m=1}^{\infty} (-1)^m \tau_{acm} (k_B T_L)^{1/2} \left(\beta_2 \varepsilon_F + \frac{k_B T_L}{m} \right) e^{\frac{m(1-\beta_2)\varepsilon_F}{k_B T_L}}$$

The expression of μ_0 for a non degenerate ensemble may be found in [6.12].

6.2.3. Results and Discussions

In the present study, the effects of degeneracy on some transport parameters such as the average energy loss rate of the non-equilibrium electrons, zero and high field mobilities have been studied in Si and InSb at low lattice temperatures. The analysis takes due account of the low temperature features like the inelasticity of the electron-acoustic phonon interactions and the true phonon distribution in place of the equipartition approximation.

The energy loss rate of the non-equilibrium electrons due to acoustic interaction $\langle \frac{d\varepsilon_{\vec{k}}}{dt} \rangle_{ac}$ has been plotted as a function of the normalised electron temperature $T_n \left(= \frac{T_e}{T_L} \right)$ for different degenerate samples ($\frac{\varepsilon_F}{k_B T_L}$= 5 and 15) of Si and InSb respectively in Fig 6.6 and Fig 6.7 using the result obtained in eq. (6.14) at the lattice temperatures T_L= 4K and 20K. Similar characteristics for the non-degenerate samples of the same materials have been plotted under the similar conditions using the results that are obtained in [6.17] in the respective figures. The average energy of the electrons in a degenerate ensemble is $\langle \varepsilon_{\vec{k}} \rangle_{deg} = k_B T_e \frac{F_{\frac{3}{2}}(\eta_e)}{F_{\frac{1}{2}}(\eta_e)}$ [6.9]. For relatively lower concentration of the carriers, the sample

being a non-degenerate one, the average energy becomes $\langle \varepsilon_{\vec{k}} \rangle_{non-deg} = \frac{3}{2} k_B T_e$. Evidently T_n at any lattice temperature is a measure of the average energy of an ensemble as has already been said earlier [6.9,6.14].

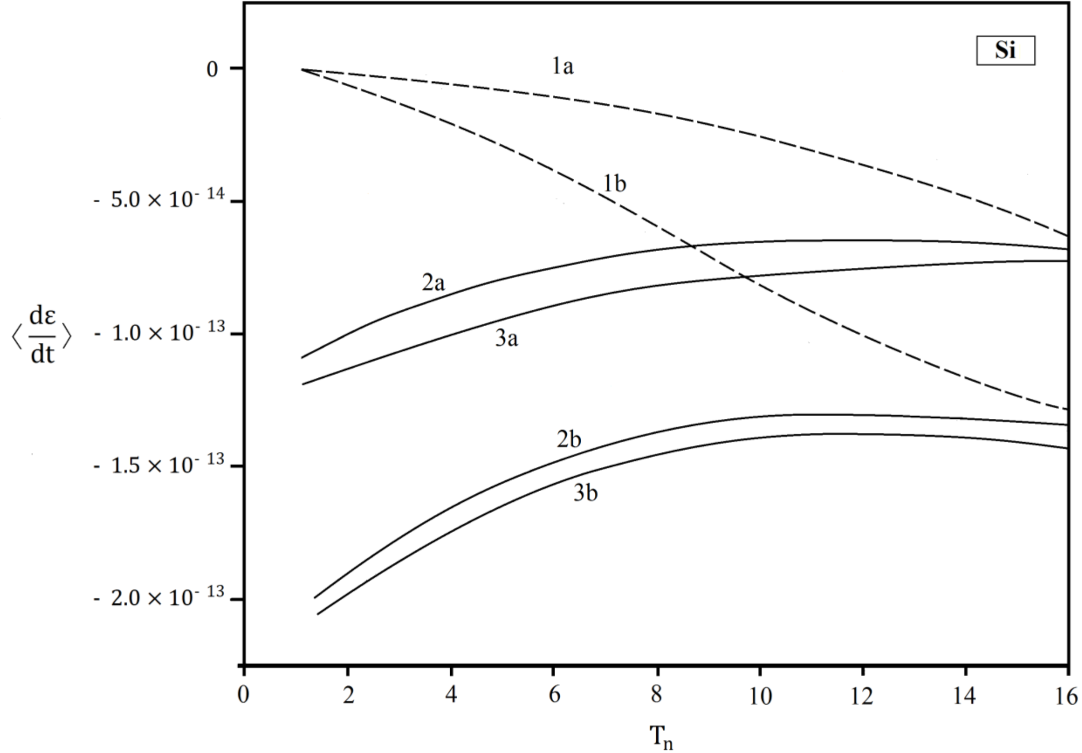

Fig. 6.6 : Dependence of $\langle \frac{d\varepsilon}{dt} \rangle$, the average energy loss rate of the non-equilibrium electrons upon the normalised electron temperature T_n. Curves marked '1' are for the non-degenerate sample of Si and those marked '2'and '3' correspond to the degenerate samples of the same material with the degeneracy parameters $\frac{\varepsilon_F}{k_B T_L} = 5$ and 15 respectively. Curves marked 'a' and 'b' are for lattice temperatures $T_L =$ 4K and 20K respectively.

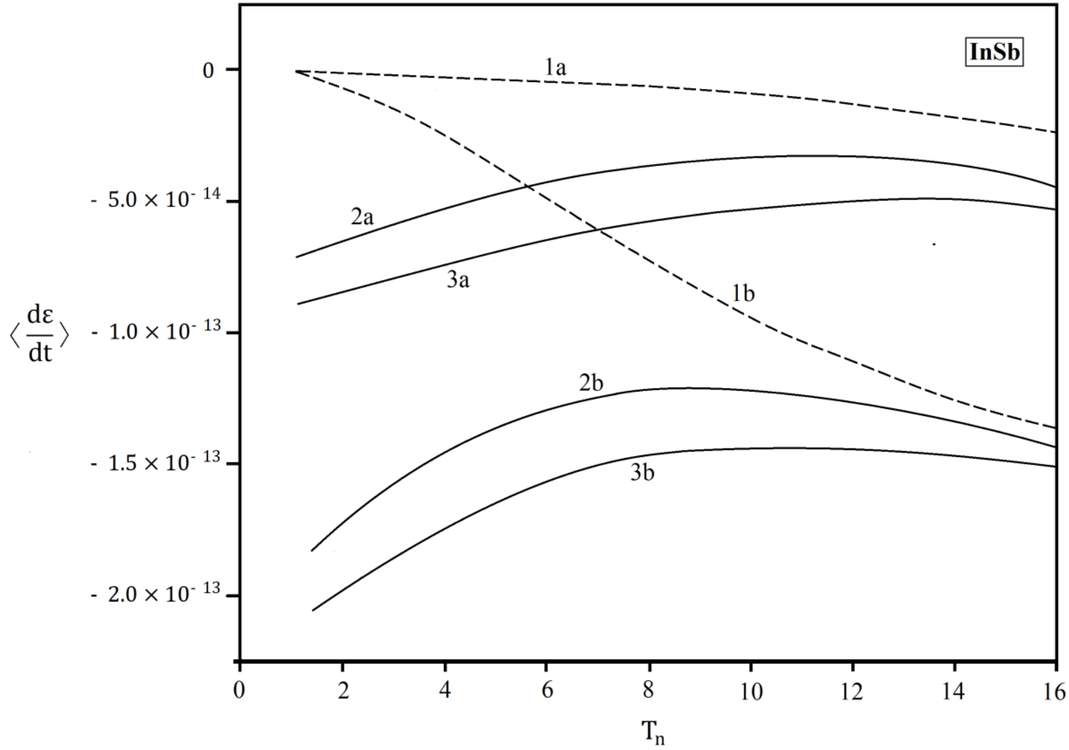

Fig. 6.7 : Dependence of $\langle\frac{d\varepsilon}{dt}\rangle$, the average energy loss rate of the non-equilibrium electrons upon the normalised electron temperature T_n. Curves marked '1' are for the non-degenerate sample of InSb and those marked '2'and '3' correspond to the degenerate samples of the same material with the degeneracy parameters $\frac{\varepsilon_F}{k_B T_L} = 5$ and 15 respectively. Curves marked 'a' and 'b' are for lattice temperatures $T_L =$ 4K and 20K respectively.

On comparing the curves 1a with 2a and 3a, and 1b with 2b and 3b of Fig 6.6 and 6.7, it may be seen that there are both quantitative and qualitative changes in the ELR characteristics due to consideration of degeneracy into account. The discrepancies in the characteristics increase on increasing the level of degeneracy $(\frac{\varepsilon_F}{k_B T_L})$ at a particular lattice temperature. The characteristic curves for the degenerate ensemble tend to the same for the non-degenerate samples at the higher values of the normalised temperatures. It is because of the fact that, at higher values of temperature, the electrons tend to obey the Maxwellian distribution because of higher energy. Hence at such higher energies, the effect of degeneracy on the energy loss rate is hardly observed.

Fig. 6.8 and 6.9 describe the zero-field mobility characteristics (μ_0) as a function of the lattice temperature for both the non-degenerate and degenerate samples of the same materials. The curves for the degenerate samples have been obtained from the eq.(6.16) and that for the non-degenerate samples are the results which are already reported in [6.12].

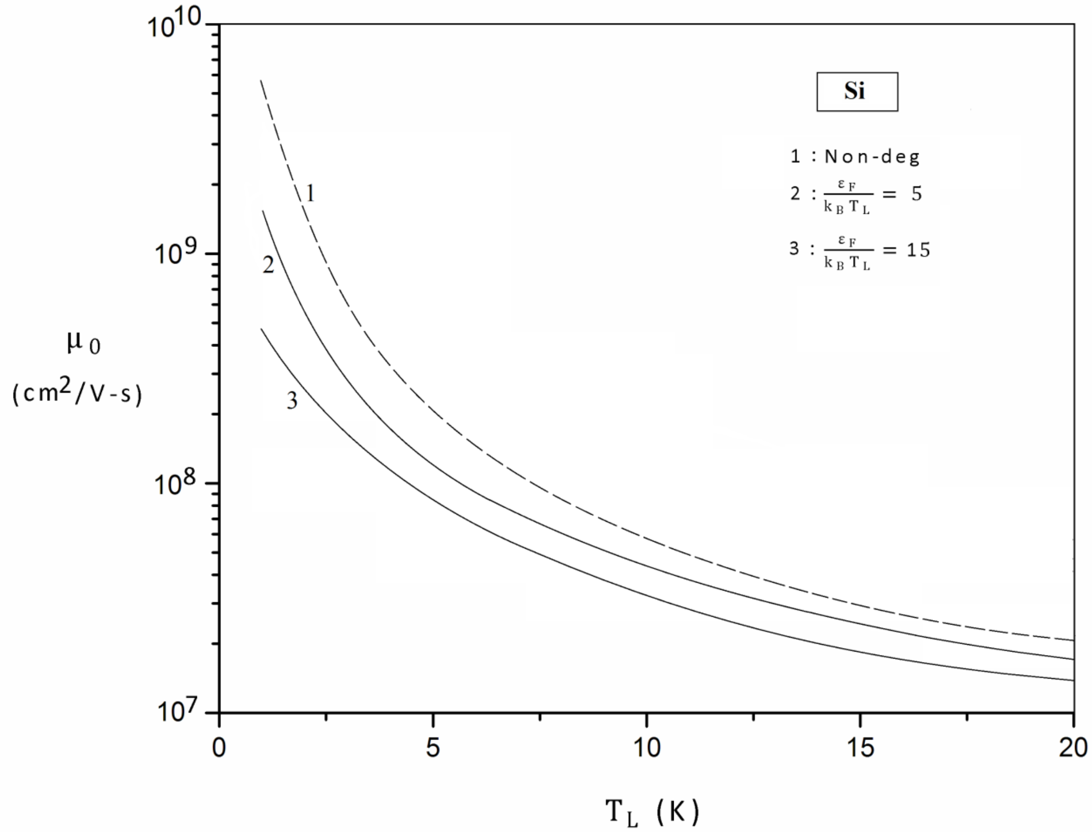

Fig. 6.8 : Dependence of μ_0, the zero field mobility upon the lattice temperature T_L for Si. Curves marked '1' represent the characteristic of a non-degenerate sample of Si and those marked '2' and '3' correspond to the same material with the degeneracy parameter $\frac{\varepsilon_F}{k_B T_L}$ = 5 and 15 respectively.

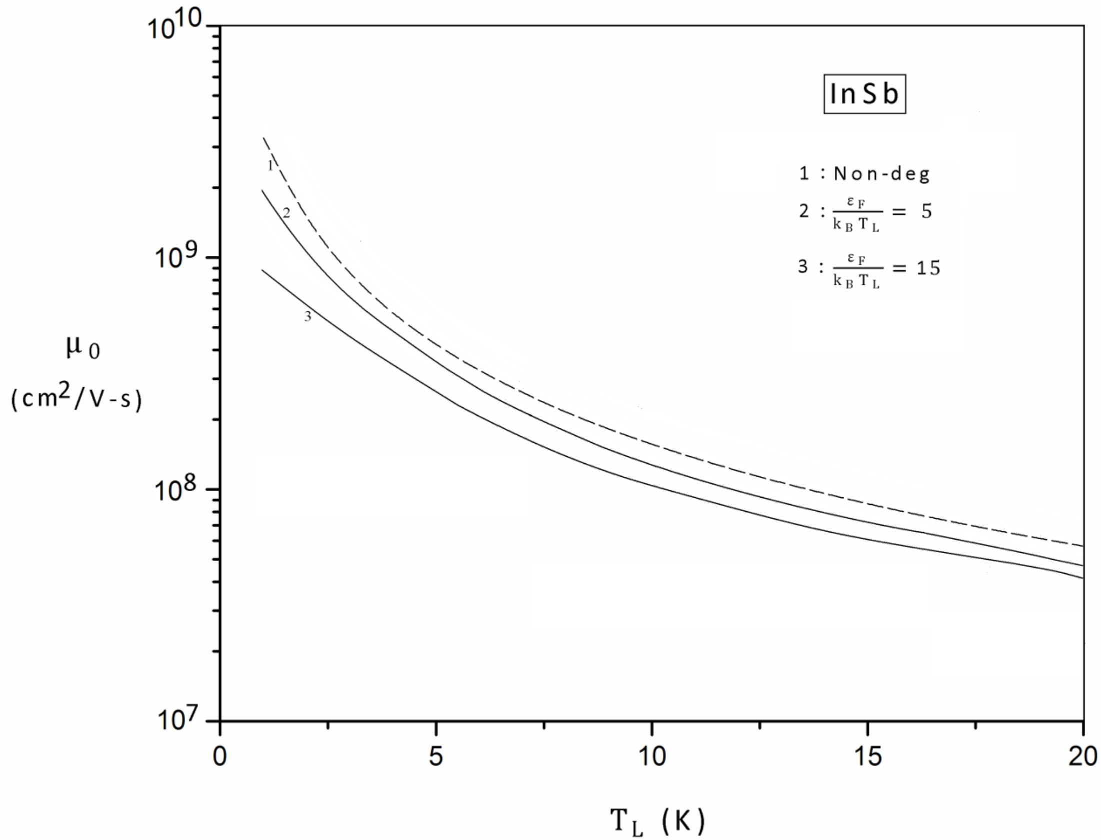

Fig. 6.9 : Dependence of μ_0, the zero field mobility upon the lattice temperature T_L for InSb. Curves marked '1' represent the characteristic of a non-degenerate sample of InSb and those marked '2' and '3' correspond to the same material with the degeneracy parameter $\frac{\varepsilon_F}{k_B T_L} = 5$ and 15 respectively.

One finds the quantitative changes in the above characteristics due to consideration of the degeneracy into account, vide curves 1 with 2 and 3 of Fig 6.8 and Fig 6.9. It may be observed that, the discrepancy in the characteristics is higher, the higher the level of degeneracy is. Again, the discrepancies decrease, the higher the lattice temperature is at a particular level of degeneracy. It is evident that, the mobility will decrease for the degenerate samples compared to that of the non-degenerate one because of the increased rate of scattering in the former material [6.15].

Finally from the energy loss rates as obtained in eq.(6.14), the high field mobility in the degenerate sample is calculated by equating the same with $eE\mu^2$ as discussed earlier, at different lattice temperatures. Similar results for the non-degenerate samples

may be obtained from [6.11]. These high field mobility values are then normalised with respect to the corresponding zero field mobilities under the similar prevalent conditions for both the non-degenerate and degenerate materials. The particular values of the zero-field mobility for Si and InSb are obtained from Fig. 6.8 and Fig. 6.9 respectively for the corresponding lattice temperatures. Then the normalised mobility $\left(\frac{\mu}{\mu_0}\right)_{\text{deg(non-deg)}}$ has been plotted as a function of the electric field E (V/cm) in Fig. 6.10 and Fig. 6.11 for Si and InSb respectively. In order to obtain such dependence, one needs to have knowledge on the fact that, how the electron temperature depends on the electric field for a material. This has already been studied by the present authors for both the non-degenerate and degenerate materials in [6.11] and [6.7] respectively under the prevalent conditions of interest here. These data are used for obtaining the field dependence of the normalised mobility at different lattice temperatures in the present analysis.

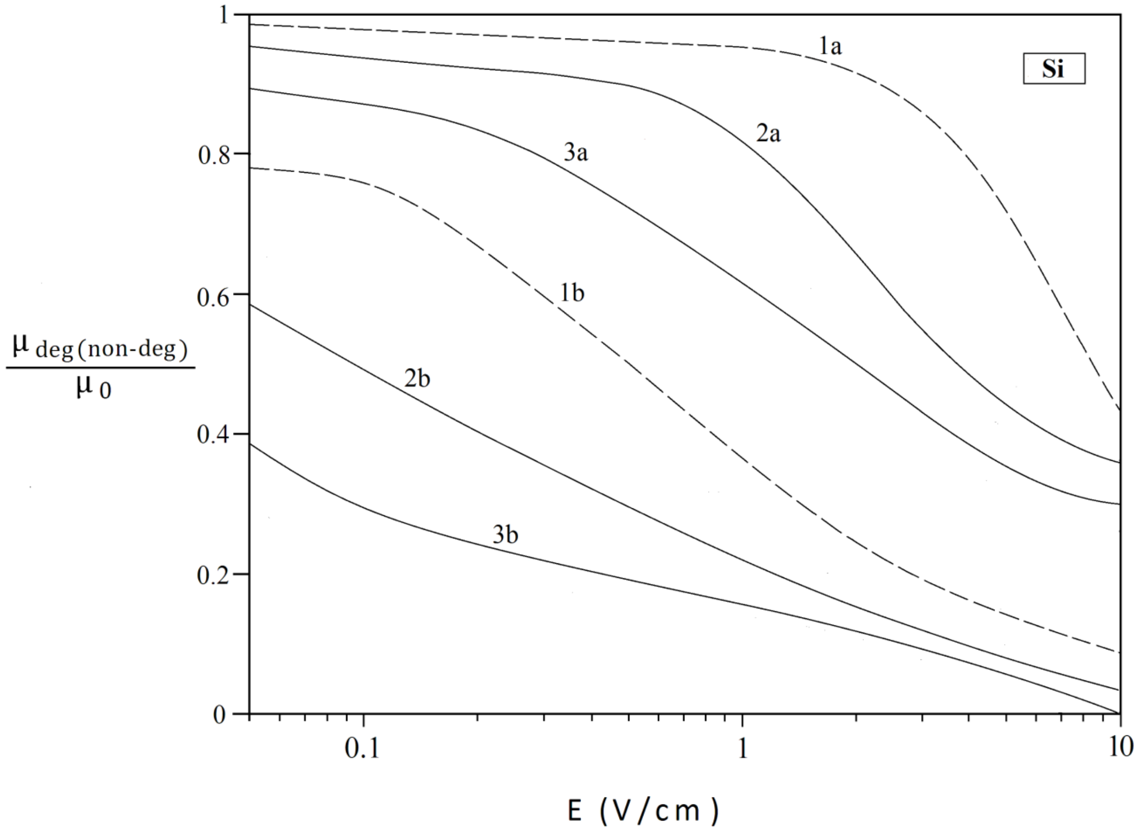

Fig. 6.10 : Dependence of $\left(\frac{\mu}{\mu_0}\right)$, the high field mobility normalised to the zero-field mobility of both the non-degenerate and degenerate samples of Si upon the electric field E. Curves marked '1' are for the non-degenerate samples and those marked '2' and '3' correspond to the degeneracy parameters $\frac{\varepsilon_F}{k_B T_L} = 5$ and 15 respectively of the same material. Curves marked 'a' and 'b' respectively are for lattice temperatures $T_L =$ 4K and 20K.

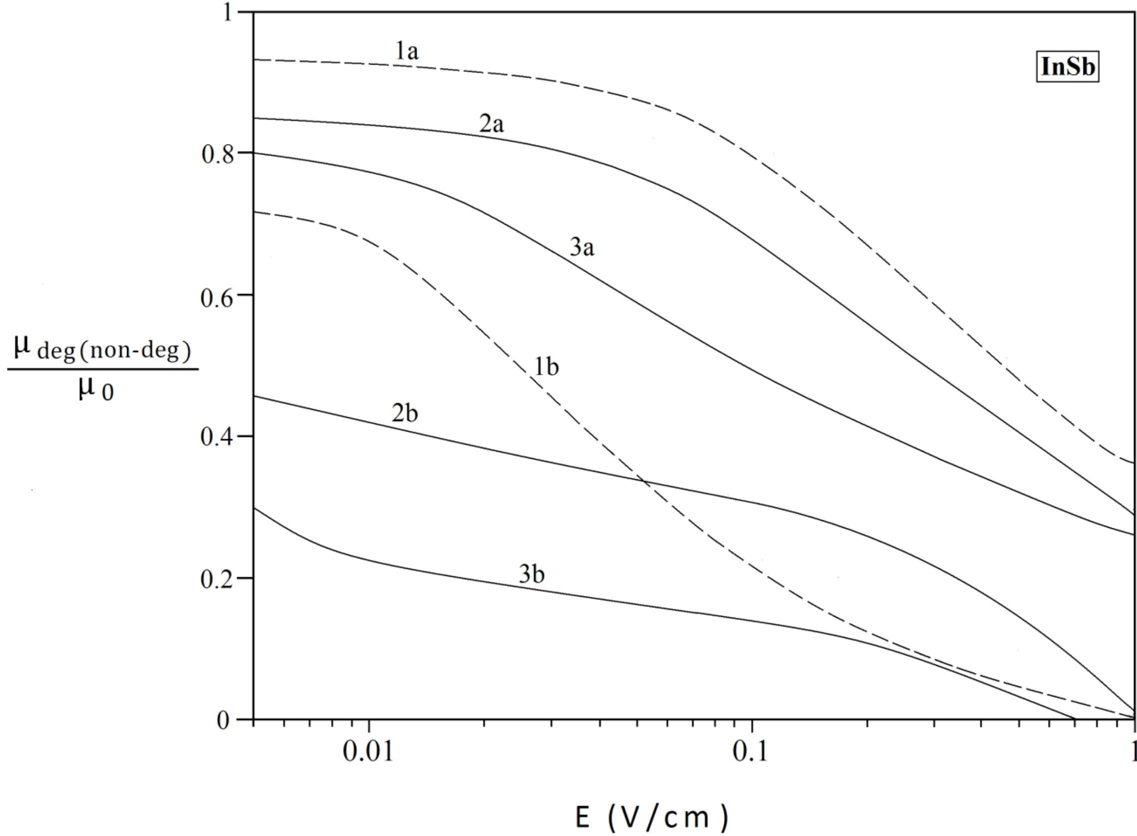

Fig. 6.11 : Dependence of $\left(\frac{\mu}{\mu_0}\right)$, the high field mobility normalised to the zero-field mobility of both the non-degenerate and degenerate samples of InSb upon the electric field E. Curves marked '1' are for the non-degenerate samples and those marked '2' and '3' correspond to the degeneracy parameters $\frac{\varepsilon_F}{k_B T_L} = 5$ and 15 respectively of the same material. Curves marked 'a' and 'b' respectively are for lattice temperatures $T_L =$ 4K and 20K.

On comparing the curves 1a with 2a and 3a, and 1b with 2b and 3b of Fig. 6.10 and Fig. 6.11, it may be seen that there are again both the qualitative and the quantitative changes in the characteristics as one considers the degeneracy of the carrier ensemble at a particular lattice temperature. The discrepancy in the characteristics becomes larger, as the level of degeneracy increases at a particular lattice temperature. Again, on comparing the curves marked 'a' with those marked 'b', one can notice that the effect of degeneracy is greater for the lower lattice temperatures. This in turn shows that the degeneracy of the carrier ensemble is a low temperature feature.

The figures reveal that, the various transport characteristics as obtained here change significantly as one takes the degeneracy of the sample into account. The present analysis has been carried out considering some of the low temperature features, such as the inelasticity of the electron- phonon collisions and the true phonon distribution. However, there are few more important low temperature features that need to be taken into account for the refinement of the theory. The impurity levels degenerate into impurity bands because of high doping. This results in the reduction of the band gap of the semiconductors and the phenomenon of band tailing occurs [6.5]. Apart from that, as the electron concentration increases, the effects of electrostatic screening of the scattering potential due to lattice imperfections become significant. Moreover, interactions of the electrons with the piezoelectric phonons is quite important at low lattice temperatures particularly in the compound semiconductors that lack inversion symmetry. However, it is apparently a formidable task to consider all the low temperature features at a time in the theoretical analysis of a problem. Of course, consideration of the above features will refine the present theory. For such study, in case of the compound semiconductors that are important from the device point of view, one needs to calculate $\left(\frac{dN_q}{dt}\right)$ for the piezoelectric interaction afresh. However, the results obtained here being realistic; stimulate for further studies on the transport phenomena in the degenerate semiconductors at low temperatures. Such result may provide an important database for the device engineers for making stimulation software of the transport problems in different semiconductors.

References:

[6.1] E.M.Conwell, in Solid State Physics, edited by F.Seitz and D.Turnbull (Academic, New York), Suppl. 9, (1967).

[6.2] Z.S.Kachlishvili, Phys. Status Solidi A33 15 (1976).

[6.3] N.Chakrabarti and D.P.Bhattacharya, Phys.Rev.B 53 6885 (1995).

[6.4] N.Chakrabarti and D.P.Bhattacharya, Phys.Rev.B 55 840 (1996).

[6.5] B.R.Nag, Electron Transport In Compound Semiconductors, Springer, Berlin, Heidelberg, New York (1980).

[6.6] S.M.Sze, Physics of Semiconductor Devices, Wiley Eastern Limited, New Delhi, (1983).

[6.7] C.Kittel, Introduction to Solid State Physics, Wiley Eastern Limited, New Delhi, (1976).

[6.8] S.Midday, S.Nag, D.P.Bhattacharya, Physica B 458 18 (2015).

[6.9] G.Bauer, Springer Tracts in Modern Physics, Springer, Berlin, Heidelberg, New York, (1974).

[6.10] A.Anselm, Introduction to Semiconductor Theory, Mir Publisher, (1981).

[6.11] B.Das, A.Basu, J.Das, D.P.Bhattacharya, Physica B 474 21 (2015).

[6.12] B.R.Nag, Theory of Electrical Transport in Semiconductors, Pergemon Press, Oxford, (1972).

[6.13] L.Reggiani, Hot Electron Transport in Semiconductors, Springer- Verlag, Berlin, (1985).

[6.14] A.Basu, B.Das, T.R.Middya, D.P.Bhattacharya, Physica B506 65 (2017).

[6.15] A.Basu, B.Das, T.R.Middya, D.P.Bhattacharya, J. Phys. Chem. Solids 100 9 (2017).

[6.16] J.S.Blackmore, Semiconductor Statistics, Pergamon Press, Oxford, (1962).

[6.17] B Das, A Basu, J Das, DP Bhattacharya, Canadian Journal of Physics 95 167 (2017).

CHAPTER – VII

Field-effect mobility of a two dimensional electron gas in an n–channel of Si-SiO_2 MOS structure

7.1. Introduction

The advancement of Si technology has made it possible to get Si-SiO_2 interface with a high degree of perfection. This prompted to replace the bipolar devices by the field effect devices, for many applications.

The MOS (Metal-Oxide-Semiconductor) structures, having similar interfaces are now widely used in digital integrated circuits. The free carriers in the conducting channel of those structures are not provided by the usual method of doping, but by the process of inversion and depletion of the surface layer. A typical concentration of about $10^{19}/m^2$ in the surface layer of SiO_2, gives rise to a rather strong surface electric field $E_s \sim 10^7$ V/m. Such a strong field effectively quantises the motion of the carriers in a direction perpendicular to the interface. But the electrons move freely on the interfacial surface. This is thus one of the structures that exhibit a quasi two dimensional ensemble of electron gas (Q2D). The study of an ensemble of Q2D has become important since the advent of the metal-oxide-semiconductor field effect transistor with easily controllable surface characteristics.

Much studies, both experimental and theoretical, have been made on the electronic transport properties of the Q2D's under various prevalent conditions [7.1]. It is well known that the transport characteristics of the Q2D in the channel of MOS, are controlled

by one or more interactions of the electrons, like the interaction with the acoustic mode lattice vibrations, and with the charged impurities near the oxide-semiconductor interface. However, the interaction with the intravalley acoustic phonons is intrinsic in nature and turns up as the most important mechanism in interpreting the available experimental results on the surface mobility characteristics at relatively higher lattice temperatures [7.2]. Though the surface-impurity scattering may seem to dominate under the condition of low surface electric fields, it is well known that, such interaction mechanism can hardly explain the details of the field-effect mobility characteristics when the surface electric field is high [7.2, 7.3]. Moreover, the carriers in high purity materials interact dominantly with the intravalley acoustic phonons, over a range of low lattice temperatures. Hence the problem of electrical transport at the low lattice temperatures turns out to be important [7.4-7.9].

Useful experimental results of the electrical transport in Q2D at the lower lattice temperatures are readily available. Shubnikov-de Hass Oscillations has been observed in the quantum well of GaAs – $Ga_xAl_{1-x}As$ heterostructures around 4.2K [7.5]. Interesting results on the mobility characteristics of the electrons in the n-type inversion layer of Si, for different crystallographic orientations at temperatures around 77K are also reported in the literature [7.7].

Wu and Thomas made theoretical analysis of the surface mobility characteristics of the thermally oxidised Silicon surface layer for the two-dimensional electron-lattice scattering at high surface electric fields, under the conditions of both high and low lattice temperatures [7.3]. The analysis is based on a number of simplified approximations. Some of them include (i) even though the lattice wave is three dimensional, it is assumed that the two dimensional electrons interact only with the two dimensional phonons, and so, takes into account only the components of the electron and phonon wave vectors $\vec{k}$ and $\vec{q}$ which are parallel to the interface. Thus, the effects of the transverse component of the phonon wave vector has been neglected, (ii) at sufficiently low temperatures, it has also been assumed that the phonons that can be excited are quite limited, hence the phonon population n_q has been taken to be effectively zero. Hence the agreement of their theoretical results with the experimental values has been hardly satisfactory.

Some efforts have already been made by many, including some of the present authors [7.8] to take into account the effects of the transverse component of the phonon wave vector in the light of Ridley's momentum conservation approximations (MCA) [7.9]. But the framework of MCA of Ridley has been developed only for an infinite rectangular quantum well. Whereas, on the surface channel of the MOS structure, which

has been considered by the Wu and Thomas [7.3], the well is actually represented by an infinite triangular potential well. Lee and Vassel [7.10] has made a refinement of Ridley's analysis of MCA, for such a well, and obtained phonon limited mobility in semiconductor heterostructures under the condition, when the lattice temperature is high.

The purpose of the present calculation is to find the field-effect mobility characteristics in a Q2D, duly taking into account (i) the effects of the transverse component of the phonon wave vector, unlike the analysis of Wu and Thomas, (ii) the full form of the phonon distribution under the condition of low temperature, instead of simply assuming $n_q = 0$, (iii) the refinement of Ridley's MCA, as put forward by Lee and Vassel, for the more realistic model of triangular potential well. The dependence of the field-effect mobility μ_{FE} on the (i) temperature, (ii) effective gate voltage and (iii) surface electric field, for an ensemble of 2DEG in Si-SiO_2 MOS structure have been obtained.

The results have shown, how each of these factors, contributes significantly, to obtain a more realistic picture of the field-effect mobility characteristics, in the channel of Si-SiO_2 MOS structure. One can note that the results of the theoretical analysis which has been made here, bring in significant improvement in their agreement with the experimental data.

7.2. Development

We consider an ensemble of a non-degenerate Q2D of the conducting channel in the $SiO_2 - Si$ interface of a MOS structure. The interface is assumed to be on the X-Y plane. The quantum well that is formed along the transverse z-direction is taken to be an infinite triangular potential well, where the electrons get confined. Thus the conduction electrons have classical free electron motion on the X-Y plane, and the motion along the z – direction, perpendicular to the interface, is quantized.

It is usually assumed that the interaction of the electrons with the acoustic mode lattice vibrations is weak enough for the first order perturbation theory to be applicable. The probability of occupancy $f(\vec{k})$ of any state $|\vec{k}\rangle$ increases when the electrons are scattered into the state $|\vec{k}\rangle$ making transition either from the state $|\vec{k}+\vec{q}\rangle$ or from $|\vec{k}-\vec{q}\rangle$, through the process of emission or absorption of a phonon of wave vector $\vec{q}$ respectively. Similarly, $f(\vec{k})$ decreases, when they are scattered out of the state $|\vec{k}\rangle$, and make transition to either of the two states, following an absorption or emission of the phonon. Taking the

algebraic sum of all these four processes into account, one can write for the net rate of change in the probability of the carrier occupancy of the state $|\vec{k}\rangle$ as [7.3,7.9,7.11]

$$\frac{\partial f(\vec{k})}{\partial t} = \frac{2\pi}{\hbar}\frac{\Omega}{(2\pi)^3}\int_q\int_{q_z}\int_\theta \left|M\left(\vec{k},\vec{k}\pm\vec{q}\right)\right|^2 f(\vec{k})\delta\left(\varepsilon_{\vec{k}} - \varepsilon_{\vec{k}\pm\vec{q}} \pm \hbar\omega_{\vec{Q}}\right) q\, dq dq_z d\theta \qquad (7.1)$$

where $\hbar = \frac{h}{2\pi}$; h being the Plack's constant; $\varepsilon_{\vec{k}}$, the electron energy $= \frac{\hbar^2 k^2}{2m_{\|}{}^*}$; $m_{\|}*$ is the effective mass of the electrons parallel to the interface, and θ is the angle between $\vec{k}$ and $\vec{k}'(=\vec{k}\pm\vec{q})$, the $\pm$ signs refer respectively to the emission or absorption of a phonon. Obviously, for the transitions from the states $|\vec{k}\pm\vec{q}\rangle$, $f(\vec{k})$ should be replaced accordingly by $f(\vec{k}\pm\vec{q})$.

Taking due account of the transverse component of the phonon wave vector q_z, the square of the matrix element for transition between the state $|\vec{k}\rangle$ and $|\vec{k}'\rangle$, due to the lattice scattering of the electrons, which are confined into a triangular potential well, may be given by [7.9,7.10]

$$\left|M\left(\vec{k},\vec{k}\pm\vec{q}\right)\right|^2 = \frac{{E_1}^2\hbar}{2\rho\Omega u_l} Q\left(N_Q + \frac{1}{2} \pm \frac{1}{2}\right)|G(q_z)|^2 \delta_{\vec{k}',\vec{k}\pm\vec{q}} \qquad (7.2)$$

It has been assumed that the electrons occupy only the lowest sub-band having energy $\varepsilon_0 = \frac{1}{2}\left[\frac{9\pi\hbar e E_S}{4{m^*}_3{}^{1/2}}\right]^{2/3}$. Here E_1 is the deformation potential constant and ${m^*}_3$ is the effective mass perpendicular to the surface, $\vec{q}$ is the component of the three dimensional phonon wave vector $\vec{Q}$ on the X-Y interface. Thus, $Q^2 = q^2 + {q_z}^2$. N_Q is the phonon population given by the Bose Einstein distribution function, and $\omega_Q = u_l Q$ [7.10].

It may be pointed out here that the quantum confinement of the electrons does not allow the momentum conservation in all the three dimensions equally. The Kronecker delta function in eq.(7.2) signifies that the momentum conservation on the plane of the interface is exact. But it is not so, for the z-direction, which is transverse to the interface. The form factor $|G(q_z)|^2$ actually describes the degree of momentum conservation along the z – direction. The expression for the form factor depends upon the nature of the potential well that is observed in a particular device system. The momentum conservation approximation (MCA) has been developed for an infinite square well by Ridley [7.9]. But in devices like MOSFET that consists of the MOS structure, the well is known to be an infinite triangular well. Ridley's model of MCA has been refined by Lee and Vassel

[7.10], for the case of triangular potential well. In the refined model, the form factor may thus be taken as

$$|G(q_z)|^2 \approx \frac{2\pi G}{z_1}\left[4\delta(q_z) + \delta\left(q_z - \frac{2\pi}{z_1}\right) + \delta\left(q_z + \frac{2\pi}{z_1}\right)\right] \tag{7.3}$$

where, $$G = \left(\frac{z_1}{4}\right)^2 \left[\frac{z_1}{2} - \frac{0.707\hbar^{2/3}}{(144{m^*}_3\pi e E_s)^{1/3}}\right]^{-2} \tag{7.4}$$

and $$z_1 = \frac{1}{2eE_s}\left(\frac{9\pi\hbar e E_s}{4{{m^*}_3}^{1/2}}\right)^{2/3} \tag{7.5}$$

e is the electronic charge, ρ is the mass density, u_l is the acoustic velocity, E_s, the surface electric field is given by $\frac{e}{K_s\epsilon_0}\left(N_{inv} + N_{dep}\right)$, N_{inv} and N_{dep} are the carrier concentrations due to inversion and depletion respectively at the interface channel, K_s is the dielectric constant and ϵ_0 is the free space permittivity.

The limits of q may be obtained from the balance condition of the energy and of the momentum component on the interface, for the electron-phonon system. Thus, for the case of elastic collisions, the limits are found to be q = 0 and q = 2k. Now carrying out the integration over θ one obtains

$$\frac{\partial f(\vec{k})}{\partial t} = \frac{{E_1}^2 {m^*}_{\|}}{4\pi^2 \rho u_l \hbar^2 k}\int_{q=0}^{2k}\int_{q_z} \frac{(q^2+{q_z}^2)^{\frac{1}{2}}}{\sqrt{1-\left(\frac{q}{2k}\right)^2}}\left(N_Q + \frac{1}{2} \pm \frac{1}{2}\right)|G(q_z)|^2 f(\vec{k})\,dq\,dq_z \tag{7.6}$$

Next, using the expression (7.3) for $|G(q_z)|^2$, the integration over q_z may be performed. In order to carry out the integration over q, the expressions for $f(\vec{k} \pm \vec{q})$ and N_Q are to be assigned. The Taylor series expansion of the distribution function of the electrons may be approximated as [7.3,7.11,7.12]

$$f(\vec{k} \pm \vec{q}) = f(\varepsilon_{\vec{k}} \pm \hbar\omega_{\vec{Q}}) = f_0(\vec{k}) \pm \hbar\omega_{\vec{Q}}\frac{\partial f_0}{\partial \varepsilon_{\vec{k}}} \tag{7.7}$$

where $f_0(\vec{k})$ is the equilibrium distribution function.

7.2.1. Mobility characteristics at high temperatures

It is well known that most of the electrons interact only with the long wavelength acoustic phonons [7.4,7.11,7.12]. As such, the crystal dispersion has been assumed to be linear. Thus at high temperatures, one can assume that the phonon energy is much smaller than the average thermal energy of the electrons i.e. $\hbar\omega_{\vec{Q}} \ll k_B T$. Hence the phonon distribution simply reduces to the form of the equipartition law i.e. $N_Q = \frac{k_B T}{\hbar\omega_{\vec{Q}}} \gg 1$. Thus, using the equipartition approximation for the phonon distribution, the integration over q may be performed and one obtains

$$\frac{\partial f(\vec{k})}{\partial t} = -\frac{9{E_1}^2 G\, m^*_{\parallel} k_B T}{\rho {u_l}^2 \hbar^3 z_1}\left[f\left(\vec{k}\right) - f_0\left(\vec{k}\right)\right] \tag{7.8}$$

Thus the inverse of the momentum relaxation time can be identified as [7.11]

$$P_{ac} = \frac{1}{\tau_{ac}} = \frac{9{E_1}^2 G\, m^*_{\parallel} k_B T}{\rho {u_l}^2 \hbar^3 z_1} \tag{7.9}$$

It may be noted that the relaxation time at high temperatures comes out to be independent of energy. As such $\langle\tau_{ac}\rangle_{\text{High Temp}} \equiv \tau_{ac}$. Thus the effective mobility of the surface layer at high temperature is obtained as

$$\left(\mu_{eff}\right)_{\text{High Temp}} = \frac{e\langle\tau_{ac}\rangle_{\text{High Temp}}}{m_\mu^*} = \frac{e\rho {u_l}^2 \hbar^3 z_1}{9{E_1}^2 G\, m_\mu^* {m_\parallel}^* k_B T} \tag{7.10}$$

where, m_μ^* is the conduction electron effective mass [7.3].

7.2.2. Mobility characteristics at low temperatures:

At the low temperatures, as the average thermal energy of the electrons tends to be comparable with the phonon energy, the equipartition approximation for the phonon distribution can hardly be made [7.4]. Though the phonon population at the low temperatures is indeed limited, putting $N_Q = 0$ as done in Wu and Thomas [7.3], seems to be an oversimplification. Under this condition since $\exp\left(-\frac{\hbar\omega_{\vec{Q}}}{k_B T}\right)$ is a rather small quantity, the phonon population in the present analysis has been chosen after some little rearrangement of the full form of the Bose Einstein distribution, as $N_Q =$

$\sum_{n=0}^{\infty} \exp\left[-\frac{(n+1)\hbar\omega_{\vec{Q}}}{k_B T}\right] \ll 1$. Obviously, the series easily converges within quite a small number of terms. Moreover, at low temperatures, N_Q is already a small quantity, so sticking only up to the first term in the Taylor series expansion of $f(\varepsilon_{\vec{k}} \pm \hbar\omega_{\vec{Q}})$ one can obtain

$$\frac{\partial f(\vec{k})}{\partial t} = -\frac{{E_1}^2 G\, {m^*}_{\parallel}}{2\pi\rho u_l\, \hbar^2 z_1 k}(2I_1 + I_2)\left[f(\vec{k}) - f_0(\vec{k})\right] \qquad (7.11)$$

Thus the inverse of the momentum relaxation time under the condition of low temperature assumes the form

$$P_{ac} \equiv \frac{1}{\tau_{ac}} = \frac{{E_1}^2 G\, {m^*}_{\parallel}}{2\rho u_l\, \hbar^2 z_1 k}(2I_1 + I_2) \qquad (7.12)$$

where

$$I_1 = \sum_{n=0}^{\infty}\sum_{m=0}^{\infty} \frac{(-1)^m}{m!}\left[\frac{(n+1)\hbar u_l}{k_B T}\right]^m (4I_{11} + 2I_{12})$$

$$I_{11} = (2k)^{(m+2)} \int_0^1 \frac{x^{(m+1)}}{\sqrt{1-x^2}}\,dx$$

$$I_{12} = \pi k\left(4k^2 + \frac{4\pi^2}{{z_1}^2}\right)^{\frac{(m+1)}{2}} - (m+1)\sum_{r=0}^{\infty}\sum_{l=0}^{\infty} \frac{\Gamma\left(r+\frac{1}{2}\right)\left(\frac{4\pi^2}{{z_1}^2}\right)^l}{\sqrt{\pi}(2r+1)r!}\binom{m}{l}\frac{(2k)^{p-2l+2}}{(m-2l-2r+2)}$$

$$I_2 = 19k^2 + 2\pi k\left(4k^2 + \frac{4\pi^2}{{z_1}^2}\right)^{\frac{1}{2}} - 4k\sum_{r=0}^{\infty}\sum_{p=0}^{\infty} \frac{\Gamma\left(r+\frac{1}{2}\right)\left(\frac{2\pi}{z_1}\right)^{-(2p+1)}}{\sqrt{\pi}(2r+1)r!}\binom{-1/2}{p}\frac{(2k)^{p+2}}{(p+2r+3)}$$

It may be noted here that unlike what has been obtained in [7.3], the relaxation time at low temperatures now indeed depends upon the energy. Moreover, the energy

dependence is quite involved. As such, in order to know the mobility of the surface layer, one has to first obtain the average value of the relaxation time for the non degenerate ensemble of electrons, which is being considered here. It is usually given by [7.11]

$$\langle \tau_{ac} \rangle_{\text{Low Temp}} = \frac{\int \tau_{ac}(\varepsilon)\varepsilon^{3/2} \exp\left(-\frac{\varepsilon}{k_B T}\right) d\varepsilon}{\int \varepsilon^{3/2} \exp\left(-\frac{\varepsilon}{k_B T}\right) d\varepsilon} \tag{7.13}$$

The integration at the numerator of (7.13) can hardly be carried out analytically. Hence one has to take recourse to numerical integration [7.13]. Thus one obtains

$$\left(\mu_{eff}\right)_{\text{Low Temp}} = \frac{e\langle \tau_{ac} \rangle_{\text{Low Temp}}}{m_{\mu}^{*}}$$

The relation between the effective mobility (μ_{eff}) and the field effect mobility (μ_{FE}) of a MOS structure is given by [7.3,7.7]

$$\mu_{FE}(V_G - V_T) = \mu_{eff}(V_G - V_T) + (V_G - V_T)\frac{\partial}{\partial V_G}\mu_{eff} \tag{7.14}$$

where, V_G is the gate voltage and V_T is the threshold voltage. Moreover, in order to obtain the dependence of μ_{FE} on the gate voltage, use is made of the well-known relation [7.14,7.15]

$$N_{inv} + N_{dep} = \frac{C_{ox}}{e}(V_G - V_T) \tag{7.15}$$

where C_{ox} is the capacitance per unit area of the oxide layer. It is given by $\frac{\epsilon_{ox}}{t_{ox}}$, where ϵ_{ox} and t_{ox} are respectively the permittivity and the thickness of the oxide layer. Typical values of t_{ox} can be taken from the experimental data of [7.7].

7.3. Results and Discussions

Deviating from the framework of the theory which has been developed in [7.3], the present analysis of the characteristics of the channel mobility of a MOS structure, takes due account of the transverse component of the phonon wave vector. The electrons in the conducting channel of the structure are assumed to be confined in an infinite triangular potential well, instead of a rectangular well. Moreover, the full form of the phonon distribution function under the condition of low temperature has also been taken

into consideration, instead of taking it to be just zero. Thus the present analysis gives more realistic details of the mobility characteristics of the surface layer in the MOS structure. Specifically, in respect of the dependence of the mobility of the surface layer upon (i) the temperature, (ii) the effective gate voltage and (iii) the surface electric field etc. Each of the dependences, thus obtained here, seems to be quite complex and are significantly different from what turns up from the theory developed in Wu and Thomas [7.3], which neglects these realistic features of the electron-phonon interaction.

For an application of the present theory, sample channels of $Si\text{-}SiO_2$ MOS structure are now considered to calculate the numerical results. It is well known that the six valleys of Si are not always equivalent. We have considered here (100) and (111) surfaces. For the (100) surface, in the four equivalent valleys $m_{\|}{}^* = (m_t{}^* m_l{}^*)^{1/2}$ and $m_\mu{}^* = \frac{2 m_t{}^* m_l{}^*}{m_t{}^* + m_l{}^*}$; whereas for the (111) surface however, $m_{\|}{}^* = \frac{3 m_t{}^* m_l{}^*}{m_t{}^* + 2\, m_l{}^*}$ and $m_\mu{}^* = \frac{2}{3} \frac{m_t{}^*(m_t{}^* + 2 m_l{}^*)}{m_t{}^* + \frac{1}{3}(m_t{}^* + 2 m_l{}^*)}$, where $m_t{}^*$ and $m_l{}^*$ are the transverse and the longitudinal masses of the electrons respectively. They are taken to be $\frac{m_l{}^*}{m_0} = 0.99$; $\frac{m_t{}^*}{m_0} = 0.19$, m_0 being the free electron mass. The values of other parameters are [7.3,7.7] :

$$E_1 = 9.8\text{ eV} ;\ u_l = 9.037 \times 10^3\ ms^{-1};\ \rho_V = 2.329\text{ kgm}^{-3};\ \epsilon_{sc} = 11.9 ;$$

$$\epsilon_{ox} = 3.7 ;\ t_{ox} = 5 \times 10^{-8}\text{ m} ;\text{and } N_{inv} + N_{dep} = 2 \times 10^{19} m^{-2}.$$

The mobility characteristics of any structure are determined by characteristics of the scattering rate of the electrons under the prevalent conditions. The dependence of the scattering rate $P_{ac} \left(= \frac{1}{\tau_{ac}}\right)$ on the carrier energy in the low temperature regime for a Q2D in the n-channel of the $Si\text{-}SiO_2$ MOS structure as obtained from the present analysis, for the similar low temperature regime is shown in Fig. 7.1 using a logarithmic scale. Two surfaces, viz. (100) and (111) have been considered. As one can see from Wu and Thomas [7.3] $P_{ac} \sim m_{\|}{}^* \varepsilon_k{}^{1/2}$ irrespective of the lattice temperature. The present theory, on the other hand, gives an altogether different picture. The scattering rate P_{ac}, under the condition of low temperature now significantly depends upon the lattice temperature. The P_{ac}, as expected, increases with the temperature. At the higher values of electron energy, however, P_{ac} tends to be independent of the temperature. The dependence of P_{ac} upon the carrier energy ε_k is now quite complex, and differs significantly from the simple power law $P_{ac} \sim \varepsilon_k{}^{1/2}$.

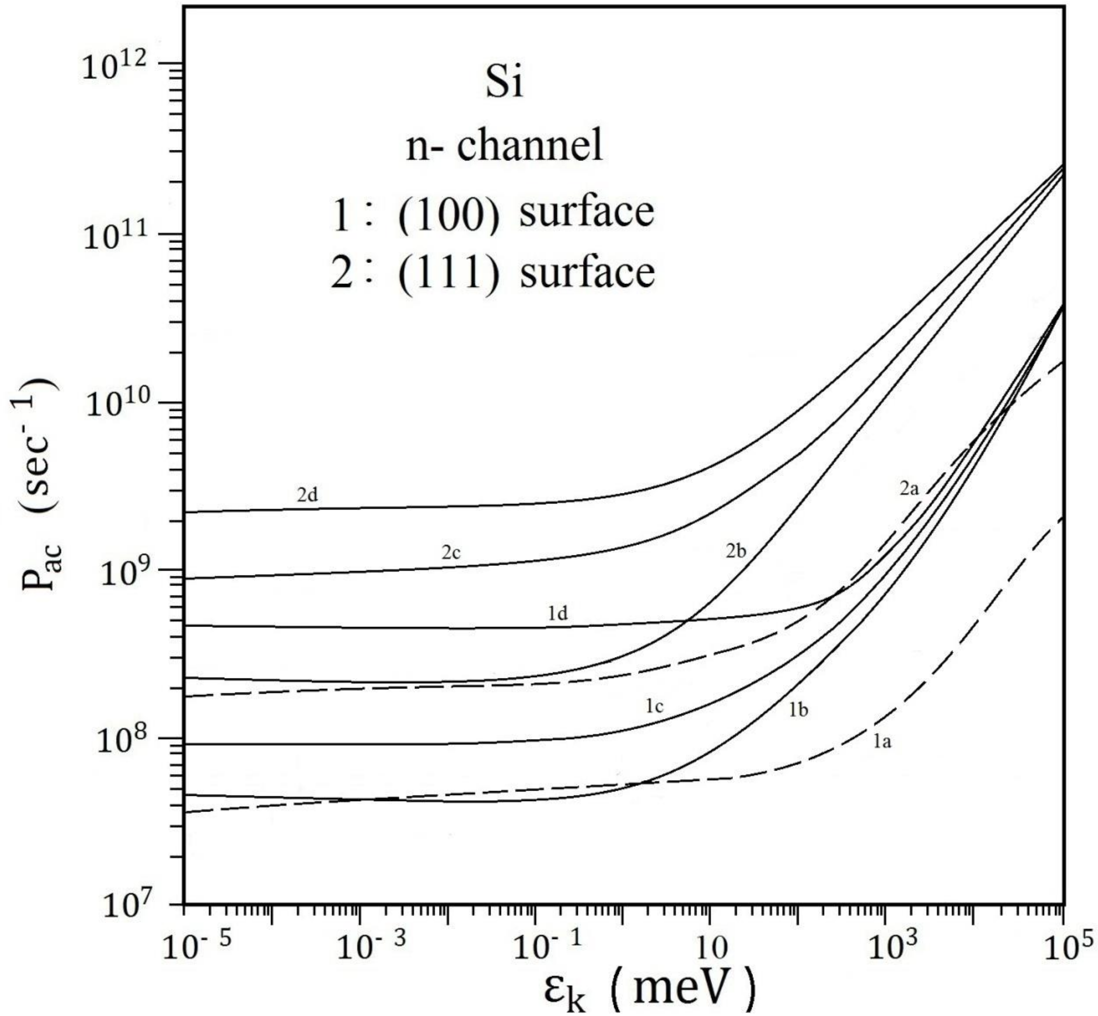

Fig. 7.1 : Dependence of the acoustic scattering rate P_{ac} upon the carrier energy $\varepsilon_{\vec{k}}$ at different lattice temperatures T for a non-degenerate ensemble of two dimensional electron gas in the n-channel of a Si-SiO_2 MOS structure for different surfaces. Curves marked 1 and 2 correspond to the surfaces (100) and (111) respectively. Curves marked 'a' are obtained from the analysis made in [7.3] considering the interaction of the two dimensional electrons with the two dimensional phonons. Curves marked 'b', 'c' and 'd' are obtained from the present analysis at lattice temperatures of 4, 10 and 20K respectively.

On the other hand, at the high temperature regime, qualitative nature of the characteristics of the scattering rate, that is obtained here, hardly differs from what turns up in Wu and Thomas [7.3], so far as its dependence upon ε_k or T is concerned. Each of them gives an energy independent of scattering rate, which is proportional to T i.e. $P_{ac} \sim T$. However, there is a significant qualitative difference of their values because of changes in the multiplicative scale factors, which depends upon surface electric field E_s in different ways for either of them. So, obviously it is interesting to see, how do these significant differences in the characteristics of the scattering rates effect changes in the characteristics of the channel mobility of the MOS Structure.

Next two figures show the dependence of the field-effect mobility upon the temperature, in the high temperature regime, for different values of the effective gate voltage $(V_G - V_T)$. Figs. 7.2 and 7.3 are for the (100) and (111) surfaces respectively. The curves marked 'a' give the results as given by the present analysis; and the curves marked 'b' are obtainable from the theoretical analysis made in [7.3].The curves marked 'c' are the experimental results reported in [7.7]. The curves 'b' show that the theoretical analysis in [7.3] predict a simple linear fall of μ_{FE} with the increase of the temperature; whereas, the results obtained from the present analysis predict that μ_{FE} falls with the increase of the temperature in a quite complex manner. Moreover, the agreement of the results given by the present analysis with the experimental values seems to be much better, compared to what Wu and Thomas predict under the similar prevalent conditions. In addition, the agreement of the results given by the present analysis with the experimental values improves as the effective gate voltage increases.

In the low temperature regime, the theory developed in [7.3] results in a temperature independent field-effect mobility. On the other hand, the present theory yields a quite complex dependence of μ_{FE} on T. Fig. 7.4 shows the $\mu_{FE} - T$ characteristics for the (100) and (111) surfaces as one can obtain from the present analysis, under the condition of low temperature, for different values of $(V_G - V_T)$. In the absence of any experimental data of the $\mu_{FE} - T$ characteristics under the similar condition of low temperature, we could not compare our theoretical results with the experiment.

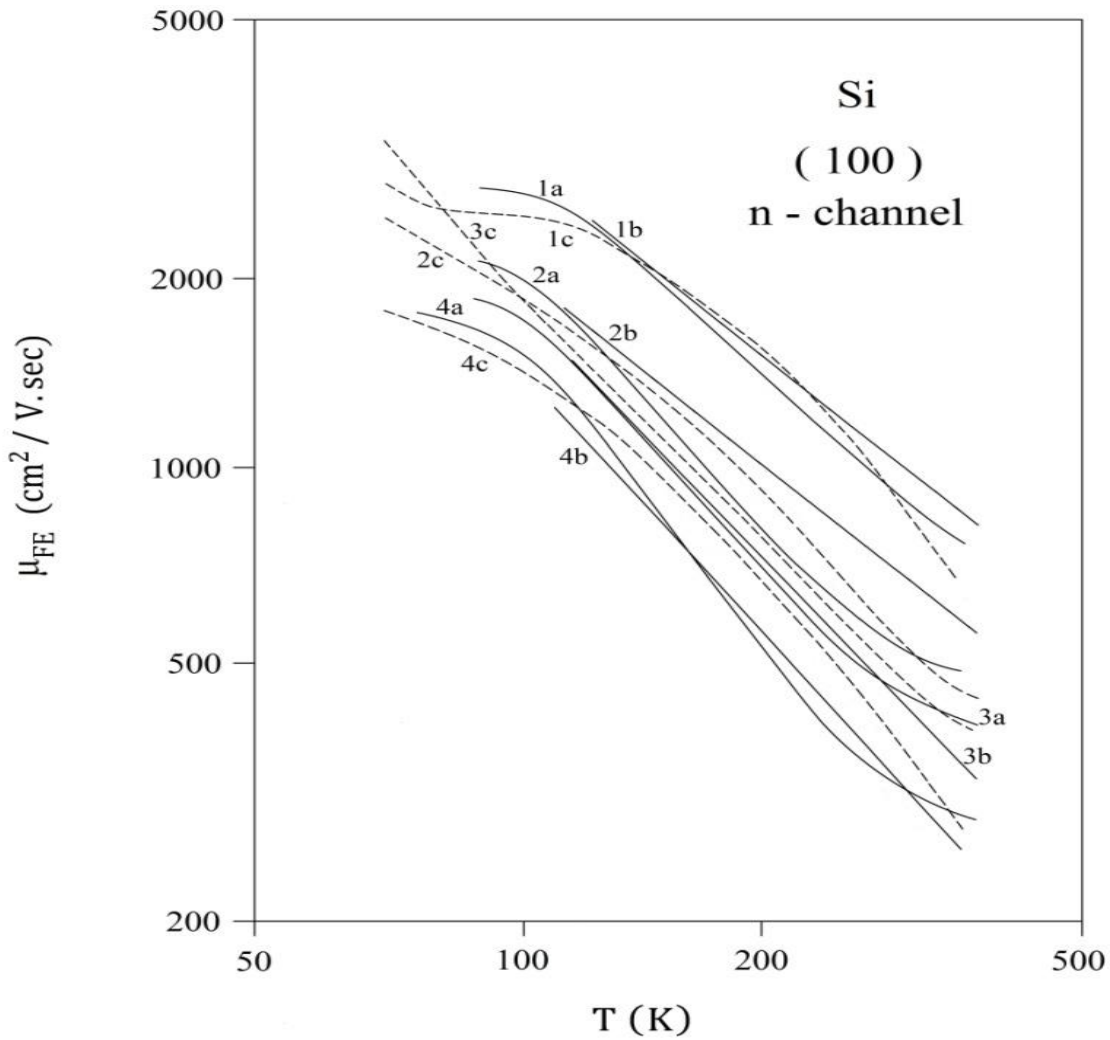

Fig. 7.2 : Dependence of the field-effect mobility μ_{FE}, upon the temperature T in the log$_2$ scale for the (100) surface taking the gate voltage $(V_G - V_T)$ as a parameter under the condition of high temperature. The curves 1-4 correspond to the gate voltages of 2, 10, 25 and 45V respectively. Curves marked 'a' and 'b' are respectively obtained from the present analysis and from what follows from [7.3]. The results are compared with the experimental data of [7.7] which are represented by the curves marked 'c'.

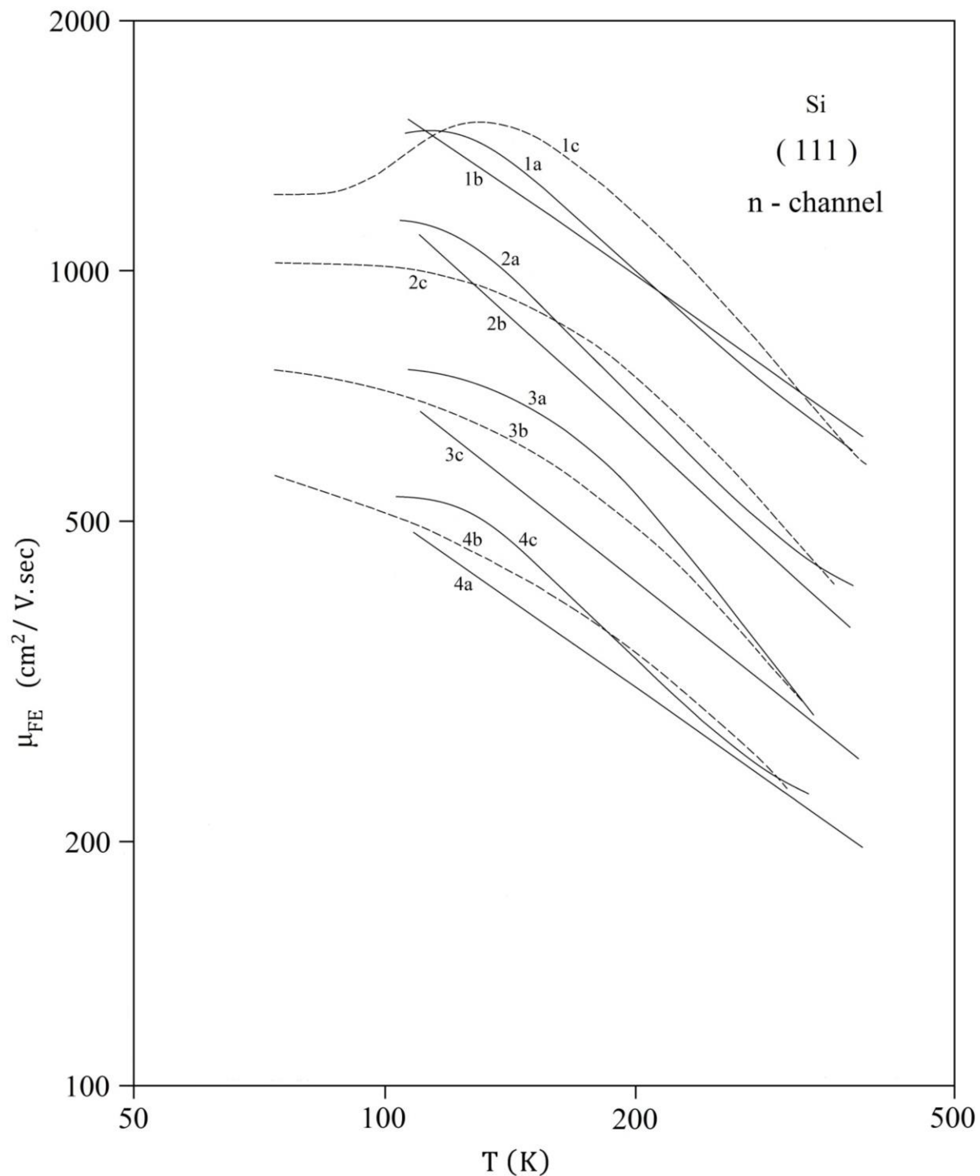

Fig. 7.3 : Dependence of the field-effect mobility μ_{FE}, upon the temperature T in the $\log_2$ scale for the (111) surface taking the gate voltage $(V_G - V_T)$ as a parameter under the condition of high temperature. The curves 1-4 correspond to the gate voltages of 2, 10, 25 and 45V respectively. Curves marked 'a' and 'b' are respectively obtained from the present analysis and from what follows from [7.3]. The results are compared with the experimental data of [7.7] which are represented by the curves marked 'c'.

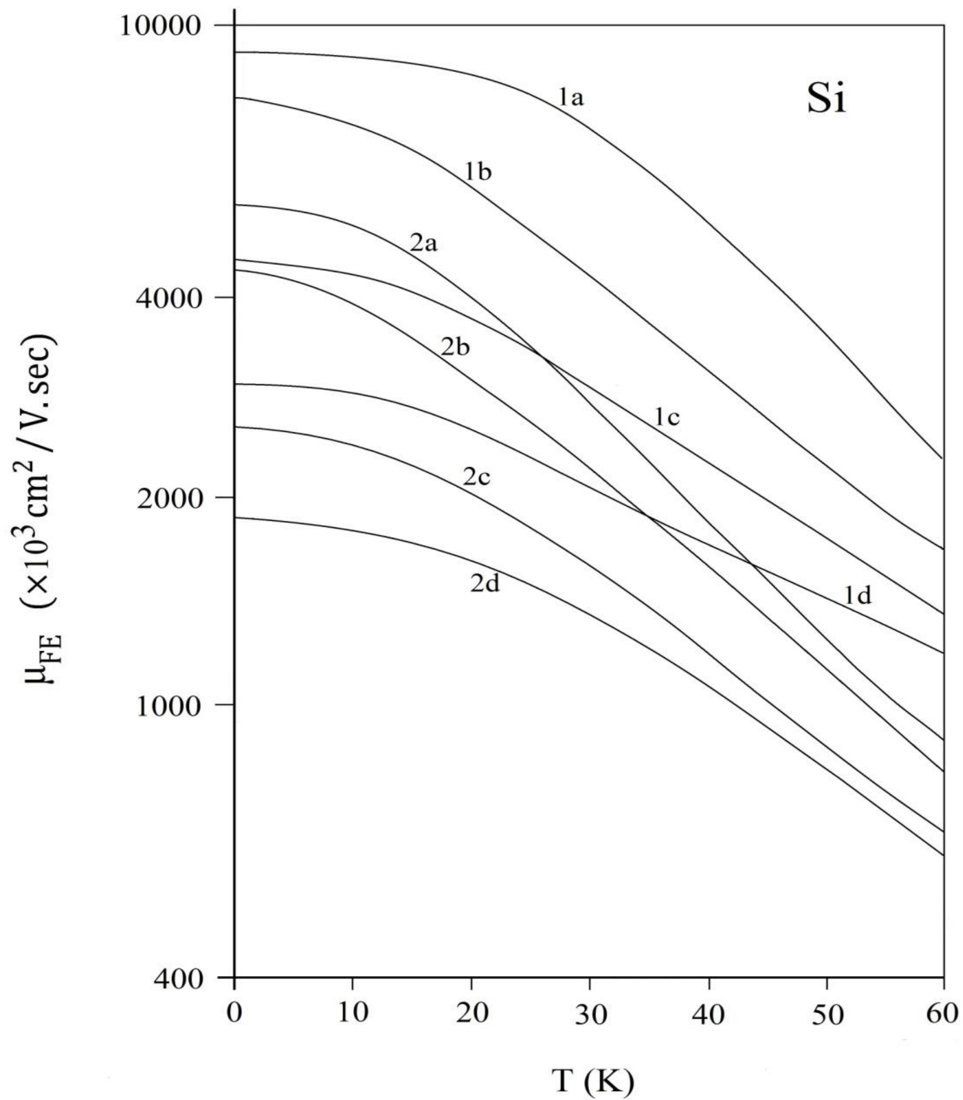

Fig. 7.4 : Dependence of μ_{FE} upon T of a two dimensional electron gas in the n-channel of the Si-SiO_2 MOS structure under the condition of low temperature as obtained from the present analysis for the surfaces (100) and (111), at different gate voltages. The curves marked 1 and 2 correspond to the surfaces (100) and (111) respectively. The curves marked 'a', 'b', 'c' and 'd' are for the gate voltages of 2, 10, 25 and 45V respectively.

Considering the (100) surface, the dependence of μ_{FE} on $(V_G - V_T)$, in the low temperature regime for different values of the temperature T is shown Fig.5. The curves marked 1, 2 and 3 are respectively for T = 4, 10 and 20 K. The curves marked 'a' are obtained from the present theory, those marked 'b' are the theoretical results from Wu and Thomas [7.3], and those marked 'c' are the experimental data T. Satô et. al [7.7]. It may be seen that the theoretical analysis in Wu and Thomas [7.3] predicts a temperature independent μ_{FE} in the low temperature regime. On the other hand, the present analysis predicts a complex dependence of μ_{FE} on T. Moreover, it may be noted, that the dependence of μ_{FE} on $(V_G - V_T)$ as obtained from the present analysis agrees in a much better way with the experimental data, compared to what the theory in Wu and Thomas [7.3] predicts. The agreement again improves as the temperature is lowered more and more.

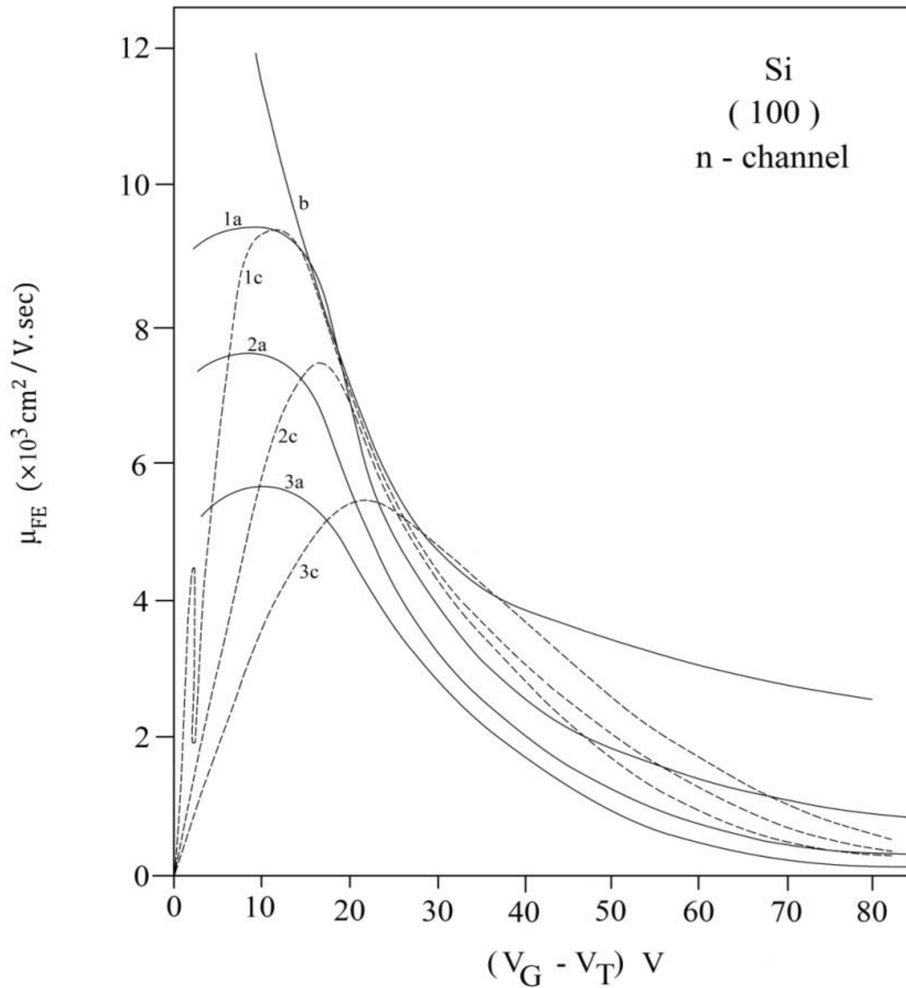

Fig. 7.5 : Dependence of the field effect mobility μ_{FE} of the two dimensional electron gas in the n-channel of the Si-SiO_2 MOS structure upon the gate voltage $(V_G - V_T)$ under the condition of low temperature, considering the (100) surface for different lattice temperatures. Curves marked 'a' and 'b' are respectively obtained from the present analysis and from [7.3]. The results are compared with the experimental data [7.7] which are represented by the curves marked 'c'. Curves marked 1, 2 and 3 are for lattice temperatures of 4, 10 and 20K respectively.

At high temperatures, the present theory predicts the same dependence of the mobility of the surface layer μ_{eff} upon the surface electric field E_s as that obtained in Wu and Thomas [7.3] viz. $\mu_{eff} \sim E_s^{-\frac{1}{3}}$. In the low temperature regime, however, the theory in

Wu and Thomas [7.3] gives a simple dependence: $\mu_{eff} \sim E_s^{-\frac{5}{9}}$. But the present theory gives a quite complex dependence of μ_{eff} on E_s. Fig. 7.6 shows the dependence of μ_{eff} upon E_s for the two surfaces (100) and (111) as obtained from the present theory at T = 4K, and the same as reported in Wu and Thomas [7.3].

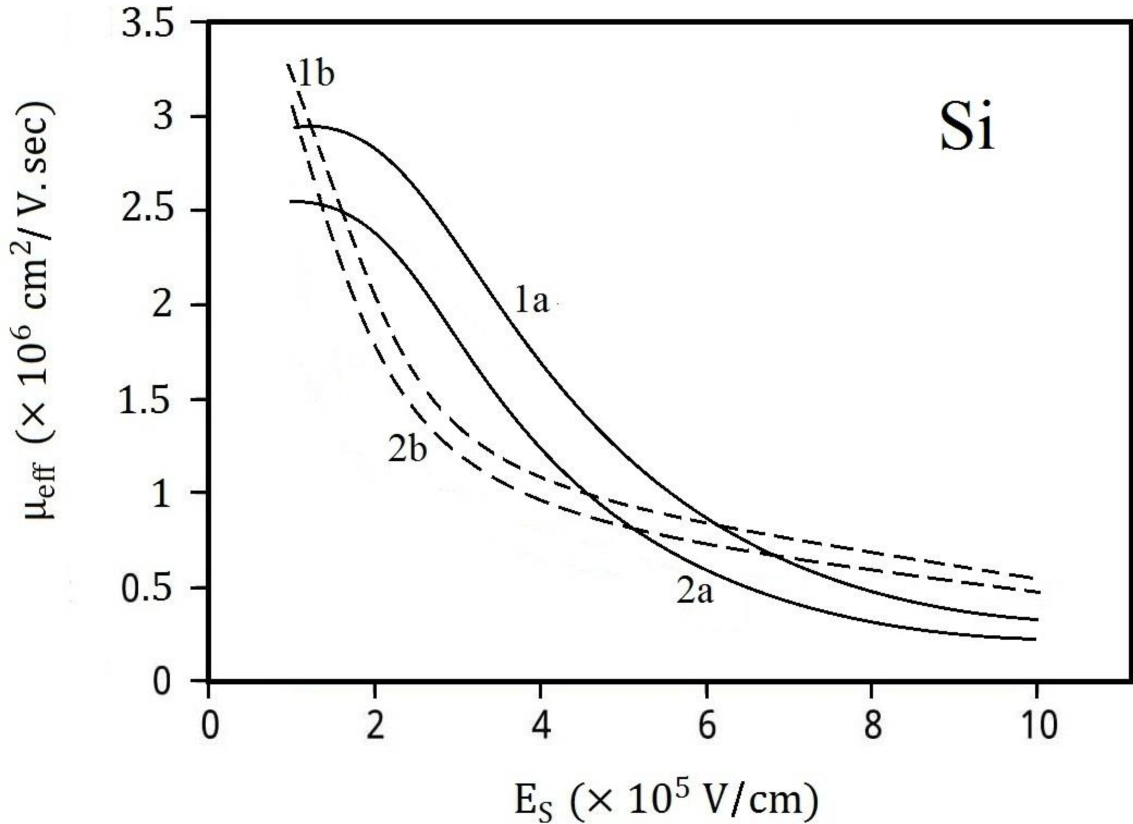

Fig. 7.6 : Dependence of the effective mobility μ_{eff} upon the surface electric field E_S for a non-degenerate two dimensional electron gas in a Si-SiO_2 MOS structure for different surfaces. Curves marked 1 and 2 correspond to the (100) and (111) surfaces respectively. Curves marked ‘a’ represents the results obtained from the present analysis, and those marked ‘b’ follow from [7.3].

From the present analysis one can see how essential it is to take into account some of the quite realistic features of the electron-phonon interaction while developing the theory of the channel mobility of a MOS structure, so that some significantly better agreement with the experimental data may be attained. The features that have been taken

into account include (i) contribution of the transverse component of the phonon wave vector, (ii) more realistic model of an infinite triangular well potential for the well produced along the direction, transverse to the Si-SiO_2 interface, instead of the infinite square well potential and (iii) the full form of the phonon population at the low temperature, instead of taking it to be zero for simplicity. Of course, there still remains enough scope for further refinement of the present theory, which would take due account of (i) the inelasticity of the electron-phonon interaction at low temperature, (ii) the variation of the deformation potential constant for high surface electric fields. The constant could assume a value larger than its bulk value (iii) apart from that the screening of the scattering potential under the condition of low temperature. The results, already obtained here being interesting, would stimulate further studies in the same line.

References:

[7.1] T. Ando, A.B. Fowler and F. Stern, Rev. Mod. Phys. 54, 437 (1982).

[7.2] F.F. Fang and A.B. Fowler, Phys. Rev. 199, 919 (1998).

[7.3] C-Y Wu and G. Thomas, Phys, Rev. B 9, 1724 (1974).

[7.4] C. Canali, C. Jacoboni, F. Nava, G. Octaviani and A. Alberigi-Quaranta Phys. Rev. B 12, 2295 (1975).

[7.5] H.L. Störmer, R. Dingle, A.C. Gossard, W. Wiegmann and M.D. Struge: Solid State Commun. 29, 705 (1979).

[7.9] H.L. Störmer, L.N. Pfeiffer, K.W. Baldwin and K.W. West, Phys. Rev. B 41, 1278 (1990).

[7.7] T. Satô, Y. Takeishi, H. Hara and Y. Okamoto, Phys. Rev. B 4, 1950 (1971).

[7.8] S. Nag , D.P. Bhattacharya, J. Phys. Chem. Sol. 79, 59 (2015).

[7.9] B.K.Ridley, J. Phys.C: Solid State Physics 15, 5899 (1982).

[7.10] J. Lee and M.O. Vassel, Jpn. J. Appl. Phys. 23, 1089 (1984).

[7.11] E.M. Conwell. High Field Transport in Semiconductors, in Solid State Physics, edited by F. Seitz and D.Turnbull (Academic Press, New York, 1997) Suppl.9

[7.12] B.R Nag , Physics of Quantum Well Devices, Kluwer Academic Publishers, Dordrecht (2000).

[7.13] S. Wolfram: Mathematica, Addison- Wesley, Redwood City, CA, (1988).

[7.14] Chenming Hu, Modern Semiconductor Device for Integrated Circuits. Pearson (2010).

[7.15] Y.Taur and T. H. Ning, Fundamentals of Modern VLSI Devices, Cambridge University Press (1998).